# RHEOLOGY MODIFICATION AND FOAMING OF POLYPROPYLENE – CLAY NANOCOMPOSITES WITH COUPLING AGENTS

By

Amit Kumar Chaudhary

A DISSERTATION

Submitted to
Michigan State University
in partial fulfillment of the requirements
for the degree of

DOCTOR OF PHILOSOPHY

Chemical Engineering

2010

# ABSTRACT

RHEOLOGY MODIFICATION AND FOAMING OF POLYPROPYLENE – CLAY NANOCOMPOSITES WITH COUPLING AGENTS

By

Amit Kumar Chaudhary

This research was motivated by the need to develop closed cell thermoplastic foam based on linear polypropylene to form the core of a wide variety of polypropylene components. This would require rheology modifiers since linear polypropylene does not have adequate tensile melt strength to prevent cell wall rupture during foaming or bubble expansion in the melt state. The objectives of this research were (1) to understand the effects of composition on melt extensional strain hardening in composites of linear polypropylene with nanoclay, compatibilizer and various coupling agents and (2) to evaluate selected nanocomposite formulations in extrusion foaming with chemical blowing agents.

Nanocomposites were prepared with organically modified montmorillonite, maleic anhydride grafted polypropylene as compatibilizer and linear polypropylene as the bulk matrix. The organoclays were also treated with amino silane coupling agents to increase the interaction between nanoclays and the compatibilizer. The effects of different polymeric compatibilizers and varying organoclay loading on the melt extensional viscosity behavior and the rate of crystallization of the nanocomposites were examined and shown to be critical for the resulting foam quality. Besides providing large numbers of nucleation sites for bubble formation during the foaming process, addition of nanoclay with appropriate compatibilizer provided strain hardening in melt extensional flow and slower crystallization.

In composites where the organoclay was used without additional treatment, hydrogen bonding on the surfaces of the organoclay holds the compatibilizer chains. Comparison of

composites with compatibilizers having different chain lengths revealed that the length of compatibilizing polymer chain that is anchored at one or more clay surfaces must be sufficient to affect the dynamics of the entanglement network during extensional flow and produce strain hardening in the melt.

Organically modified nanoclays and the compatibilizer have mainly electrostatic or hydrogen bonding type interactions, which are weaker forces of attraction. Amino silane coupling agents were grafted on the clay faces and/or edges to replace these weaker forces of attraction with stronger chemical bonds. Chemical reactions between the silated clays and appropriate compatibilizer resulted in nanocomposites with significantly greater strain hardening compared to the unsilated clay nanocomposites. These nanocomposites were further evaluated for extrusion foaming using a chemical blowing agent. The nanocomposites exhibiting uniform strain hardening over a range of strain rates resulted in foams with small cell size and highest cell densities within the scope of this research.

Since recyclability drives the substitution of thermoset polyurethane foams with closed cell PP foams, the effect of re-processing on the melt strain hardening behavior was investigated. Various nanocomposites were annealed and extruded through a uniform cross-section die to study the effect of heating and shear flow on the structural morphology and strain hardening of the nanocomposites. The results indicated that annealing had no negative impact on morphology or strain hardening of the nanocomposites. However, extrusion of these nanocomposites indicated that nanocomposites prepared using multiple hydrolysable groups resulted in formation of layered aggregates that are difficult to orient during uniaxial extensional flow and thus resulted in loss of the strain hardening behavior.

DEDICATED

TO

MY FAMILY

AND

IN THE MEMORY OF MY LATE BROTHER

# ACKNOWLEDGEMENTS

Achieving success in any endeavor required not only personal efforts but also the support of coworkers, colleagues and family. I have been fortunate enough to have this support during the entire course of my graduate studies here at Michigan State University. First and foremost, I would like to express my deepest gratitude to my academic advisor, Dr K. Jayaraman, for his advice and constant encouragement. Apart from being encouraging and supportive of my ideas, I thank you for the endless discussions and guidance to help shape my hypothesis into realities. I would also like to thank my committee members Dr R. Narayan, Dr A. Lee and Dr L. Matuana for serving on my committee and providing valuable guidance during the course of my research.

I would also like to express my gratitude to my fellow colleagues, John, Tanmay, and Katie, who helped me get started with my research during the early stages of my graduate studies. I would also like to thank Mr. Mike Rich for training me on various equipments and allowing me to use the facilities at the Composite Materials and Structure Center lab. I would also like to thank Mr. Brian Rook for helping me with various instruments and equipments during the course of my research. Further I would like to extend my sincere appreciation to Dr A. Pastor and Ms E. Danielewicz for training me on various microscopy tools along with sample preparations.

I would also take this opportunity to thank my parents and grand parents for their immense faith and unconditional love, which helped me stay miles away from home and earn a doctoral degree from Michigan State University. I couldn't have done it with you – Mom and Dad. Finally I would like to say "Thank you" to my wife Deboleena, for her constant support and

understanding through difficult times. Her love and support turned the tortuous path of graduate research work into a smooth one.

I want to take this opportunity to thank the chemical engineering staffs, Jennifer Somerville, Jennifer Peterman, Donna Fernandez, Lauren Brown, and Nichole Shook for all the help. I cannot thank Ms. JoAnn Peterson enough for her help and support during my initial tough days here at MSU. Finally, to my friends and lab-mates, thanks for all the laughs and unforgettable moments. You have all made my stay at Michigan State University a truly enjoyable experience.

# TABLE OF CONTENTS

# LIST OF TABLES

# LIST OF FIGURES

# 1. INTRODUCTION

## 1.1. Overview and Objectives

During the last few decades, polymeric materials have evolved into a global industry and have gained ever-increasing acceptance as an integral part of modern technology by steadily replacing other materials in a wide variety of applications. In order to satisfy the growing needs of the current market, nearly few 100 million tons of polymeric materials are produced worldwide, as compared to 5 million tons produced around six decades ago.

Ease of processing, light weight, economy and versatility makes these polymeric materials a preferred and competing commodity. The weight of these polymeric materials can further be reduced by foaming them with suitable blowing agents. Polymer foams, also referred to as sponge, expanded or cellular plastics are a class of polymeric materials that are extensively used as a common consumer product due to their economic and performance advantages, starting from styrofoam coffee cups to polyurethane foam seat cushions in automobiles. Polymer foams were first introduced in early 1940s and since then its use in modern technology continues to grow at a rapid pace across the globe due to their light weight, excellent strength/weight ratio, superior insulating and energy absorbing ability, buoyancy, comfort features and many more, most of which are absent in the unfoamed resin. The polymer foam industry is expected to grow steadily due to the unique advantages offered by these materials compared to traditional materials. In U.S. alone, the polymer foam consumption for the year 2010 is estimated to be around 7.5 billion pounds and is expected to reach around 8.6 billion pounds by the year 2015 at an annual growth rate of around 2.5% for all polymeric foams produced from commercial polymers.

With the growing need for energy and cost efficient systems primarily in automotive, aerospace and construction industries, polymer foams have evolved as another promising area of intensive research. With the advancement of foaming technology over the past few decades, the foaming technology has evolved from being purely empirical to more fundamental, relying on science and technology. Foams can be prepared from any polymer, by the introduction of a secondary gaseous phase within the polymer matrix. Different polymers are selected for different industrial foam applications depending upon their properties, their ease of manufacture, and the economics of the foaming system**.** This has led to foaming of nearly all types of polymeric resin – thermoset [1-8], thermoplastic [9] and even biopolymers [10-18] and has thereby led to the expansion of polymer foam application from automotive, construction, packaging, furnishing, transportation, sports industries all the way up to its use in tissue engineering [19-21] and drug delivery system [21-23]. Various polymers have been used for foaming applications, for example, polyurethane (PU) [1-8], polystyrene (PS) [24-28], poly-vinyl chloride (PVC) [29-33], polycarbonate (PC) [34-36], polyolefins (polyethylene (PE), polypropylene (PP)) [37-49], poly (ethylene terephthalate) (PET) [50], poly (lactic acid) (PLA) [51, 52]. Amongst all polymer foams, polyurethane (PU) foam continues to be the largest product segment in the global polymeric foams market followed by polystyrene (PS) foam. Even though PU foams cannot be recycled, thereby causing a strong impact on environmental issues, its market is expected to grow at a rate of 2.6% annually. This is due to the fact that PU leads to the production of closed cell foams with a wide range of densities and hardness, forming both rigid and flexible foams depending on the final application. Also due to the high impact resistance properties of PU foams, it is widely used in automotive industries for its use in door and instrument panels along with cushioning of seats. The production of such automotive interiors involves multistep

fabrication and thus produces as lot of non-recyclable scrap. This demands a sooner replacement of this material with more environmental friendly and recyclable polymer foam.

Thermoplastic polyolefins (TPO) has all the required properties necessary to replace PU foams from automotive industry [53, 54]. TPO is a two phase blend of semi-crystalline polypropylene and ethylene-octene elastomer. This material is widely used in the automotive industry for the production of various automobile exterior and interior parts such as bumper fascia, claddings, wire insulations etc. because of its weatherability, low density, low cost, high impact strength and scratch resistance [53-56]. However, utilization of TPO foam has not been implemented successfully due to various technological challenges involved in its production and has not yet been fully developed. Nonetheless, there lies a significant amount of interest in developing foamed TPO products due to its attractive economic and environmental properties. Polypropylene is the major component of the TPOs and has various attractive properties, for example, it can be used at higher service temperatures, has good stiffness, excellent chemical and abrasion resistance and above all has low material cost and is easily processable. However, PP has poor impact properties. Even though polyethylene has better impact properties than PP, PE has failed to satisfy the market demands for high performance and high heat resistance foamed polymers. Even though rheologically PE is more favorable for foam production than PP, PP foams are preferred for applications where stiffness, chemical resistance, good heat and sound insulation, and higher end use temperatures is required. The addition of elastomers to the PP matrix improves the impact strength of the resulting material by improving its ductility and crack resistance [55-57], thereby making it the most desirable polymer for foaming applications. However, foamability of linear polypropylene is also largely restricted by its rheological [47, 58, 59] and thermal properties [60, 61]. This research primarily focuses on understanding

foamability and modifying the rheological properties of linear polypropylene by the use of organically modified montmorillonite nanoclays that can lead to successful production of polypropylene foam, thereby leading to TPO foams for various interior and exterior applications in the automotive industry.

## 1.2. Polymer Foams: General Introduction

Thermoplastic foams are cellular plastics having dispersed, usually spherical or hexagonal, voids in a continuous thermoplastic polymer matrix. These materials possess unique physical, mechanical and thermal properties, usually governed by the matrix, the foam cellular structure (for example, cell size, cell density and bulk density).

Thermoplastic polymer foams represent a class of light weight materials that find immense potential in a variety of applications, such as, transportation, insulation, packaging, sealing materials, sports, impact and sound absorption and many more [62]. Thermoplastic foams have been classified by cell size, expansion ratio and cell wall integrity. These classifications are independent of processing technology and the polymer used, and they reflect different applications and different physical properties of the foams. Polymer foams with an average cell size above 100 μm are classified as conventional (coarse) foams, between 10 and 100 μm as fine-celled foams, and foams below 10 μm are known as microcellular foam. Microcellular foams were first introduced by Suh et al. [63] in 1980s. Microcellular foams have large number of small cells, which reduces the stress concentration around the cells due to reduction in cell size. Compared to conventional and fine-celled foams, microcellular foams are known to exhibit superior impact strength, high toughness and stiffness to weight ratio, high

thermal stability, low thermal conductivity, high fatigue life, and reduced material weight and overall cost.

Foams are also classified as either rigid or flexible depending on whether their glass transition temperature is below or above ambient temperature and on their cell morphology. Rigid foams are selected for applications where high mechanical strength is required, such as in building and construction, transportation, packaging, furniture, decorative moldings, food and drink containers, and floatation devices. Flexible or semi-flexible foams are used in gasketing, sports applications, shock and sound attenuation, shoes, furniture cushioning, textile and primary seals in automobiles.

Polymer foams are also classified as closed cell or open cell foams depending upon the cell structure. Closed cell foams have cell cavities that are closed and isolated from each other surrounded by cell walls. This leads to foams with better insulation properties and higher mechanical strength. Open cell foams have cell cavities that are interconnected and the cell walls are broken and not continuous. The open cell foams are superior materials in terms of absorptive capability.

The foaming of polymeric materials can be achieved by various methods, such as use of blowing agents, mechanical whipping of air and dispersion of hollow microspheres [62]. The most widely used process is the expansion of molten polymer containing a blowing or foaming agent. Blowing agents used in the foaming processes can be classified into two categories – physical blowing agents (PBA) and chemical blowing agents (CBA) [64]. Chemical blowing agents are chemicals that function by releasing a gas due to heat-induced decomposition above a critical decomposition temperature. The gas thus generated (commonly nitrogen or carbon dioxide) is dissolved in the hot melt under high pressure, which later nucleates and grows into

bubbles as the pressure is reduced. These can either be endothermic or exothermic, or a combination of both. Proper selection of the CBA allows a good temperature control in the foaming process. Most widely used CBAs are azodicarbonamide, benzene sulfonylhydrazide, and sodium bicarbonate. PBA are substances that form gaseous products under the foaming conditions (high temperature and/or reduced pressure). In this case a homogeneous mixture of polymer melt and physical blowing agent is first obtained by directly metering the physical blowing agent into the polymer melt at high pressure. Subsequent increase in temperature or reduction in pressure results in bubble nucleation and growth. Commonly used physical blowing agents are volatile liquids such as, hydrocarbons, alcohols, inert gases such as nitrogen, and carbon dioxide. Amongst all, $CO_2$ is the most favorable PBA, as it is inexpensive, nontoxic, and environmentally benign. However, due to limitation in solubility in the polymer melt and the high rate of diffusion out of the melt, significantly limits the development of $CO_2$ as an industrial scale foaming agent.

Polymer foams can be manufactured by a variety of continuous to batch processes, for e.g., continuous extrusion, injection molding, rotational molding, compression molding, and lamination of foams, or foam board production [62]. Irrespective of the type and nature of blowing agent, the polymer matrix and the foaming technology, in general, the foaming process involves three fundamental steps:

- Bubble / cell nucleation
- Cell growth
- Cell stabilization

Nucleation is a classical phenomenon that exists in processes like condensation and crystallization. Colton et al. [65] presented a theoretical model for cell nucleation in amorphous

thermoplastic microcellular foams based on the classical nucleation theory. The process of cell nucleation within a polymer melt takes place when the polymer melt gets supersaturated with the blowing agent and a sudden pressure drop results in phase separation. If the nucleant is generated from a single homogeneous phase of dissolved gas in a polymer melt without impurity or dirt, the process is called *homogeneous nucleation*. However, if cells are formed at solid/liquid interface, e.g., at the surface of foreign particles, the process is called *heterogeneous nucleation*. Fletcher [66], in his study presented the effect of nucleant size on heterogeneous cell nucleation. In heterogeneous nucleation, high nucleation efficiency can only be achieved when nucleation is energetically favored and the nucleant is well dispersed in the polymer matrix. According to the theory developed [65, 66], heterogeneous nucleation rate is primarily a function of particle concentration and dimensions, nature of polymer-gas-particle surface interactions, and pressure of the system. Qualitatively, it was inferred that a small contact angle and a large surface curvature results in an increase in heterogeneous nucleation rate.

Once the gas bubbles are nucleated, they will continue to grow by diffusion of gas from polymer melt phase into the bubble, until eventually they are stabilized or ruptured. The growth process is very complicated due to several factors governing the polymer melts rheological response to the deformation introduced by the expansion of the gaseous phase. With the continuation in cell growth, the probability of cells coming in contact with each other increases, causing neighboring cells to share a common cell wall. This decreases the cell wall thickness, as a result of which they become highly stretched and unstable. This could eventually lead to cell coalescence because of which the average cell size increases and cell density decreases. One of the important factors in controlling cell growth and thereby reducing cell coalescence is the stability of the cell walls, which depends upon the tensile melt strength or melt strain hardening

of the surrounding polymer matrix. Strain hardening or tensile melt strength of a polymer melt is defined as the degree of resistance to extensional flow. Therefore, polymers with higher tensile melt strength are expected to increase the cell wall stability and thereby prevent cell coalescence leading to polymer foams with higher cell density, lower cell size and narrow cell size distribution. Higher melt viscosity would also reduce cell coalescence by slowing down the drainage of polymer from the cell wall during the foam solidification period.

In order to obtain a controlled and uniform cellular structure of the polymer foam, heterogeneous nucleating agents such as, talc, silicon oxide, titanium oxide, and zinc oxide are commonly added to the polymer matrix. Work done by Baldwin et al. [67] indicates that production of microcellular foams using an extrusion system requires stringent processing conditions – high pressure drop or pressure drop rate and processing temperature close to the glass transition temperature (for amorphous polymers), resulting in a narrow operating window. In order to ameliorate these strict processing conditions, work was done to incorporate nucleating agents in the polymer matrix to produce microcellular foams. Work done by Park et al. [68] using talc (microfillers) as the heterogeneous nucleating agent in the polymer matrix, showed an increase in cell density and better control over cell size distribution compared to microcellular polymer foam without any nucleating agents. This encouraged researchers to explore the use of nanoparticles as heterogeneous foaming nucleating agent in polymer matrix for the production of microcellular foams.

## 1.3. Polymer Nanocomposites

Traditionally, polymeric materials have been filled with various natural or synthetic micron sized inorganic fillers forming polymer composites, thereby improving their material

properties and reducing cost. Commonly used micro fillers are in the form particles (calcium carbonate), fibers (glass or cellulose fibers), or plate-like (glass flake, mica, talc). Even though these materials impart significant improvement in various material properties, they are often associated with few drawbacks, for example, increase in density, brittleness and opacity [69-74]. Polymer nanocomposites, on the other hand, are a different class of composite in which the fillers incorporated have at least one dimension in the nanometer scale.

Polymer nanocomposite is a field of research that has been studied in great detail over the past two decades. Interest in polymer nanocomposites has been results of improvements in their various physical and mechanical properties due to the addition of a small amount of anisotropic nanoparticles in the polymer matrix. These small additions are effective at low concentrations due to the large surface area to volume ratio of the nanofillers. This surface to volume ratio can significantly alter the macroscopic properties of polymers, imparting high thermal and dimensional stability, enhanced mechanical properties, high heat deflection temperature, improved flame retardance, reduced gas permeability and increased barrier properties without a significant increase in density and opacity [73, 74]. Polymer nanocomposite was first introduced by Toyota Motor Co. by developing nylon–6/montmorillonite nanocomposites [75, 76] in late 1980s. In the time since their introduction, this field has expanded to work on many different polymer systems such as polyolefins, polyamide, polystyrene, poly(methyl methacrylate), poly(ethylene terephthalate), polycarbonate, polyvinyl alcohol, polyacrylic acid, and polyethylene oxide [73, 74]. The derived nanocomposites have been extended for various applications such as solar calls, electronic devices, and structural applications. Commonly used nanoparticles used in polymer nanocomposites are layered silicates (nanoclay), fibers (carbon

nano fibers, and rod-shaped (carbon nano tubes). Amongst all the nanofillers, nanoclays are most widely studied probably because of its availability and cost.

Polymer/layered silicate (PLS) nanocomposites are synthesized by dispersing nano silicates in the polymer matrix either by in situ polymerization, solution blending or melt mixing. Amongst these, melt mixing is the most economical process and is widely used for commercial purposes. Nanoclays are high aspect ratio particle (100 – 300), that provide considerable enhancement in various material properties at low weight fractions (0.5 – 5 wt%) compared to traditional fillers (glass, mica, talc), which are incorporated at a higher weight fractions (10 – 40 wt%). This result in significant increase in density of traditional composites compared to nanocomposites. Most common nanoclays used in the synthesis of these PLS nanocomposites is montmorillonite that are obtained naturally in the form of tactoids comprised of several layers. These nanolayers are comprised of aluminum-oxygen-hydroxyl octahedral layers sandwiched between two silicon-oxygen tetrahedral sheets and are generally called 2:1 smectite clays. These nanolayers are held together by Van-der Walls forces of attraction and are thus difficult to separate from each other. Since most engineering polymers are hydrophobic in nature, dispersion of these tactoids into discrete nanolayers is further hindered by the hydrophilic nature of these layered silicates. The extent of dispersion of these clay platelets defines whether the final nanocomposite is intercalated or exfoliated (Figure 1.1). In intercalated structure, the polymer chains penetrate between layers of clay galleries and increase the inter-platelet spacing but retain a well-ordered multilayer morphology of alternating polymer and clay layers. In case of exfoliated nanocomposites, the nanoplatelets are completely separated from one another and are well dispersed within polymer matrix. There is no repeating pattern of polymer and clay layers in exfoliated nanocomposites as seen in intercalated composites. Due to better dispersion of clay

platelets, exfoliated nanocomposites will have higher effective particle concentration at the same weight percentage of nanoclay loading.

In order to achieve better dispersion of these nanolayers, the naturally occurring montmorillonite has to be organically modified to synthesize polymer compatible nanoclay. In order to facilitate the interaction between the hydrophilic clay layers and hydrophobic polymers, the galleries of the clay tactoids are intercalated with long chain alkyl ammonium surfactants [77-81]. The ammonium ion is attached to the clay face and the dangling hydrocarbon tails swells the clay galleries to facilitate polymer chain intercalation and thus improves dispersion of these nanolayers in the polymer matrix. The functionality present in the polymer chain along with its extent of hydrophobicity defines the selection criteria of the surfactant to be intercalated in the naturally occurring montmorillonite. Reichert et al. [82] studied the effectiveness of alkyl chain length of the surfactant towards dispersion of the organically modified nanosilicates in the polypropylene matrix and reported that the extent of dispersion of organosilicates improves with the increase in alkyl chain length of the surfactant. Manias et al. [83] and Ton That et al [84] reported that multiple alkyl tails of the surfactant results in better dispersion of nanoclay in the polypropylene matrix. However, the selection criteria are different for polymers having functional groups (nylon, polystyrene) as opposed to polyolefins [85].

Even with the organic functionalization of montmorillonites, the intercalation of hydrophobic polyolefins in the organically modified montmorillonites is difficult and is generally facilitated by the use of less hydrophobic compatibilizers. These compatibilizers are, in general, polyolefins functionalized by grafting hydroxyl groups or more commonly maleic anhydride groups at the ends of the polyolefin chains [78, 86, 87]. Okada et al. [88] were the first to demonstrate the use of polypropylene-grafted maleic anhydride (PP-g-MA) as a

compatibilizer to synthesize PP-clay nanocomposites. The importance of such polar compatibilizers for the use in non-polar clay nanocomposite preparation is well demonstrated by various researchers [86, 89-94].

## 1.4. Polymer Nanocomposite Foams

In recent years, the integration of the polymer nanocomposite technology with the traditional polymer foaming process, has led to synthesis of polymer nanocomposite foams with greatly improved characteristics in terms of reduced average cell size and increased average cell density. The presence of nanoparticles provides additional surface to facilitate heterogeneous nucleation of the large number of cells during the foaming process. The heterogeneous nucleation effect of nanoparticles has been reported for various polymers, for example, polystyrene, nylon, poly (lactic acid), polycarbonate, polyurethane, poly (vinyl chloride), poly (ethylene terephthalate), and polypropylene.

The use of nanoclay in foaming polystyrene to obtain closed cell foams with narrower cell size distributions and high cell densities was demonstrated by Lee and coworkers [9, 26, 28, 95-99]. Han et al. [28] foamed polystyrene (PS) / clay nanocomposites in a continuous extrusion foaming process using carbon dioxide as foaming agent and studied the influence of nanoparticles on cell size, cell density and mechanical properties of the foam. They observed an eight fold increase in cell density and the average cell size decreased by approximately 40% upon addition of 7.5 wt% organically modified nanoclay. This is attributed to the much higher surface area made available for nucleation of bubbles by well dispersed nanolayers.

Shen et al. [99] presented a direct impact of aspect ratio of nanoparticles on cell size and cell density of PS / carbon nanofibers (CNFs) nanocomposite foam. They studied the foaming of

PS / CNFs nanocomposites via continuous extrusion process (melt compounding) using carbon dioxide as foaming agent. In order to overcome Van der Waals forces of attraction amongst the CNFs and to improve mixing and dispersion of CNFs uniformly in the polymer matrix, higher level of shear was applied during the extrusion process. The intensive shear exerted by the twin screw extruder resulted in significant break-up of CNFs (average CNF length reduced from ~60 μm to ~0.28 μm). In order to study the effect of change in aspect ratio of the CNFs, they made PS / CNFs nanocomposites via solution blending (minimum shear on the CNFs) with the help of ultrasonication, instead of high shear mixing, to achieve complete dispersion of CNFs in the polymer matrix. Solution blending resulted in nanocomposites with average fiber length of several dozens of microns, indicating minimum damage to the CNFs compared to that in the extrusion process. PS / CNFs composite made via these two processes (melt compounding and solution blending) were subsequently foamed in a batch process. The average cell density of the solution blended sample ($5.7x10^8$ cells/$cm^3$) was found to be higher than that of the melt compounded one ($1.85x10^8$ cells/$cm^3$) and the average cell size was also smaller (10.2 μm for solution blended sample and 14.9 μm for melt compounded one).

Work done by Zeng et al. [27, 95] also looked into the importance of aspect ratio of nanoparticles along with its surface properties in foaming of PS nanocomposites. Two types of nanoparticles were selected for preparing PS nanocomposites – plate-like nanoparticles (nanoclay) [95], nanofibers (carbon nanofibres (CNFs) and single wall carbon nanotubes (SWCNTs)) [27]. The synthesized nanocomposites were subsequently foamed in a batch process using carbon dioxide as the foaming agent. During the synthesis of PS / SWCNTs nanocomposites, it was found that the dispersion of SWCNTs in the PS matrix was poor and resulted in large amount of ball shaped aggregates at higher levels. However, the results indicate

that even with poor dispersion of SWCNTs in the PS matrix, the resultant nanocomposite foam with 0.1wt% SWCNTs displays a much higher cell density and a smaller cell size compared to exfoliated PS / clay nanocomposites with 5wt% nanoclay. PS / CNFs nanocomposites with well dispersed CNFs (1wt%) also resulted in foams with higher cell density and a smaller cell size compared to the exfoliated PS / clay nanocomposites. However all three nanocomposites significantly increased the cell density and reduced the cell size compared to pure PS foam. One important factor leading to lower cell density and higher cell size of PS / clay nanocomposite foams compared to CNFs and SWCNTs system is lower aspect ratio. However, in order to explain the comparatively poor performance of exfoliated PS / clay nanocomposites towards heterogeneous nucleation even at such higher clay levels (5 wt%), Zeng et al. found that polymer-gas-particle contact angle (θ) was 105.5°compared to 20° for PS /CNFs system. This indicated that poor wetting property of nanoclays is responsible for lower cell density and higher cell size compared to that of CNFs system. These results indicate that low particle loading of high aspect ratio nanoparticles having favorable wettability (low contact angle) serve well as heterogeneous nucleating agents during the foaming process for producing microcellular foams under mild processing conditions.

Apart from increasing the nucleation efficiency, high aspect ratio of nanoparticles offers the potential for cell wall reinforcement. Since the thickness of foam cell walls is in the micron and sub-micron regime [100], the nanoscale dimension of the nanoparticles make them desirable elements to reinforce the cell walls, resulting in foams with enhanced mechanical properties [99]. The success behind microcellular foams can be attributed to the mechanism of cell structure evolution, which can be due to increased cell nucleation, controlled cell growth, reduced cell coalescence, and enhanced cell stability. Any one of the above mentioned factors or a

combination of these factors can result into foams with superior physical and mechanical properties.

## 1.5. Polypropylene Foams

Linear polypropylene, in today's market, is one of the most widely used polymeric materials due to its outstanding combination of cost performance, excellent physical properties, strong and continuous expansion of process versatility, and environmental friendly processes and materials during manufacturing, use, and recycling stages. Due to its outstanding functional characteristics and low material cost, polypropylene foams have been considered as a substitute for other thermoplastic foams in industrial applications. With the growing attention towards total recyclability and to take advantage of the benefits of polypropylene, these materials are considered to be the best replacement for thermoset (polyurethane) foams. Even though polypropylene has higher rigidity compared to other polyolefins and it offers better impact strength than polystyrene along with a higher service temperature range and good temperature stability, continuous foaming of polypropylene foams is largely restricted by the semi-crystalline nature of the polymer [60, 61, 101] and its rheological properties [47, 58, 59].

The evolution and control of the cellular structure in semi-crystalline polymer foams is quite different from that of amorphous polymer foams. The semi-crystalline nature of the polymers makes the foaming process more complicated because of simultaneous nucleation and growth of gas bubbles and crystals. Reignier et al. [61] have demonstrated with batch foaming of poly-(e-caprolactone) that crystallization affects both bubble nucleation and growth. Park and coworkers [46, 60, 102] have investigated foaming of polypropylene with supercritical $CO_2$. Work done by Doroudiani et al. [60] indicated that the cellular structure of semi-crystalline

polymer foams is difficult to control because of the fact that the gas would not be able to diffuse into the crystallites leading to non-uniform bubble nucleation. Hence, early onset of crystallization, before the gas bubbles are nucleated, could lead to reduction in bubble nucleation efficiency resulting in non-uniform foaming with regions of sparse and dense bubbles. Naguib et al. [46] reported that both early and delayed onset of crystallization is detrimental to foam cellular structure (Figure 1.2). In their work done on foaming of branched PP using N-butane as a blowing agent in a tandem foam extrusion system, they report an optimum melt temperature for maximum expansion ratio of the foam samples. They observed a decrease in foam extrudate diameter as a function of the distance from the die when the melt is at a higher temperature, due to delayed onset of crystallization causing the gas to diffuse out of the sample. On the contrary, a lower melt temperature resulted in early onset of crystallization leading to insufficient foaming. Park et al. [45, 103, 104] have reported effects of other processing parameters – melt temperature and pressure, on continuous foaming of polymers with a physical blowing agent.

The most important rheological property for producing superior quality foam is the ability of the polymer melt to show strain hardening under uniaxial extensional flow. Linear PP does not have adequate tensile melt strength or strain hardening under uniaxial extensional flow, a necessary property for producing superior quality foam, particularly in crystallizing polymers. Strain hardening, is defined as the transient extensional viscosity rise above the linear viscoelastic curve, at a constant strain rate. Polymers that do not demonstrate strain hardening under uniaxial extensional flow, develop thinner cell walls during bubble expansion in the foaming process, which results in coalescence of bubbles and even open-cell foams [105, 106]. An increase in extensional viscosity during the expansion process provides stability to the cell walls and has been shown to be important for producing good quality foams [58, 100]. Ghijsels

et al. [107] studied the temperature dependency of tensile melt strength for polyolefins and showed that the tensile melt strength of polypropylene decreases with increase in temperature. As mentioned earlier, melt strain hardening behavior of a polymer is an important parameter for foaming applications. Due to weak tensile melt strength at higher temperature, the processing window for foaming polypropylene is extremely narrow, the lower limit being determined by the melting temperature of polypropylene (160°C - 165°C) and the upper temperature limit being determined by minimum accepted tensile melt strength that can result in microcellular foams. Burt [108] reported in his work that the operating temperature range for producing acceptable polypropylene foam, using linear polypropylene, is merely 4°C as opposed to 50°C for polystyrene.

The mechanism of polymer deformation during bubble growth in a polymer foaming process is biaxial stretching. Munstedt et al. [48, 109, 110] has measured the biaxial extensional viscosity for linear PP as well as branched PP using lubricated squeezing flow and have observed that the biaxial extensional viscosity shows similar trends to the uniaxial extensional viscosity. In particular, they concluded that if strain hardening is observed in uniaxial extensional flow, it will be observed in biaxial extensional flow as well. This is useful because more reliable equipment and procedures are available for measurement of uniaxial extensional viscosity of melts than for the measurement of biaxial extensional viscosity of polymer melts. Hence uniaxial elongational flow measurements may be used to identify relevant trends in the biaxial extensional viscosity.

Various approaches have been adopted to produce melt strain hardening of linear PP and eventually improve its foamability. Chemical or radiation crosslinking is a common method used for introducing strain hardening property in the resulting polymer melts [44, 111, 112]. Crosslinking the polymer results in melt strain hardening of PP and results in better foam;

however, the crosslinking process leads to loss of recyclability, chain scission and oxidative degradation of the PP, which affects its physical properties [113-115]. Another approach to impart strain hardening behavior in polypropylene is to introduce tree type branching network. It is well established that branched polypropylene show strong strain hardening character [110, 116, 117]. Blends of linear and branched PP have also resulted in polymer melt showing strain hardening in uniaxial extensional flow [116, 118-120]. Due to the presence of strain hardening property in blends of linear and branched PP, it has been reported [48, 58] that such blends foam better than the linear resin, leading to smaller cell sizes and higher cell densities compared to linear PP. These blends typically have around 20 wt% of the branched polymer that increases the overall cost of the polymer material significantly.

Successful application of nanoparticles to serve as heterogeneous nucleating agent to improve foamability of amorphous polymers led to its use to improve the foamability of linear polypropylene foam. However, the extent of success in producing good quality polypropylene foams with the assistance of nanoparticles was limited due to the absence of strain hardening property of the linear polypropylene melt in uniaxial extensional flow. Numerous work has been done on foaming linear polypropylene in a wide array of processes, starting from continuous extrusion process [48, 49, 121-123], injection foaming process [42], and batch foaming process [41, 124, 125]. Gendron et al. [121] have reported extrusion foaming of nanocomposites based on linear PP and branched PP having 2 wt% of organically modified nanoclay, with direct carbon dioxide injection as the blowing agent to produce low density foams (0.2 – 0.3 gm/cc). In addition to the nanoclay, they had also added 0.5 wt% of talc to serve as nucleating agent. They observed severe coalescence in linear PP foam samples that showed mild improvement with the addition of nanoclay at low concentrations (0.3 wt%) of the blowing agent. However, they

observed severe collapse in foam cellular structure of the PP/clay nanocomposite foam with increase in the blowing agent concentration from 0.3 wt% to 0.5 wt%. However, foam samples produced from branched PP system resulted in better cellular structure. But no significant improvement in cellular structure was observed upon the addition of the nanoclay on top of 0.5 wt% of talc. Branched PP with talc as the nucleating agent resulted in foams with cell sizes in the range of 250 – 600 μm. Similar results were obtained with both talc and nanoclay present in the branched PP matrix. However, in the absence of talc, branched PP/clay nanocomposite resulted in poor foam with cell sizes of the order of 600 – 1000 μm. This was probably due to poor dispersion of the nanoclays, hence suggesting the reduced capability of nanoclay serving as efficient nucleating agent in polypropylene matrix. In the absence of strain hardening in linear PP matrix, even in the presence of both talc and nanoclay, they observed foams with large coalesced zones, thereby indicating the importance of strain hardening in the polymer melt for foaming applications.

Carreau et al [42] reported foaming studies of both linear and branched PP nanocomposites containing 2 wt% of organically modified montmorillonite nanoclay in an injection foaming process, using 1 wt% of a chemical blowing agent (azodicarbonamide). With controlled injection foaming conditions, they were able to produce high density linear PP foams with good cellular structure. They observed a small drop in average cell size from 60μm to 45μm, due to the addition of clay in linear PP matrix. An even better cellular structure was obtained for branched PP and its nanocomposite foams. The addition of nanoclay in the branched PP system resulted in a small reduction in the average cell size from 40μm to 35 μm. Zheng et al. [49] also reported extrusion foaming of linear PP/clay nanocomposites with supercritical carbon dioxide as the foaming agent. They reported improvement in cellular structure and

reduction in average cell size and increase in average cell density with the addition of nanoclay. The linear PP foam had cell sizes in the range of 150 – 500 μm, which reduced to around 50 – 80 μm upon addition of 1 wt% of nanoclay. This improvement in foam quality can be attributed partly to the use of supercritical carbon dioxide as the foaming agent that provides greater pressure drop during the foaming process, usually not achievable by liquid carbon dioxide and other chemical blowing agents. However, its use in industrial application demands stringent safety regulations and cost. It has also been shown that production of polypropylene foam with smaller cell size (20 – 60 μm) is possible by the use of a non-conventional batch foaming process [41, 124, 125]. This limited improvement in foam quality by the use of nanoclays in linear polypropylene is primarily because of absence of strain hardening behavior in PP melts and crystalline nature of the polymer. This is not the case with amorphous polymers like polystyrene that show strain hardening behavior under uniaxial extensional flow [126, 127] and do not have any crystallization issues, leading to the successful application of nanoparticles in improving foamability of amorphous polymers. This suggests that there is clearly a need for preparing and foaming linear PP/clay nanocomposites that display significant strain hardening under uniaxial extensional flow.

Takahashi et al. [128] studied the extensional flow behavior of polyethylene composites with microscale fillers (glass beads, glass fiber, talc) and found that strain hardening goes down with filler addition. Similar observations were made while studying extensional flow behavior of ethyl-vinyl acetate / nanoclay nanocomposites [129]. Similar to the effect of fillers on strain hardening behavior in microcomposites, Gendron et al. [121] and Carreau et al. [42] also observed no improvement in melt strain hardening under uniaxial extensional flow upon the addition of nanoclays to linear PP. However, Seong et al. [130] reported in their work done on

polyamide-6/clay nanocomposite that melt strain hardening behavior can be obtained in a nanocomposite if the organically modified nanoclay tactoids are completely exfoliated. Recently, nanoclays were used by Okamoto et al. [131] to introduce strain hardening property in maleated polypropylene melt. Pathak and Jayaraman [132] have found that selection of high molecular weight maleated polypropylene and the composition of the nanocomposite were critical to obtain significant strain hardening in uniaxial extensional flow of the nanocomposite melt. In their subsequent work, Okamoto et al. [100] evaluated the performance of maleated polypropylene / clay nanocomposite for foam applications. They reported reduction in cell size and an increase in cell density upon addition of nanoclay to the maleated polypropylene foam. However, it is well established that functionalizing with maleic anhydride results in polypropylene with unacceptable mechanical properties [133]. Hence there lies a strong need for preparing and foaming linear PP/clay nanocomposites that display significant strain hardening under uniaxial extensional flow.

## 1.6. Research Objectives

The objective of this research is to develop novel and controlled approach to impart strain hardening behavior to linear polypropylene by the addition of organically modified nanoclays and maleic anhydride grafted polypropylene without the loss of recyclability and economy and investigate foamability of the resulting nanocomposites in a continuous extrusion foaming process using chemical blowing agents for the manufacture of low-density polypropylene foams. While formulating these approaches, one needs to develop understanding of the role of compatibilizer and organically modified nanoclay, towards imparting strain hardening property to the linear PP/clay nanocomposite melt.

To address this bigger objective, this research is categorized into three specific research problems:

a) To synthesize linear polypropylene/clay nanocomposites showing strain hardening behavior under uniaxial extensional flow and investigate the specific material properties affecting foamability of linear polypropylene/clay nanocomposites. This was then used to demonstrate superior foamability of TPO nanocomposite that is prepared from strain hardening PP/clay nanocomposite, compared to TPO without any nanoclays.

b) To study the effect of additional nanoclay treatment by carefully chosen silane coupling agents on the strain hardening property of linear polypropylene-clay nanocomposites and their foamability.

c) To develop basic understanding on the effect of compatibilizer molecular structure on the strain hardening behavior of the linear polypropylene/clay nanocomposites under uniaxial extensional flow.

d) To investigate the effect of thermal annealing and melt processing by extrusion through a uniform die on strain hardening behavior of polypropylene-clay nanocomposites, in the context of recyclability.

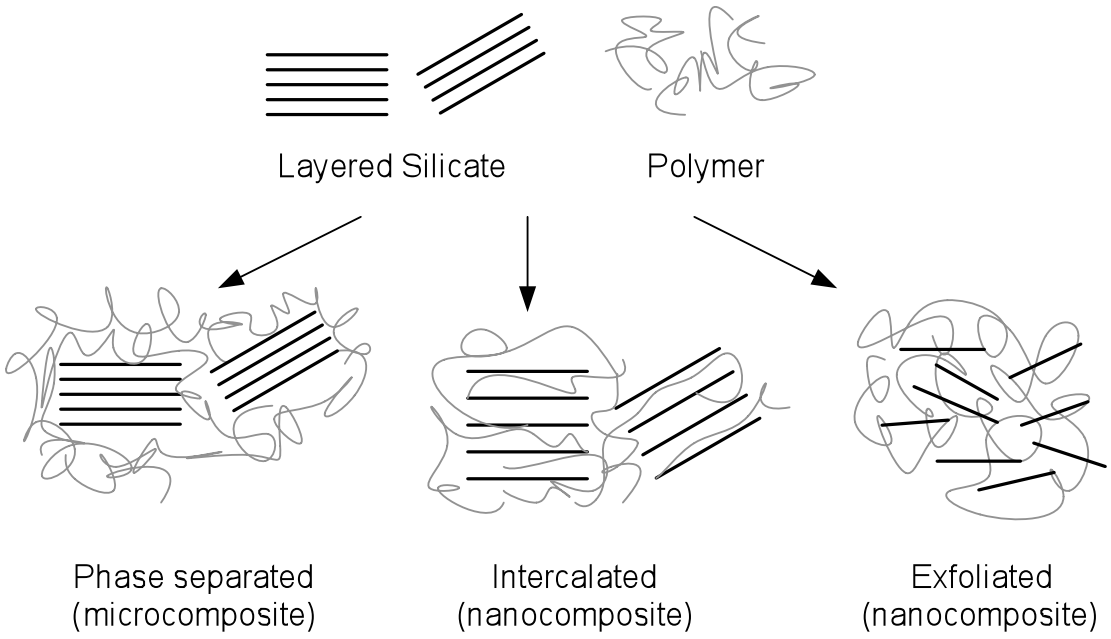


**Figure 1.1:** Classification of layered-silicate polymer nanocomposites based on the extent of dispersion of the nanolayers.

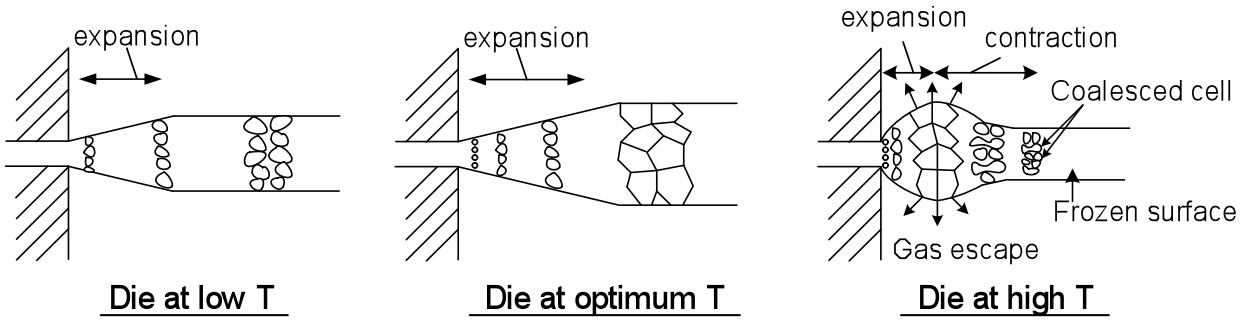


**Figure 1.2:** Effect of die processing temperature on evolution of cellular structure of semi-crystalline polymer foam [46].

# 2. POLYPROPYLENE / CLAY NANOCOMPOSITES – PREPARATION AND CHARACTERIZATION PROCEDURES

## 2.1. Materials

Linear polypropylene, Profax 6523, was used as the matrix polymer for most of the study. In order to prepare PP/clay nanocomposite, maleic anhydride grafted polypropylene was used as a compatibilizer. A tree type branched polymer (PF-814) was used to prepare a blend of linear and branched PP. This was done so as to compare the foaming results of linear PP/clay nanocomposites with the blend of linear and branched PP. Since the ultimate objective of this study is to replace polyurethane foam with TPO foam, a TPO blends was made by blending an ethylene–octane copolymer (Engage 8480) with linear PP. The details of all the polymers (melt flow rate (MFR), molecular weight (Mw), and supplier) used in this study are presented in Table 2.1.

The nanoclays used in this study were organically modified montmorillonite clay provided by Nanocor. Two different organoclays were used for the synthesis of the PP/clay nanocomposites: (a) I.44P: with 35 wt% of dimethyl-di-octadecyl ammonium cation and (b) Nanocor I.30P: with 24 wt% octadecyl ammonium cation. Both these organoclays have same molecular equivalent of organic surfactants in the clay galleries.

The chemical blowing agent used in this study was Cell-span 693K (gas volume 70cc/gm), provided by Phoenix Plastics with the active ingredient being azodicarbonamide. Four different silane coupling agents were used for the treatment of nanoclays:

a) N-aminoethyl-Aza-2,2,4-trimethylsilacyclopentane (Diamino monomethoxy-Silane)

b) N-(2-aminoethyl)-3-aminopropylmethyldimethoxysilane (Diamino dimethoxy-Silane)

c) N-(2-aminoethyl)-3-aminopropyltrimethoxysilane (Diamino Trimethoxy-Silane)

d) Phenyl trimethoxy silane.

## 2.2. Nanocomposite Preparation

The nanocomposites for the scope of this research were prepared by melt mixing technique. For the preparation of polymer/clay nanocomposites, both continuous and batch mixing process have been used for research purpose as well as on commercial scale. Twin screw extruder has been used as a continuous mixing process for the preparation of polymer/clay nanocomposite. Batch mixing process has been increasing used, primarily for research purpose, for the preparation of polymer nanocomposites at small scale. Common batch mixers used for this purpose include Banbury mixers [134-137], DACA mixers [138] and Gelimat mixers [139]. The residence time and shear rate in all these mixing techniques were optimized so as to result in nanocomposites with best possible dispersion of the nanoplatelets with minimal degradation of the polymer and the organically modified clay.

In this study a 75 cc Banbury batch mixer, manufactured by CW Brabender Instruments Inc., with two counter rotating Banbury screws was used for the preparation of polypropylene/clay nanocomposites. Prior to compounding, maleated polypropylene pellets and the nanoclay powder were dried in a vacuum oven at 80ºC and 20" Hg vacuum, for 12 hours. The dried polymers were then premixed with the nanoclay power in a plastic beaker, according to the proportions required for a 47gm batch nanocomposite formulation. This homogenized polymer – clay mixture was then fed to the preheated Banbury mixer bowl. For majority of the research, the nanocomposite was prepared by melt mixing at 180ºC, 150rpm for 10 minutes. The mixing temperature of 180ºC was chosen based on the fact that most polypropylene has a melting temperature of around 165 ± 2ºC. This mixing protocol was chosen so as to maximize

shearing time and minimize polymer and/or clay thermal and/or shear degradation and has been optimized in our lab through previous work [135, 140]. In order to minimize oxidative thermal degradation, a constant nitrogen purge was maintained inside the mixing bowl. For part of the study additional mixing conditions used were: (a) 200ºC, 80 rpm, 10 minutes mixing time and (b) 200ºC, 40 rpm, 10 minutes mixing time. This was done so as to study the effect of shearing on nanocomposite structure and its effect on strain hardening under uniaxial extensional flow. The reason for increasing the temperature was to match the actual melt temperature of 180ºC mixing case, which was measured to be 200ºC due to additional heat generated due to shear at 150 rpm. The final nanocomposite was then collected from the mixing bowl as clumps with the help of a brass scraper. These clumps were used directly for the preparation of samples for rheological studies and structural characterization of the final nanocomposite, while for foaming studies these clumps were granulated in a mini granulator.

## 2.3. Silane Treatment of Nanoclays

In order to carry out silane treatment of the nanoclays, 15g of an organoclay was dispersed in 500ml of a solvent (80 wt% methanol + 20 wt% de-ionized water) using a magnetic stirrer. In a separate flask, 4.5gm of silane was diluted with 200ml of the same solvent. This diluted silane solution was slowly added to the clay dispersion and left under constant stirring condition for 6 hrs under ambient conditions. After 6 hrs, the clay suspension was filtered and washed at least 3 times using the same solvent to remove any unreacted silane. The resulting clay cake was then left for 24 hrs in a vacuum oven at 80ºC, 20” Hg pressure for curing. The cured clay was then powdered in a mortar-pestle and sieved with a No. 200 sieve. The powdered clay

was used for various characterizations and for the preparation of the nanocomposites with linear polypropylene, using PP-g-MA as a compatibilizer.

Three different solvent systems were chosen for the study:

(a) A mixture of 80 wt% methanol and 20 wt% de-ionized water,

(b) A mixture of 80 wt% methanol and 20 wt% de-ionized water, and

(c) De-ionized water.

The organoclays were easily dispersed in the first solvent, however in order to disperse the clay in the second solvent, a lab sonicator was used to prepare the clay dispersion. Since the nanoclays used for silane treatment is already pretreated with organic surfactants, it was next to impossible to disperse the clay in de-ionized water. Hence an aqueous cake of the organoclay was obtained from Nanocor, an unfinished product obtained from an intermediate step during the production of the organoclay, which was easily dispersed in de-ionized water.

## 2.4. BET Surface Area Measurements

Brunauer, Emmett, and Teller in 1938 proposed a theory [141] with an objective to explain the physical adsorption of gas molecules on a solid surface that can further be used as the basis for an important analytical technique for the measurement of the specific surface area of the surface. This theory was invariably known by the initials of the authors, BET theory. This theory is an extension of Langmuir theory [142] for monolayer molecular adsorption and is applicable to multilayer adsorption. The fundamental hypotheses of the BET theory are:

1. The surface is homogeneous
2. Gas molecules physically adsorb on a solid surface in layers infinitely
3. There is not interaction between each adsorption layers

4. Langmuir theory can be applied to each layer.

Based on these hypotheses, the BET equation is given as:

$$\frac{1}{v\left[\left(P_0/P\right)\text{-}1\right]} = \frac{c\text{-}1}{v_m c}\frac{P}{P_0} + \frac{1}{v_m c} \qquad (2.1)$$

where, P and $P_0$ are the saturation and equilibrium pressure of the adsorbates, $v$ and $v_m$ are the total and monolayer adsorbed gas volume and c is the BET constant, given by equation (2.2):

$$c = \exp\left(\frac{E_A - E_L}{RT}\right) \qquad (2.2)$$

where, $E_A$ is the heat of adsorption of the first layer and $E_L$ is the heat of liquefaction of the second and higher layers.

This theory is widely used to calculate the total surface area ($S_{total}$) of solids by physical adsorption of gas molecules, using equation (2.3)

$$S_{total} = \frac{\left(v_m N s\right)}{V} \qquad (2.3)$$

where, 'N' is Avogadro's number, 'V' is the molar volume of adsorbent gas and 's' is the cross section area of the adsorbing species.

In the present work, Micrometrics (Gemini V) Surface area and pore size analyzer is used to determine the surface area of the various organically modified montmorillonite nanoclays, using nitrogen as the adsorbent gas. Prior to subjecting the nanoclays for BET surface area analysis, around 1.5gms of clay samples were degassed at 120ºC with nitrogen as the purge gas for 24 hours. The sample was then weighed accurately and subjected to the BET surface area analysis following the adsorption procedure. Helium gas was used to estimate the free volume in the sample tube followed by the adsorption of nitrogen gas, under liquid nitrogen temperature, to

calculate the total volume. These informations were then used to estimate the specific surface area (area/gm) of the clay samples.

## 2.5. X-Ray Diffraction

X-ray diffraction (XRD) technique was used for structural characterization of various organically modified montmorillonite and its resulting polypropylene/clay nanocomposites. This technique is based on the fact that if a crystal was an assembly of regularly spaced atoms, then they can act as scattering sites for X-ray beam that has a wavelength approximately equal to the inter atomic distance in a crystal. Thus it can provide insight to the microsctructure of the crystal by diffracting the X-ray beam. A mathematical expression for such diffraction phenomenon was proposed by Bragg and is given by equation 2.1, known as Bragg's Law of diffraction.

$$n\lambda = 2d\sin(\theta) \qquad (2.4)$$

Where 'n' is the order of reflection, 'λ' id the wavelength of the X-ray beam, 'd' is the spacing between atoms or planes, and 'θ' is the angle of diffraction. The first order reflection is only considered in this work [143].

The X-ray diffractometer used in this study was a Rigaku Rotaflex Ru-200BH X-ray diffractometer, which is equipped with a Ni-filtered Cu Kα radiation source and operated at 45kV and 100mA. This instrument has four diffraction slits; one between the X-ray source and the sample (1/6º); two between the sample and the goniometer (1/6º and 0.3º) and the last slit is mounted on the detector (0.3º). The selection of the optimal diffraction slits combination was on the basis of previous work done in our lab. To obtain the X-ray diffraction pattern of the clay samples, the powder clay samples were compacted on a 1"x1" cavity on a glass slide. For the polymer nanocomposite specimens, a 20x40x1 $mm^3$ sample was compression molded at 200ºC

and 10 tonnes pressure in a Wabash compression molder. All measurements are recorded for a 2θ scan range of 0.5º to 10º, at a rate of 0.5º/min and at equal increments of 0.01º.

Natural montmorillonite clay has a mean interlayer basal spacing of the (001) plane (d-spacing) of about 0.95nm. The organic treatment by various octadecyl ammonium surfactant leads to intercalation of the surfactant molecules inside the clay galleries resulting in an increase in d-spacing. For the nanoclay treated with octadecyl ammonium cation (single tail alkyl chain), the mean d-spacing increase to about 2.34 nm and the clay treatment with dimethyl-di-octadecyl ammonium cation results in a mean d-spacing of about 2.54 nm.

## 2.6. Transmission Electron Microscopy

Transmission electron microscopy (TEM) is a valuable analytical tool, where a beam of electrons is transmitted through an ultra thin sample. The high energy electron beam interacts with the sample during transmission and produces an image containing finest details of the internal structure of the specimen. The electron beam produced from an electron gun is controlled using a series of lenses (condenser and objective lens) before it passes through the sample. Even though TEM is a powerful tool to produce high resolution images, up to the nano-dimensions of specimens, it comes with various limitations. The biggest drawback is that TEM can scan very small area of a given sample (usually around 0.3 $mm^2$). Another limitation is the sample preparation. Since the technique relies on transmission of electron beam through the sample, the thickness of the sample has to be less than about 90nm. Moreover, the thickness should be uniform or else it will produce images with varying degree of brightness due to variation in sample thickness. Hence, this technique is difficult to be used with a lot of materials. A sectioning device called an ultra-microtome is generally used to prepare samples. For polymer

samples, the sectioning has to be done below its glass transition temperature in order to preserve the structure of the specimen under investigation. Since the glass transition temperature of polypropylene samples below 0ºC, cryo-sectioning is required to provide enough rigidity so as to facilitate uniform sectioning of the sample and to maintain its structure. Cryo-sectioning is a technique where thin, uniform sections of specimen are produced by cutting the material with a diamond tip knife, below room temperature. The low temperature is maintained using liquid nitrogen as a coolant.

The ultra microtome used for this study was PTXL ultra-microtome (RMC, Boeckeler Instruments) connected to a CRX cryo unit. In order to prepare the sample, a small rectangular piece (1-2 $mm^2$) was cut out of a compression molded sample. The cut sample was then mounted on the ultra-microtome maintained at -120ºC using concentrated sucrose solution. This section close to 90nm was then cut and mounted on 200 mesh size formvar coated copper grids. These sections were then used to study the dispersion and structure of nanoclay layers in various PP/clay nanocomposites using JEOL 100CX TEM at 120KeV acceleration voltage.

## 2.7. Differential Scanning Calorimetry

Differential scanning calorimetry (DSC) is a thermoanalytical technique that measures the change of the difference in heat flow rate to the experimental sample and to a reference sample while both are subjected to a controlled temperature program. Throughout the experiment both the experimental and the reference sample are maintained at a constant temperature. The reference is generally an empty sample holder (hermetically sealed aluminum pan). This technique was used to determine the melting temperature, crystallization temperature, fractional crystallinity, and rate of crystallization of the pure polymer or polymer/clay nanocomposites. The

principle underlying this technique is that, when the polymer sample undergoes a physical transformation (phase change), which is associated with a change in enthalpy, the instrument either increases or decreases the amount of heat flow to the sample so as to maintain both the experimental and the reference sample at the same temperature.

The differential scanning calorimeter used in the present study was a TA Q-Series instrument – DSC Q10TA. The sample (8-10mg) was heated to 200 °C (5°C /min ramp), then cooled to 40 °C (-5°C /min ramp) under nitrogen atmosphere and the entire cycle was repeated. Results are reported from the second run as the first run is primary to remove any thermal history present in the sample. The peak obtained from the heating cycle denotes the melting temperature (Tm) and the peak from the cooling cycle represents the crystallization temperature (Tc). The fractional crystallinity ($X_C$) and the average rate of crystallization (k) in each sample were obtained by the following relations.

$$X_c = \frac{\Delta H_c}{207w} \tag{2.5}$$

$$k = \frac{X_c}{t_c} \tag{2.6}$$

where, w is the weight fraction of polymer in the sample, $\Delta H_c$ is the enthalpy of crystallization of polymer in the sample obtained by computing the area under the crystallization peak, the quantity 207 J/g refers to the enthalpy of crystallization of 100% crystalline PP and $t_C$ refers to the time span over which crystallization is completed.

## 2.8. Thermo-gravimetric Analysis

Thermo-gravimetric analysis or thermal gravimetric analysis (TGA) is a technique used to determine weight loss (or weight gain) of a sample as a function of temperature under controlled atmosphere. As a sample is heated, it can undergo weight loss due to drying, due to liberation of gases from chemical reactions or oxidative decomposition.

The Thermo gravimetric analyzer, TA instrument TGA Q500 series, was used in this study to study the percentage weight change with respect to change in temperature for different organically modified montmorillonite clays and the chemical blowing agent. A high precision platinum pan was used to and the experiment was carried out under an inert nitrogen atmosphere. About 6 – 10mg of sample was used in this study. A high resolution temperature ramp procedure was selected to increase the temperature from room temperature to 800°C at a ramp rate 10°C/min. This procedure allows maintaining an almost constant temperature when the sample is undergoing weight change at a particular temperature, thereby resulting in greater accuracy.

## 2.9. Rheology

Rheology is the science of flow and deformation [144] that gives valuable information about the microstructure of a material. In this study, we have used rheological studies to investigate the role of various organically modified montmorillonite nanoclays on the melt rheological properties of polypropylene, under both shear and uniaxial extensional flow.

### 2.9.1. Shear Rheology

Rheology involving simple shear flow is the most common type of rheological study, generally, used to investigate the linear viscoelastic response of a material (in this case molten polymer). Linear viscoelastic studies of polymer melt produces valuable information about its molecular structure. For this study, simple shear flow is produced by sandwiching the test material between a set of smooth parallel plates, where one of the plates is stationary while the other one is mobile. This moving plate produces a shear deformation that is analyzed using relationships derived from equation of motion using the following assumptions [144]:

1. Steady, laminar, isothermal flow
2. $\upsilon_\theta$ (r, z) only, $\upsilon_r = \upsilon_z = 0$
3. Negligible body forces
4. Cylindrical edge

Based on these assumptions, the equation of motion for parallel plate geometry transforms into:

$$\theta: \qquad \frac{\partial \tau_{\theta z}}{\partial z} = 0 \tag{2.7}$$

$$z: \qquad \frac{\partial \tau_{zz}}{\partial z} = 0 \tag{2.8}$$

$$r: \qquad \frac{1}{r}\frac{\partial}{\partial r}\left(r\tau_{rr}\right) - \frac{\tau_{\theta\theta}}{r} = -\rho\frac{\upsilon_\theta^2}{r} \tag{2.9}$$

Further, using these relationships and assuming a "no-slip" condition at the plate surfaces, the relationship between the shear stress and the torque generated is given as:

$$\tau_{12}(R) = \frac{M}{2\pi R^3}\left[3 + \frac{d\ln M}{d\ln \dot{\gamma}_R}\right] \tag{2.10}$$

In the present study, we have used strain controlled small amplitude oscillatory shear type flow to obtain various linear viscoelastic properties of the polymer melt. The oscillatory strain and stress in such flow is given as:

$$\gamma = \gamma_0 \sin(\omega t) \tag{2.11}$$

$$\tau = \tau_0 \sin(\omega t + \delta) \tag{2.12}$$

The oscillatory stress can further be decomposed into an in-phase plastic or elastic component and an out-of-phase viscous component, which are used to obtain an in-phase plastic or elastic or storage modulus (G') and an out-of-phase viscous or loss modulus (G") respectively. These are defined as:

$$G' = \frac{\tau_0'}{\gamma_0} \tag{2.13}$$

$$G'' = \frac{\tau_0''}{\gamma_0} \tag{2.14}$$

In order to generate the mentioned and many more such linear viscoelastic polymer melt rheological properties, strain controlled oscillatory shear measurements were performed on an AR2000 rheometer from TA Instruments with 40mm diameter steel parallel plates. The linear viscoelastic regime for various PP and PP/clay nanocomposites was first determined by running a strain sweep tests at a fixed frequency. The strain beyond which the storage modulus starts changing as a function of strain is defined as the non-linear viscoelastic range and before that is the linear viscoelastic range. A strain of 1% was selected for testing as this value of strain was well within the linear viscoelastic limit for various polymeric materials used in this study. In order to generate linear viscoelastic data as a function of angular frequency, an oscillatory frequency sweep test was run with angular frequency ranging from 0.01 to 100 rad/s at 180ºC

and 1% strain. An oscillatory time sweep was also conducted at a frequency of 1 rad/s for 1 hour to observe the stability of the nanocomposite melt with respect to time. In this test, a constant value of the storage modulus over time within ± 5% was considered as a stable nanocomposite with minimal changes in the microstructure. To ensure minimal oxidative thermal degradation, a continuous purge of nitrogen was maintained during the tests.

### 2.9.2. Extensional Rheology

As opposed to shear rheology, extensional rheology is a study of material properties under shear free elongational flow. Extensional flow is of particular importance in various commercial processing, for example, fiber spinning, foaming, blow molding, thermoforming, film blowing etc, however, material properties determined from shear flow alone cannot be applied for the prediction of such processes. This makes elongational or extensional flow behavior of polymer melts a very important property that needs attention for our research. Due to the presence of shear stresses at stationary boundaries, homogeneous extensional flows are more difficult to be produced compared to simple shear flows [145]. In this work, polymer melts are subjected to uniaxial extensional flow in order to study its extensional rheological behavior.

Uniaxial extension is an axi-symmetric deformation, where a tensile stress is applied along the longest dimension and the other free surfaces of the specimen are under compression. In order to study the uniaxial flow behavior of polymer melts used in this research, TA ARES rheometer mounted with “Extensional Viscosity Fixture” (EVF) has been used. The design of the fixture is based on the original concept by Meissner [146]. This fixture consists of two cylinders, one stationary connected to the transducer to measure the force and the other rotating around the stationary one to wind up the sample (Figure 2.1). The extensional force ($F_S(t)$) measured by the

transducer and the sample area ($A_S(t)$) , both a function of time, is converted to the extensional stress ($\sigma_E(t)$) as follows:

$$\sigma_E(t) = \frac{F_s(t)}{A_s(t)} \tag{2.15}$$

This is then used to calculate the transient uniaxial viscosity ($\eta_E(t)$) at a particular strain rate as follows:

$$\eta_E(t) = \frac{\sigma_E(t)}{\frac{d}{dt}\varepsilon_H} \tag{2.16}$$

In order to measure the transient extensional viscosity of the various polymer melts used in this study, a constant Hencky stain ($\varepsilon_H$) of 3 and four different strain rates (0.1, 0.5, 1.0, 2.0 $s^{-1}$) have been used. The lowest test temperature has been maintained at 180ºC, well above the melting point of various polymer melts used in this study (165 ± 3ºC). A higher temperature of 200ºC has also been used for few tests to observe the behavior of the transient extensional viscosity at higher temperatures. Since these tests are very sensitive to the sample condition, care has been taken so that the test specimens are free of any voids or inhomogeneities. The test samples were prepared by compression molding the polymer chunks into 18 x 10 x 0.75 $mm^3$ rectangular specimens. The polymer chunks were allowed to melt in the compression molder at 200ºC and then the melt was subjected to a pressure of 1 tonnes for 5mins followed by 5 tonnes for 5 mins. The melt was then cooled to room temperature using cooling water maintaining the pressure of 5 tonnes. The samples were then carefully removed from the mold and examined for any defects (voids, cracks, grain boundaries, foreign particles and uniform shape). The state of the stretched specimen was also inspected immediately after the test, so as to observe any

sagging of the polymer melt due to gravity effect and any non-uniform stretching in order to ensure that there was uniform stretching in the central portion of the specimen during the test.

## 2.10. Polymer Foaming Procedure

Continuous extrusion foaming process was used to prepare PP nanocomposite foams. A single screw extruder was used for this purpose with a 2mm diameter die (L/D=15) and a tapered transition from the extruder barrel. The optimum temperature for extrusion of foam from each compound was selected based on the crystallization temperature of the compound. Park et al. [45, 103, 104] have reported effects of die temperature and pressure, on continuous extrusion foaming of polymers with a physical blowing agent. Naguib et al. [46] reported that both early and delayed onset of crystallization is detrimental to foam cellular structure. In their work done on extrusion foaming of branched PP using n-butane as a blowing agent, they report an optimum melt temperature that provides maximum expansion ratio in the foam samples. They observed foam collapse away from the die when the melt is at a higher temperature, due to delayed onset of crystallization causing the gas to diffuse out of the sample. On the contrary, a lower than optimum melt temperature resulted in early onset of crystallization leading to insufficient foaming. The conclusions of these studies were used to maintain the optimum temperature in the extruder for the foaming experiment. The extruder has four different temperature zones: three in the barrel and one in the die. The first three temperature zones were maintained at 180°C, 200°C and 170°C respectively for all foaming experiments done using cell span 693K as the blowing agent. The decomposition profile of the blowing agent with increase in temperature was obtained from TGA (Figure 2.2). According to the TGA result, majority of the blowing agent is decomposed by 215°C. However, in order to avoid thermal degradation of the material in use

and to take advantage of maximum volume of gas produced from the blowing agent, the second zone was maintained at 200ºC. The first temperature zone was maintained at a lower temperature compared to the second zone so as to prevent any loss of gas from the hopper due to early decomposition. The second temperature zone is the region where maximum decomposition of the blowing agent is expected. The fourth temperature (die temperature) zone was maintained at approximately 35°C above the crystallization temperature; this was found to be optimal in our foam extrusion work, as it helped to maintain a constant pressure drop of 4000psi with various polymer samples during the foaming experiments. The third temperature zone was maintained in between the second zone and the die temperature. The chemical blowing agent (CBA) was used at 3 wt% in this study. The CBA was premixed with the granulated polymer in a bag and was fed through the hopper. The extruder was operated at a constant speed of 20 rpm in this study. While flowing through the single screw extruder the CBA and the PP nanocomposite fuse to form a homogeneous melt. Near the die exit, due to steep pressure drop through the die, the gas laden polymer melt started to nucleate bubbles and the extruded polymer foam strand continued to expand until it solidified under ambient conditions. The polymer strands were collected for further foam characterization.

## 2.11. Characterization of Foam Samples

### 2.11.1. Density Measurement

Archimede's principle is used for determining the density of the foam extrudates using a Sartorius YDK 01 density measurement kit. According to Archimede's principle when a solid is immersed in a liquid, it is subjected to the force of buoyancy. The value of this force is same as

that of the weight of the liquid displaced by the volume of the liquid. This kit is equipped with a hydrostatic balance that enables the measurement of weight of the foam samples in air (W(a)) as well as in water (W(l)). For the present study, water is used to do these measurements and equation 2.17 is used to obtain the density of foam samples. A minimum of three measurements are done with different specimen for a particular foam sample in order to get an average value of density.

$$\rho = \frac{W(a).\rho(l)}{W(a) - W(l)} \qquad (2.17)$$

### 2.11.2. Scanning Electron Microscopy

Scanning electron microscope (SEM) is an electron microscope that provides topographical information of the surface by scanning it with a high energy electron beam. The beam of electrons interacts with the surface of the specimen, thereby providing with important information about its surface topography and chemical composition along with various other properties.

Scanning electron microscopy is based upon "electron in" – "electron out" process in ultra-high vacuum (UHV) environment. As the primary electron beam is scanned across the surface, electrons of a wide range of energies are emitted from the surface in the region where the beam is incident. These electrons include backscattered electrons and Auger electrons, but the vast majority of these are the secondary electrons formed in multiple inelastic scattering processes. These secondary electrons are collected by the detector, converted to a voltage and amplified. The amplified voltage is then applied to the grid of the cathode-ray tube (CRT) and modulates or changes the intensity of the spot of light on the surface. For example, if the beam is on a projection on the surface, a large number of secondary electrons will be detected, causing a

large voltage in the detector and results in a bright spot on the surface of the CRT. If the beam of electron then moves to a depression on the sample, fewer electrons will be detected, resulting in a darker spot on the surface of the CRT. The contrast in the micrograph arises from variations in the surface topography. Consequently, the secondary electron micrograph is a direct image of the real surface structure.

Since an electron beam is bombarded on the specimen, care needs to be taken to avoid any accumulation of electron on the sample, called charging of the sample, leading to hot spots in the image. For samples that are conductive this is not an issue, however for non-conductive polymer samples, the specimen need to be coated with conductive gold or osmium tetraoxide particles. SEM technique is used in this research to study the cellular structure of the foam extrudates of various PP and PP/clay nanocomposite samples using JEOL 6400 scanning electron microscope. Foamed extrudates were cryogenically fractured to maintain the structural integrity of the foam cells and the fractured surface was coated with osmium tetroxide particles. SEM micrographs were taken from these fractured surfaces at a magnification of 60X. The cell size, cell size distribution and cell density were evaluated using ImageJ software. A minimum number of five SEM images were used to get an average value these parameters. The cell density (N) was calculated using the following equation:

$$N = \left( \frac{n}{A} \right)^{3/2} \tag{2.18}$$

where n is the number of cells in the defined area A, derived from SEM micrographs.

| Name | Polymer Type | Supplier | Mol. Wt | Melt Flow Rate (g/10 min) | Maleic anhydride content (wt%) |
|---|---|---|---|---|---|
| Profax 6523 | Linear PP | Lyondell-Basell | 390,000 | 4.0 | -- |
| Profax PF 814 | Branched PP | Lyondell-Basell | -- | 3.0 | -- |
| Exxelor PO 1015 | PP-g-MA, copolymer | ExxonMobil Chemical Co. | 180,000 | 150.0 | 0.25-0.5 |
| Exxelor PO 1020 | PP-g-MA, homopolymer | ExxonMobil Chemical Co. | 80,000 | 430.0 | 0.5-1.0 |
| Bondyram 1001CN | PP-g-MA, copolymer | Polyram Ind. | -- | 100.0 | 0.75-1.0 |
| Bondyram 1001 | PP-g-MA, homopolymer | Polyram Ind. | -- | 100.0 | 0.75-1.0 |
| AC 950 | PP-g-MA, homopolymer | Honeywell Ind. | 22,000 | -- | 4.0 |
| Engage 8480 | Ethylene Octene elastomer | Dow Chemical Co. | -- | 1.0 | -- |

**Table 2.1:** Details of various polymers used in this study.

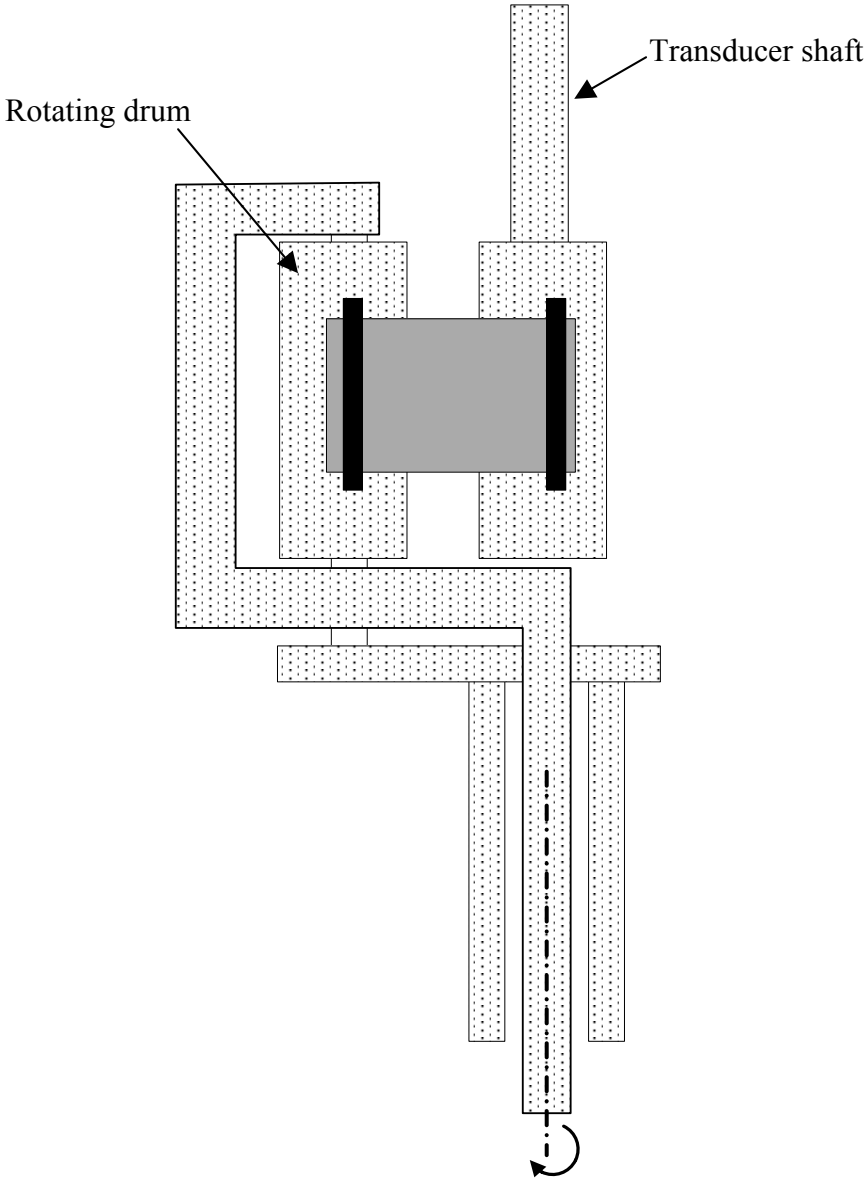


**Figure 2.1:** A schematic of Extensional Viscosity Fixture (EVF) used for the measurement of uniaxial elongational viscosity of polymer melts.

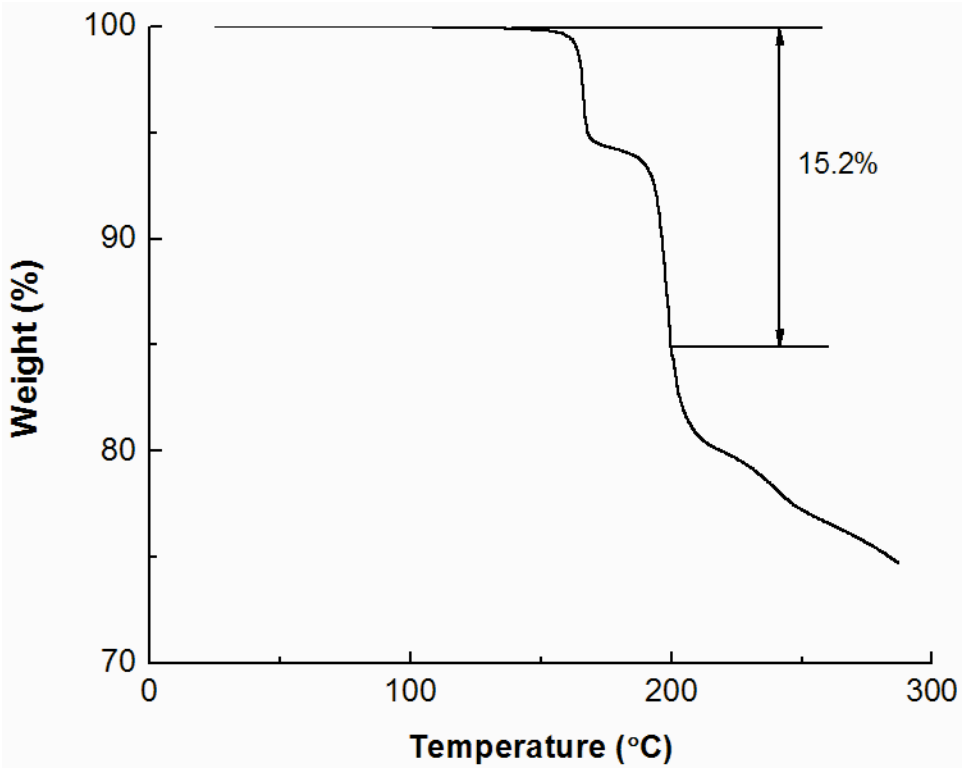


**Figure 2.2:** Thermal decomposition profile of Cell span–693k, as obtained from thermo-gravimetric analysis. At 200°C, 15.2 wt% of the chemical blowing agent is decomposed to produce gas (primarily nitrogen) for foaming various polymers used in this study.

# 3. EXTRUSION OF LINEAR POLYPROPYLENE/CLAY NANOCOMPOSITE FOAMS

## 3.1. Introduction

A variety of thermoplastic polymer foams have been produced with polystyrene [27, 95] poly (lactic acid) [51], poly (ethylene terephthalate) [50] and polycarbonate [36]. Amongst the various foamed polymers, polyurethane and polystyrene continues to dominate the foam market today. Polypropylene foams are expected to replace polystyrene and polyurethane foams in various applications, because polypropylene can be used at higher service temperatures, and has greater stiffness, excellent chemical, abrasion and impact resistance and low material cost along with total recyclability. However, continuous foaming of linear PP has been largely restricted by its rheological properties [47, 58, 108] and the semi-crystalline nature of the polymer [60, 61]. Linear PP does not show strain hardening under extensional flow, a necessary property for producing good foam particularly in crystallizing polymers [58, 100]. Polymers without strain hardening property develop thinner cell walls during bubble expansion in the foaming process, which results in coalescence of bubbles and even open-cell foams [47, 105, 106]. The semi-crystalline nature of the polymer also makes the foaming process more complicated because of simultaneous nucleation and growth of gas bubbles and crystals. Reignier et al. [61] have demonstrated with batch foaming of poly–(ε-caprolactone) that crystallization affects both bubble nucleation and growth.

Blends of linear PP and branched PP foam better than the linear resin [48, 58, 59], leading to smaller cell sizes and higher cell densities than with the linear resin. This is because an increase in the extensional viscosity of the blends during the expansion process provides stability to the cell walls [116, 118-120]. These blends typically have 20 wt% of the branched polymer

and add to the cost significantly. Partial crosslinking also increases the tensile melt strength of PP [44, 111, 112] and results in better foam; however, the crosslinking process leads to loss in recyclability, chain scission and oxidative degradation of the PP, which affects its physical properties [113-115]. This section of the research describes an alternative and novel method of introducing strain hardening property in linear PP melts that has the potential for lower cost and easier recyclability. This method incorporates small amounts of organoclay with an appropriate maleated PP as compatibilizer.

The use of nanoclay in foaming polymers to obtain closed cell foams with narrower cell size distributions and high cell densities was demonstrated for the amorphous polystyrene by Lee et al. [9, 95]. They reported over 50% reduction in average cell size and around six to ten fold increase in cell densities of the polystyrene nanocomposite foam by the addition of 5wt% organically modified nanoclay. This is attributed to the much higher surface area made available for nucleation of bubbles by well dispersed nanolayers [9, 42, 147]. The enhanced nucleation efficiency has also been reported for foaming of various other polymer nanocomposites [95, 147-150].

Other workers [41, 42, 49, 121] have tried this approach with the semi-crystalline polypropylene with limited improvement in foam quality produced in continuous extrusion or injection molding process. For example, Carreau et al. [42] reported foaming studies of both linear and branched polypropylene nanocomposites containing 2 wt% of nanoclay in an injection foaming process, using 1wt% of a chemical blowing agent (azodicarbonamide). They observed a 25% drop in average cell size, due to the addition of clay in linear PP. An even smaller reduction in cell size (12.5%) was observed for branched PP foam samples due to the addition of clay. Gendron et al. [121] have reported extrusion foaming of nanocomposites based on linear PP and

branched PP having 2 wt% nanoclay, with direct carbon dioxide injection as the blowing agent. They observed large coalesced zones in linear PP foam samples when foamed with lower concentrations of $CO_2$. Addition of 2wt% of nanoclay to the linear PP matrix slightly improved the cellular structure of the foam samples, however, when foamed with higher concentrations of $CO_2$, the PP-clay nanocomposite again led to formation of large coalesced regions. With the addition of nanoclay to the branched PP matrix, they obtained foams with cell sizes in the range of 600–1000 μm. However, when they added 0.5wt% of talc serving as nucleating agent, they obtained foams with cell sizes in the range of 250 – 600 μm. However, no further reduction in cell size was observed when both talc and nanoclay was added to the branched PP matrix. With their research they showed that the efficiency of nanoclay serving as nucleating agent is greatly dependent on the level of nanoclay dispersion obtained in PP nanocomposites and that its nucleating ability is inferior to talc. Carreau et al. [42] and Gendron et al. [121] also reported uniaxial extensional flow behavior of linear PP/clay nanocomposite melt and observed no improvement in melt strain hardening upon addition of nanoclay to linear PP. There is clearly a need for preparing and foaming polypropylene clay nanocomposites that display significant strain hardening in extensional flow.

The use of nanoclay to introduce strain hardening in maleated polypropylene melts alone was demonstrated first by Okamoto et al. [100] and this was shown with a high molecular weight polypropylene. Pathak and Jayaraman [132] have found that selection of a high molecular weight maleated polypropylene and the composition of the nanocomposite were critical to obtain significant strain hardening in uniaxial extensional flow of the nanocomposite melt.

The objective of the present research is to investigate differences in foam quality produced from two sets of polypropylene clay nanocomposites, all prepared with good

dispersion of clay – one set that does not display melt strain hardening and another that has much improved strain hardening behavior under uniaxial extensional flow. These nanocomposites were prepared by using different ratios of compatibilizer to clay and two different grades of the compatibilizer. The foams were produced in a single screw extruder with the same proportion of a chemical blowing agent in all cases. It is worth noting here that the literature on foaming polymer nanocomposites has been focused largely on physical blowing. The results showed that besides providing a greater concentration of nucleating sites for foaming the polymer matrix, addition of nanoclay with appropriate compatibilizer has the potential for producing melt strain hardening and altering the crystallization kinetics favorably in extrusion of closed cell polypropylene foams. In order to compare the foaming results of linear PP/clay nanocomposite foams with a blend of linear and branched PP in the same process, a blend of linear and branched PP was prepared and foamed using the same process. Since the final objective of this research is to foam TPOs for automotive application, this technology was extended to foam TPOs.

## 3.2. Materials and Experimental Procedures

Linear polypropylene (Profax 6523) was used in this part of the research along with two grades of polypropylene-grafted-maleic anhydride (PP-g-MA): Exxelor PO-1015, labeled as PP-g-MA1 is a random copolymer of propylene and ethylene, and AC-950, labeled as PP-g-MA2 is a homopolymer. A tree type branched polypropylene, PF 814, was used at 20 wt% to prepare an 80:20 blend of linear and branched PP so as to compare the foaming results with linear PP/clay nanocomposite system. The nanoclay used in this study was organically modified montmorillonite clay, I.44P. The chemical blowing agent used in this study was Cell-span 693K.

In order to prepare a TPO material, Engage 8480 was used as the elastomer. The details of all materials are provided in section 2.1.

Five different PP-clay nanocomposites were compounded for this study. A TPO blend and TPO nanocomposite, derived from a strain hardening PP/clay nanocomposite, was also prepared for foaming studies. The details of the composition are tabulated in Table 3.1. A 47g Banbury batch mixer at 180°C and at a rotation speed of 150 rpm for 10 minutes was used for the preparation of all the nanocomposites. However, to prepare a blend of pure polymers the same mixer was used at 200ºC and at a rotation speed of 30 rpm for 10 minutes. This was done because at higher rotation speed the entanglements formed amongst the branches of the branched PP are lost [116], affecting the strain hardening behavior of the polymer melt (Figure 3.1). The compounded materials were then foamed in a single screw extruder using 3 wt% of the chemical blowing agent. XRD, DSC, extensional rheology was used for detailed characterization of the polymer materials, and SEM and its image analysis along with density measurements was used to characterization the foam samples. The details of all the preparation and characterization procedures are provided in Chapter 2.

## 3.3. Results and Discussion

### 3.3.1. Morphology of Nanocomposites

X-ray diffraction (XRD) patterns obtained for all the PP nanocomposites along with the nanoclay (I.44P) in the range of $2\theta = 1–10^{o}$ are presented in Figure 3.2. Lack of distinct features in the XRD curve implies the existence of random-well dispersed clay platelets, however, presence of distinct peaks indicates presence of ordered clay stacks and the corresponding $2\theta$

value can be used in equation 2.4 to calculate the spacing of the stacked platelets. The mean interlayer spacing of the (001) plane (d-spacing) for the nanoclay used in this study was found to be 2.54nm ($2\theta = 3.48^{o}$). The d-spacing of the (001) plane was found to be higher in all the PP nanocomposites here, confirming intercalation by polymer. A comparison between PPNC-N1 and PPNC-N2 indicates a larger d-spacing of 3.53 nm in PPNC-N2, than in PPNC-N1 (2.85nm). The higher maleic anhydride content in PP-g-MA2 (2.6 wt% bound maleic anhydride) compared to PP-g-MA1 (0.5 wt% bound MA) allows greater hydrophilic interaction between the polar montmorillonite surface and the maleic anhydride groups of the polymer chains and results in greater intercalation of the polymer chains within the clay galleries. A comparison between PPNC-N1 and PPNC-S1 nanocomposites, which have similar clay loadings and different proportions of the same compatibilizer (PP-g-MA1) shows an increase in d-spacing with an increase in the proportion of compatibilizer, thus indicating that similar extents of nanolayer intercalation can be achieved by increasing the weight fraction of the lower maleic anhydride content compatibilizer. Further increases in the proportion of this compatibilizer provided very little change in the extent of intercalation as seen by comparing PPNC-S1, PPNC-S2 and PPNC-S6.

### 3.3.2. Uniaxial Extensional Rheology

Although gas expansion within foaming polymers creates biaxial extensional flow in the melt, uniaxial extensional flow measurements are relevant because measurements of biaxial extensional viscosity in lubricated squeezing tests display trends that are similar to trends in measurements of uniaxial extensional viscosity – cf. Munstedt et al. [48, 109]. In particular, they conclude that if strain hardening is observed in uniaxial extensional flow, it will be observed in

biaxial extensional flow as well. This is useful because more reliable equipment and procedures are available for measurement of uniaxial extensional viscosity of melts than for the measurement of biaxial extensional viscosity of polymer melts.

The melt extensional viscosity transients for the linear PP and its nanocomposites at 180 °C and several strain rates are presented in Figure 3.3 and 3.4. For all specimens, as expected, the transient extensional viscosity curves measured at different strain rates superimpose at low strains to give the linear viscoelastic limit. Strain hardening of the melt is defined as an upward deviation of the extensional viscosity from this linear viscoelastic envelope usually at strains greater than one.

For a quantitative estimation of strain hardening effect in the nanocomposites, the strain hardening parameter ($\chi$) is defined as follows:

$$\chi = \frac{\eta_E^+(t,\ \dot{\varepsilon})}{\eta_{E0}^+(t)} \qquad (3.1)$$

where, $\eta_E^+(t)$ is the transient extensional viscosity as a function of time and strain rate and $\eta_{E0}^+(t)$ is the transient extensional viscosity in the linear viscoelastic regime. The linear viscoelastic $\eta_{E0}^+(t)$ may be determined in one of two ways: (a) as 3 times the transient shear viscosity growth curve at very low strain rates or (b) by extrapolating the superimposed portion of the curves for different strain rates. The two methods give the same result for homogeneous melts but may give different results for filled polymer systems and polymer clay nanocomposites in particular because of differences in orientation of anisotropic filler particles in elongational and shear flows [128, 131, 151]; hence method (b) was used for this paper.

The transient extensional viscosity data for the linear PP melt did not show strain hardening. The extensional viscosity data for molten PP-g-MA compatibilizer did not show any strain hardening either. Amongst the PP nanocomposite melts, PPNC-N1 and PPNC-N2 showed no strain hardening behavior. However, the transient extensional viscosity curves for PPNC-S1, PPNC-S2 and PPNC-S6 show significant strain hardening of the polymer melt at all strain rates tested. The strain hardening parameter, estimated at a Hencky strain of 2.25, is plotted against strain rate for three strain hardening melts in Figure 3.5; these curves shows that strain hardening in PPNC-S1, PPNC-S2 and PPNC-S6 melts decreased with increasing strain rate similar to the trend shown by blends of linear PP with up to 20 wt% of branched PP [116] as well as blends of linear PP with small amounts of crosslinked polymer [152, 153]. The melts of PPNC-S1, PPNC-S2 and PPNC-S6 displayed similar strain hardening behavior indicating that 3 wt% of organoclay and a 4:1 weight ratio of PP-g-MA to clay were adequate for producing this effect in linear polypropylene/organoclay nanocomposites. The latter amounted to 0.20 g-mol bound maleic anhydride on the compatibilizer chains per kg organoclay as presented in Table 3.1 which represents one requirement for forming sufficient physical junctions (presumably by hydrogen bonding) between the hydroxyl groups at the organoclay edges and the compatibilizer chains which may also form bridges between clay particles.

The other requirement arises from the density of trapped entanglements along the bridging compatibilizer chains. This may be seen from the fact that when the lower molecular weight compatibilizer was used with more bound maleic anhydride amounting to 0.80 g-mol per kg organoclay, the resulting nanocomposite melt did not display strain hardening. Hence, strain hardening in the nanocomposite melts is analogous to that reported for blends containing small amounts of crosslinked polymer. Just as blends of linear polypropylene with small amounts of

chemically crosslinked polymers contain trapped entanglements on chain segments between crosslinks or junctions which respond to stretching differently from entanglements and chain segments in the bulk [152], interactions between the surface or edge of the nanolayer and the maleated polymer can form a network of physical junctions or anchor points between which bridging compatibilizer chains trap entanglements to produce a similar effect. Thus, in addition to good dispersion and sufficient interaction between the compatibilizer and the clay surface or edge, the molecular weight of the compatibilizer should be high enough so as to form a sufficient number of trapped entanglements along the compatibilizer chain between clay surfaces or edges.

The melt extensional viscosity transients for blend of linear (80 wt%) and branched PP (20 wt%) at 180 °C is presented in Figure 3.1. The blend prepared at 30 rpm at 200ºC is used for the foaming experiments in this study. As expected, the blend show significant deviation from the linear viscoelastic regime at higher Hencky strain for all strain rates tested, indicating significant strain hardening of the polymer melt. This blend was used for foaming along with other linear PP/clay nanocomposites and a comparison of foam qualities was made later in this study.

The uniaxial extensional viscosity behavior of TPO and TPONC melt at 180ºC is presented in Figure 3.6. The TPO resulting from a blend of linear PP (70 wt%) and an elastomer (30 wt%), shows absence of strain hardening behavior at all strain rates. However, the TPONC resulting from the blend of PPNC-S2 (70 wt%) and the same elastomer (30 wt%), shows significant improvement in the strain hardening behavior at all strain rates. This clearly demonstrates that if the bulk linear PP component is a strain hardening one then the resulting TPO nanocomposite would also show strain hardening behavior under uniaxial extensional flow.

Hence, if PPNC-S2 results in a good quality closed cell foam then TPONC should also lead to similar foam properties.

### 3.3.3. Crystallization Behavior

Nonisothermal crystallization exotherms obtained from cooling ramps in DSC tests are presented for all PP nanocomposites in Figure 3.7 and 3.8. The cooling rate for all the DSC tests was 5°C /min. The fractional crystallinity ($X_C$) and the average rate of crystallization (k) in each sample were obtained by using equation 2.5 and 2.6 respectively. These results are tabulated in Table 3.2.

It is clear from Table 3.2 that both compatibilizers crystallize more slowly than the linear PP [42]. PP-g-MA1 being a random copolymer displayed a lower rate of crystallization from the melt than PP-g-MA2 which is a homopolymer. Amongst the four nanocomposites, studied in this work, PPNC-N2 has the highest rate of crystallization. The average rates of crystallization for PPNC-N1, PPNC-S1, PPNC-S2 and PPNC-S6 (each containing PP-g-MA1) are all about half of the rate for PPNC-N2 (which contains PP-g-MA2). This may be traced to the fact that PP-g-MA1 crystallized at about half the rate of PP-g-MA2.

The nonisothermal crystallization exotherms for the blend of linear and branched PP is presented in Figure 3.8. The fractional crystallinity and average rate of crystallization for L80B20 is presented in Table 3.2. The average rate of crystallization for L80B20 is similar to the PP/clay nanocomposites prepared using PP-g-MA2. This is probably because there is nothing that would either interfere or slow down the folding of the polymer chains during crystallization, thereby resulting into a blend that shows higher rate of crystallization.

### 3.3.4. Extruded Foam Structure

It is evident from the preceding sections that addition of nanoclay and a suitable compatibilizer to linear polypropylene has the potential to produce three different effects: (a) greater surface area for nucleation of voids, (b) changes in crystallization rate of the polypropylene and (c) strain hardening in the melt state. PPNCs resulting in first two effects are commonly observed due to the addition of nanoclays and PP-g-MA respectively, however a combination of nanoclay and compatibilizer resulting in strain hardening behavior in linear PP nanocomposites has not been reported previously. The five different polypropylene nanocomposites of this work exhibit combinations of these effects to different extents as shown in Table 3.3. Extruded foam samples were inspected visually to determine whether they were open cell or closed cell foams. The foamed linear PP without any nanoclay particles turned out to be open cell foam. Some open cell structure was seen in PPNC-N2 foam as well. The rest of the nanocomposite foams were all closed cell foams. The scanning electron micrographs for all the extruded foam samples are presented in Figures 3.9 – 3.17. The scanning electron micrograph of linear PP foam sample, (Figure 3.9), shows evidence of severe cell coalescence and large scale inhomogeneity, with regions of very low cell density. The micrograph of PPNC-N2 foam presented in Figure 3.10 shows some improvement in quality with homogeneous cellular structure; however the cells are still larger in size and the cell size distribution shows that most of the cells are greater than 200 μm. The homogeneous nature of the cellular structure may be attributed to the increased surface area for heterogeneous nucleation in PPNC-N2 over the neat linear PP, but the absence of any strain hardening characteristics led to cell coalescence leading to large size cells in the foam. The cell size distributions obtained from image analysis of the micrographs are plotted for the various extruded foams in Figures 3.18 – 3.24. The bulk

densities, average cell sizes and cell number densities of the extruded polypropylene nanocomposite foam samples are listed in Table 3.4. The bulk density of all the foam samples are about 0.3g/cc indicating similar level of expansion was achieved during the foaming process irrespective of the nature of the polymer melt. Thus any difference in cell size and cell size distribution of the foam samples is not due to different levels of expansion achieved during foaming but due to the additional surface area, slower rate of crystallization and, most important, the strain hardening behavior of the polymer melt. Recall that neither PPNC-N1 nor PPNC-N2 showed extensional melt strain hardening and both have the same level of nanoclay, but PPNC-N1 crystallizes slower than PPNC-N2. Hence a comparison between PPNC-N1 foam and PPNC-N2 foam would establish the effect of slower crystallization on foam characteristics. It is evident from the SEM micrograph of PPNC-N1 foam in Figure 3.11 that it has better cellular structure compared to PPNC-N2 foam. The cell density for PPNC-N1 foam is six fold greater than that of PPNC-N2 foam and the average cell size in PPNC-N1 foam is significantly lower as well. A slower rate of crystallization of the polymer matrix in PPNC-N1 allows a greater rate of bubble nucleation in the melt and also allows more uniform expansion of the bubbles. This is also evident from the cell size distributions of the two nanocomposite foams presented in Figures 3.18 and 3.19. The cell size distribution of PPNC-N2 foam has 30% of cells greater than 200μm in size with a small fraction of smaller cells whereas the cell size distribution for PPNC-N1 is more uniform, indicating that greater surface for nucleation and slower rate of crystallization of the polymer melt can definitely help in producing better foams. Even though the cellular structure of PPNC-N1 is better than PPNC-N2 foam due to slower crystallization kinetics, the final foam property of PPNC-N1 foam is not acceptable with a lot of larger size cells and a broad cell size distribution.

Next, the effect of strain hardening in melt extensional flow may be seen by comparing the cell size distribution of the foam produced with PPNC-S1 against that of the foam produced with PPNC-N1. It is clear from Table 3.4 that PPNC-S1 resulted in foam with smaller average cell size (86.5μm) and higher cell density ($1.3x10^6$cells/$cm^3$). The cell size distribution presented in Figure 3.20 for PPNC-S1 also shows that the cells are mostly present in a narrow cell size range of 40-100μm as opposed to the broad distribution in case of PPNC-N1. Since the clay loading in PPNC-S1, the average rate of crystallization, amount of blowing agent used and the pressure drop during foaming is very similar to that in PPNC-N1, the improvement in foam quality with PPNC-S1 is solely due to the strain hardening of the polymer melt under uniaxial extensional flow. The enhanced strain hardening behavior of the PPNC-S1 melt stabilizes the cell walls and limits coalescence. The absence of strain hardening in PPNC-N1 resulted in cell coalescence and led to larger cells.

Finally, the cell structures of foams produced with the three strain hardening nanocomposites PPNC-S1, PPNC-S2 and PPNC-S6 may be compared. The three nanocomposites differ only in clay and compatibilizer loading, however maintaining the strain hardening property. All the three PPNCs show significant strain hardening behavior under uniaxial melt extensional flow and have similar crystallization rates. From the SEM micrographs in Figures 3.12 – 3.14 and the results in Table 3.4, it is evident that the three extruded foams have comparable average cell sizes and average cell densities. The cell size distributions for PPNC-S1, PPNC-S2 and PPNC-S6 nanocomposite foams (Figures 3.20 – 3.22) are also comparable. This indicates that high quality foams can be produced with only 3 wt% of nanoclay and using compatibilizer to clay ratio of 4, if the polymer nanocomposite melt has appropriate rheological and thermal characteristics.

Further, foaming studies were done on a blend of linear and branched PP (L80B20) to compare its results with those of linear PP/clay nanocomposites, in the same system. The scanning electron micrograph of L80B20 extruded foam samples is presented in Figure 3.15 and its cell size distribution is presented in Figure 3.21. The average cell size and cell size density is also presented in Table 3.4. A comparison between PPNC-S6 and L80B20 foam samples clearly shows that PPNC-S6 resulted in superior quality foams with smaller average cell size and higher cell density. This is probably because of absence of any nanoparticles for heterogeneous nucleation, despite the fact that the blend shows significant strain hardening characteristics. As already established in our research along with other studies, presence of nanoparticles, serving as additional nucleating sites for the cells, can significantly improve the foam characteristics. Further, the faster rate of crystallization could also be a reason for poor foam characteristics of the L80B20 foam. Hence, judicious selection of compatibilizer along with nanoclays can result in an affordable approach for the production of superior quality linear PP foams compared to that produced from blend of linear and branched PP.

Since the final objective of this research is to produce good quality TPO foams, foaming studies were carried out on TPONC along with a control TPO. The SEM images of the two foams are presented in Figures 3.16 and 3.17. From the micrographs it is clear that a strain hardening PP component of the TPO can significantly improve the foam characteristics of the TPO. Hence, the presence of strain hardening PP component and an elastomer can produce good quality TPO foam that has necessary physical and mechanical properties to replace PU foams from automotive applications.

Results presented in this section on foams extruded from polypropylene-clay nanocomposites with a chemical blowing agent, show progressive improvement in the quality of

foam samples as one or more of the following features were present in the nanocomposites: high surface area, slower crystallization and melt strain hardening in extensional flow. The maleated polypropylene having low levels of maleic anhydride content and high molecular weight along with slow crystallization kinetics led to the nanocomposites displaying slower crystallization kinetics and strain hardening in melt extensional flow that are critical factors in foaming linear semicrystalline polymers. This knowledge was further implemented to produce TPOs, showing strain hardening behavior that further results in good quality closed cell foams. These results demonstrate the effect of compatibilizer type on the thermal and rheological properties of the polypropylene – clay nanocomposites. Further increases in melt strain hardening can be achieved by silane treatment of the nanoclays used for making polypropylene nanocomposites, leading to further improvement in the quality of extruded foams. This work is presented in the subsequent chapters.

## 3.4. Conclusion

When several polypropylene clay nanocomposites all with good dispersion of the dialkyl amine treated organoclay were foamed by extrusion with a chemical blowing agent, systematic variations in foam quality were obtained based on differences among them in melt strain hardening and in crystallization behavior. Even among nanocomposites without any melt strain hardening, decreasing the rate of crystallization led to closed cell foams with smaller cell size and higher cell density. Among nanocomposites where significant strain hardening was observed in extensional flow along with the slower rates of crystallization, the extruded polypropylene nanocomposite foams displayed the smallest cell sizes and the greatest cell density by reducing cell coalescence. These enhancements may be attributed to attachment of high molecular weight

PP-g-MA chains to the surfaces of nanolayers due to hydrogen bonding, providing greater constraints on chain stretch relaxation and also slowing down the crystallization.

| Specimen | PP 6523 (wt%) | PP-g-MA (wt%) | | Nanoclay (wt%) | g-mol bound MA / kg organoclay | PF 814 (wt%) | Engage 8480 (wt%) |
|---|---|---|---|---|---|---|---|
| | | PP-g-MA1 | PP-g-MA2 | | | | |
| PPNC-N1 | 68.0 | 24 | -- | 8.0 | 0.80 | -- | -- |
| PPNC-N2 | 68.0 | -- | 24 | 8.0 | 0.15 | -- | -- |
| PPNC-S1 | 40.0 | 52.8 | -- | 7.2 | 0.37 | -- | -- |
| PPNC-S2 | 76.0 | 21.0 | -- | 3.0 | 0.36 | -- | -- |
| PPNC-S6 | 85.0 | 12.0 | -- | 3.0 | 0.2 | -- | -- |
| L80B20 | 80.0 | -- | -- | -- | -- | 20.0 | -- |
| TPO | 70.0 | -- | -- | -- | -- | -- | 30.0 |
| TPONC | 53.2 | 14.7 | -- | 2.1 | 0.36 | -- | 30.0 |

**Table 3.1:** Composition of various nanocomposites and polymer blends used in this study.

| Specimen | Fractional crystallinity | Time span $t_c$ (min) | Average rate of crystallization ($min^{-1}$) |
|---|---|---|---|
| PP | 0.44 | 2.9 | 0.15 |
| PP-g-MA1 | 0.34 | 3.9 | 0.09 |
| PPNC-N1 | 0.35 | 5.0 | 0.07 |
| PPNC-S1 | 0.36 | 5.1 | 0.07 |
| PPNC-S2 | 0.38 | 5.0 | 0.07 |
| PPNC-S8 | 0.39 | 5.1 | 0.08 |
| PP-g-MA2 | 0.36 | 2.7 | 0.13 |
| PPNC-N2 | 0.44 | 3.4 | 0.13 |
| L80B20 | 0.42 | 3.9 | 0.11 |

**Table 3.2:** Crystallization parameters of various nanocomposites and polymer blends estimated from non-isothermal crystallization study in a DSC.

| Polymer | Surface area | Average rate of crystallization | Melt strain hardening |
|---|---|---|---|
| PPNC-N2 | B A S E C A S E | | |
| PPNC-N1 | = | _ | = (None) |
| PPNC-S1 | = | _ | + |
| PPNC-S2 | _ | _ | + |
| PPNC-S6 | _ | _ | + |
| L80B20 | x | = | + |

(-): lower than base case, (+): higher than base case, (=): same as base case, (x): absent

**Table 3.3:** Comparison of various PP nanocomposites and polymer blends.

| Polymer | Density ($g/cm^3$) | Average Cell Size ($\mu m$) | Average Cell Density ($no./cm^3$) |
|---|---|---|---|
| Linear PP | 0.4 | -- | -- |
| PPNC-N2 | 0.4 | 170.9 | $0.1 \times 10^6$ |
| PPNC-N1 | 0.37 | 132.7 | $0.6 \times 10^6$ |
| PPNC-S1 | 0.3 | 86.5 | $1.3 \times 10^6$ |
| PPNC-S2 | 0.3 | 87.0 | $1.2 \times 10^6$ |
| PPNC-S6 | 0.3 | 87.9 | $1.2 \times 10^6$ |
| L80B20 | 0.35 | 112.1 | $0.8 \times 10^6$ |
| TPO | 0.43 | -- | -- |
| TPONC | 0.4 | 83.1 | $1.0 \times 10^6$ |

**Table 3.4:** Characteristics of various foam extrudates of polymer blends and polymer nanocomposites foamed in a single screw extruder using 3 wt% of azodicarbonamide.

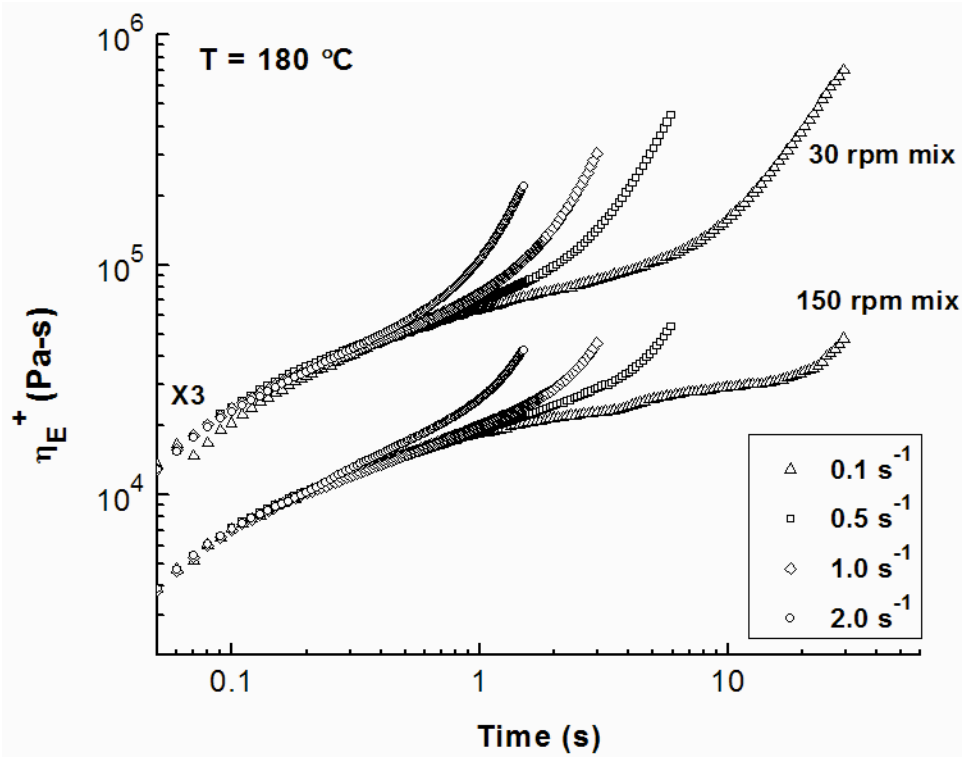


**Figure 3.1:** Melt extensional viscosity of polymer blend of linear and branched PP mixed at two different mixing conditions. The blend prepared at low mixing rpm show greater strain hardening behavior.

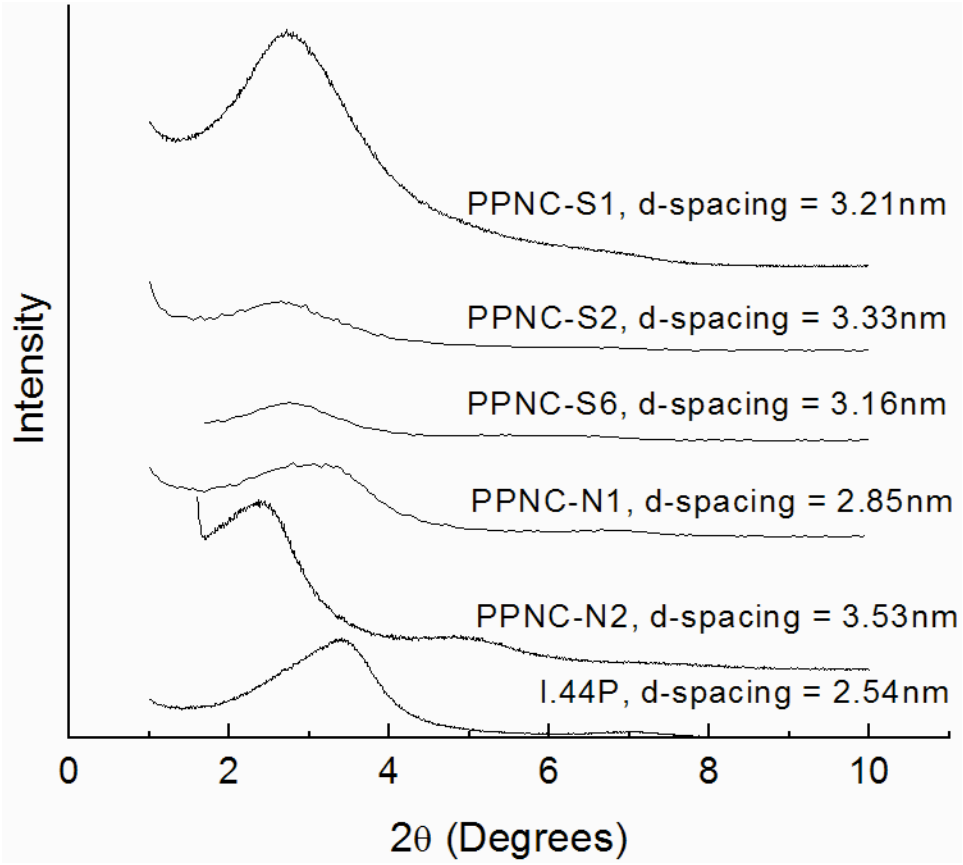


**Figure 3.2:** X-ray diffraction patterns of various linear polypropylene–clay nanocomposites along the X-ray diffraction pattern of the nanoclay.

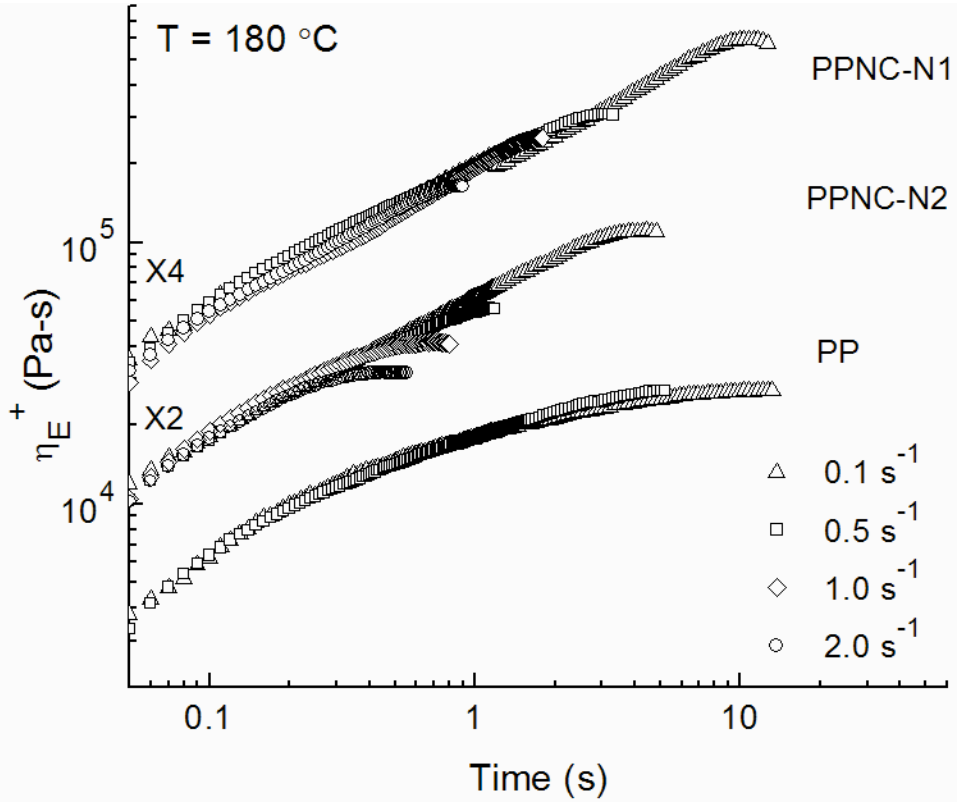


**Figure 3.3:** Melt extensional viscosity of PP, PPNC-N1 and PPNC-N2 under uniaxial extensional flow. None of the polymer melt show strain hardening behavior under uniaxial extensional flow.

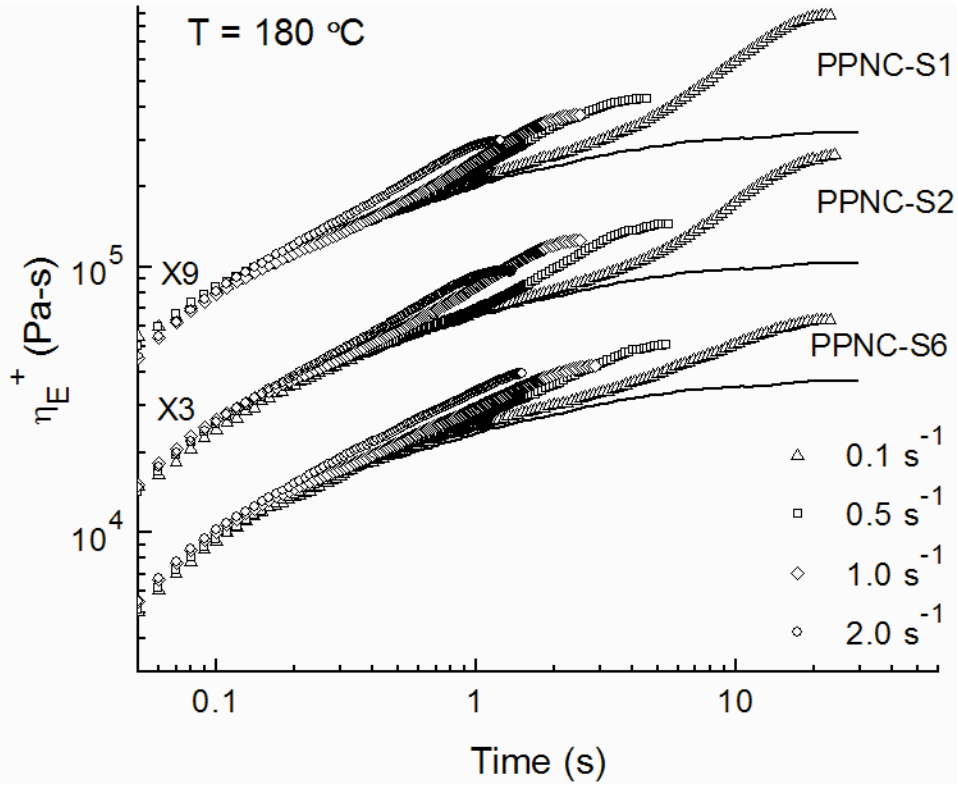


**Figure 3.4:** Melt extensional viscosity of PPNC-S1, PPNC-S2 and PPNC-S6 nanocomposites under uniaxial extensional flow. All polymer melts shows significant strain hardening phenomena under uniaxial extensional flow.

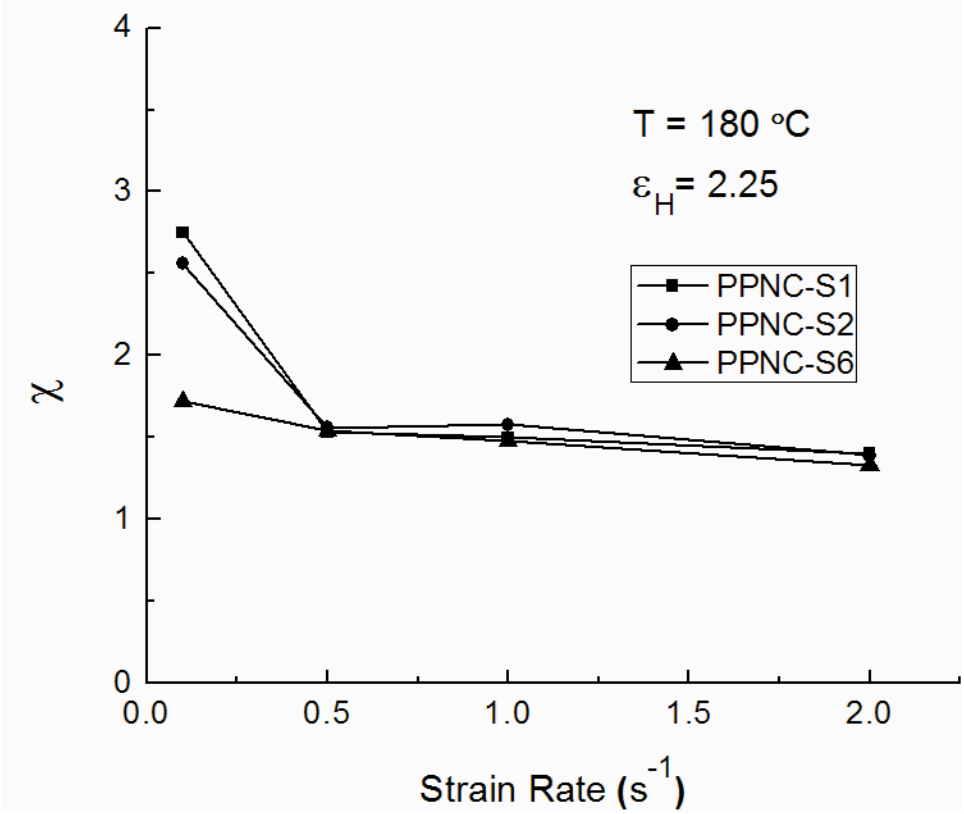


**Figure 3.5:** Strain hardening parameter of PPNC-S1, PPNC-S2 and PPNC-S6 nanocomposites.

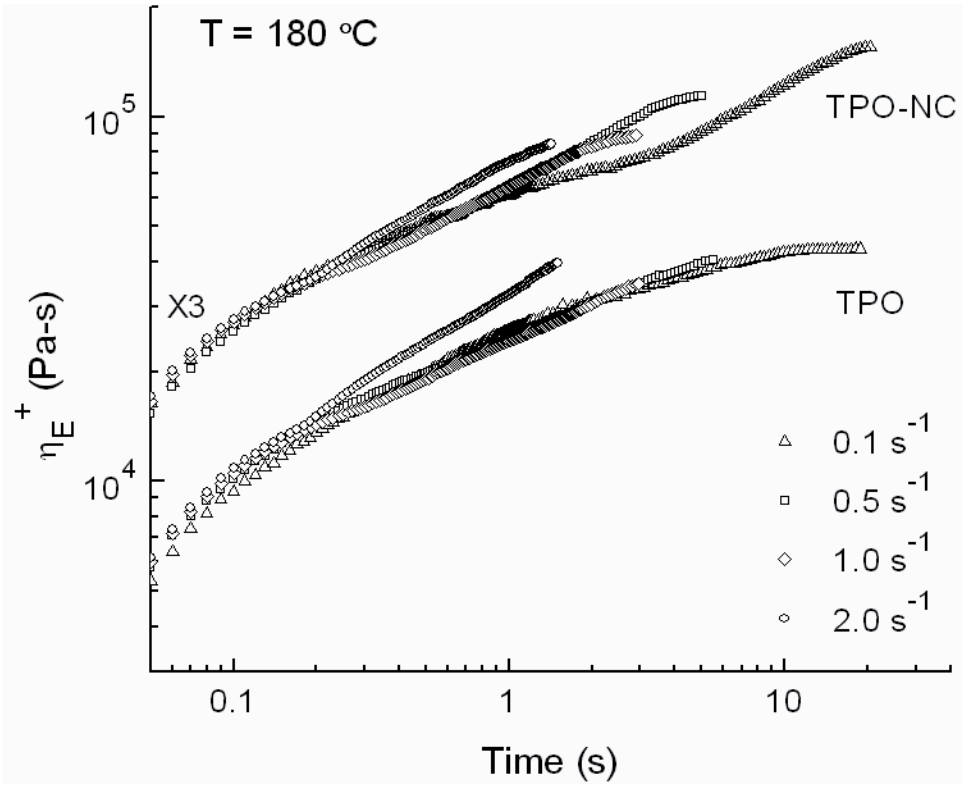


**Figure 3.6:** Melt extensional viscosity of TPO and TPONC under uniaxial extensional flow.

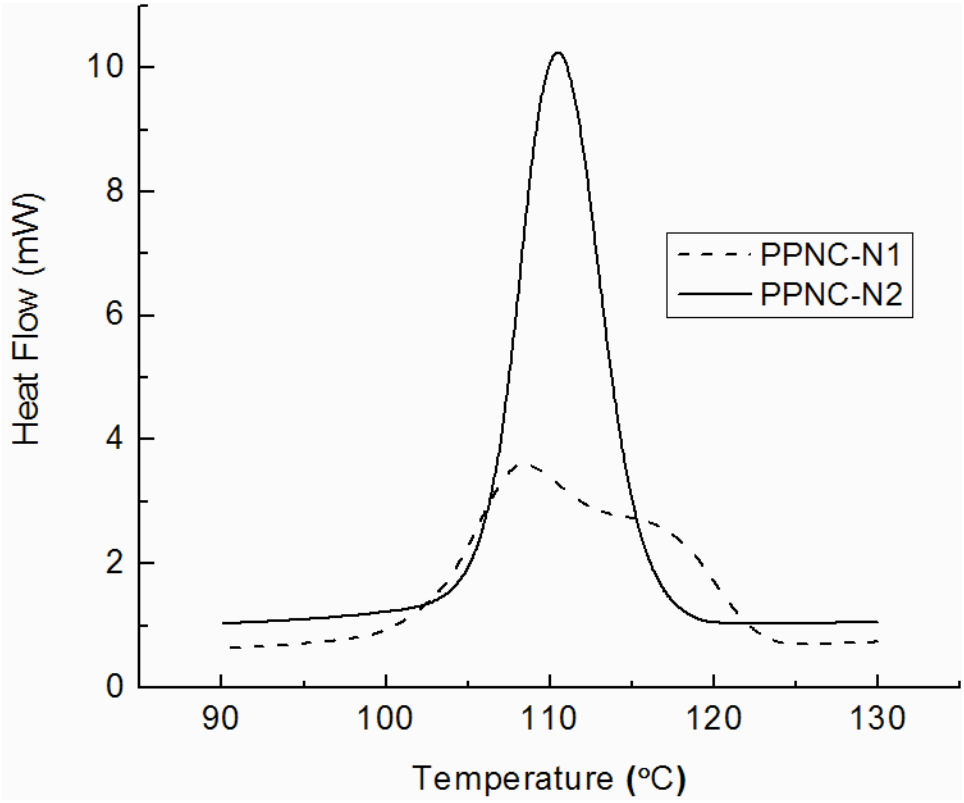


**Figure 3.7:** Non-isothermal crystallization of PPNC-N1 and PPNC-N2 nanocomposites having same wt% of different PP-g-MA and same organoclay.

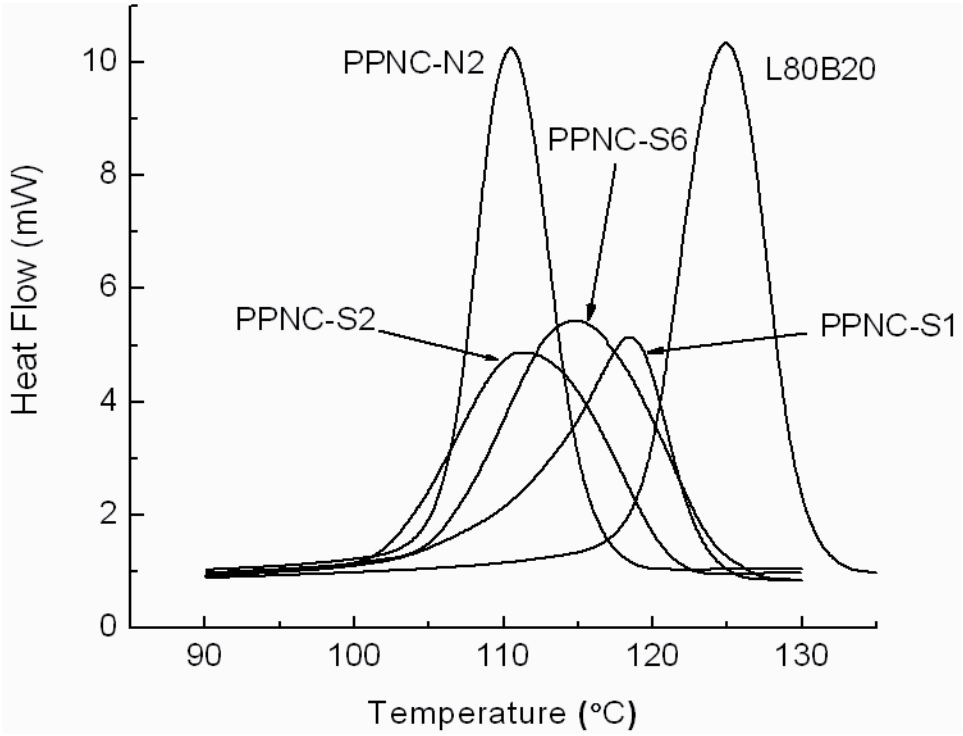


**Figure 3.8:** Non-isothermal crystallization of PPNC-S1, PPNC-S2, PPNC-S6, PPNC-N2 nanocomposites and L80B20 polymer blend.

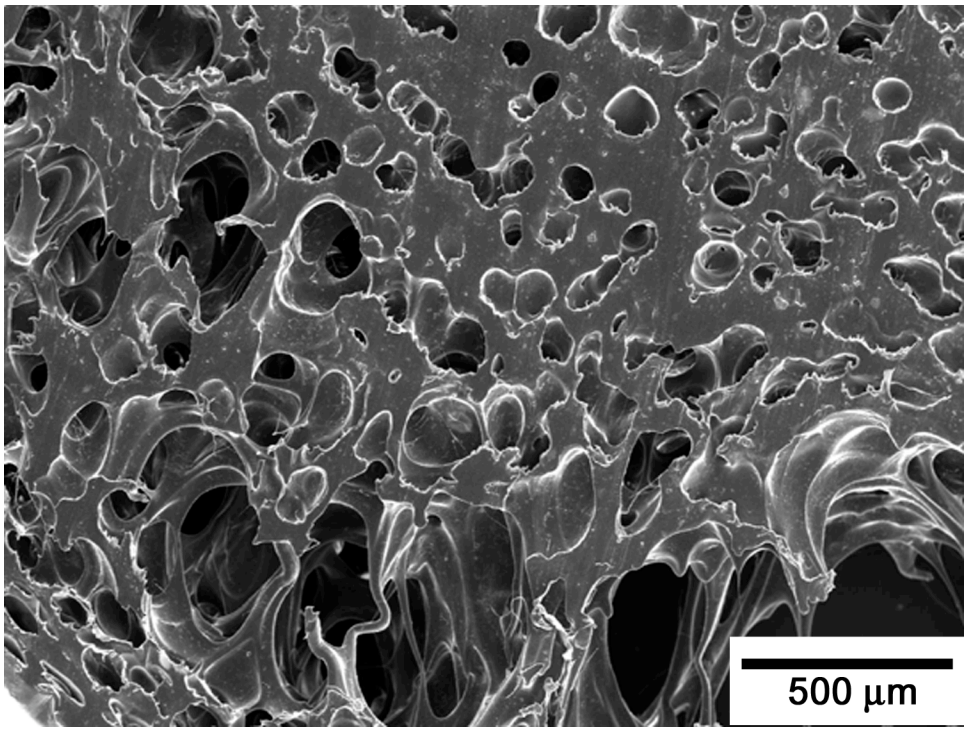


**Figure 3.9:** Scanning electron micrograph of linear polypropylene foam extrudate.

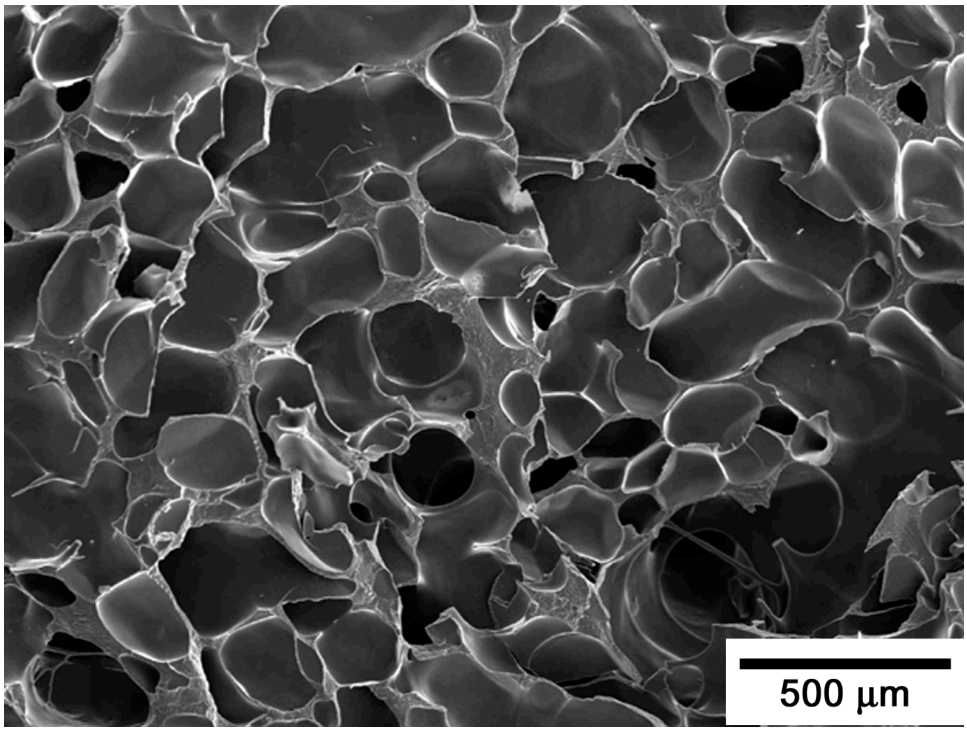


**Figure 3.10:** Scanning electron micrograph of PPNC-N2 foam extrudate.

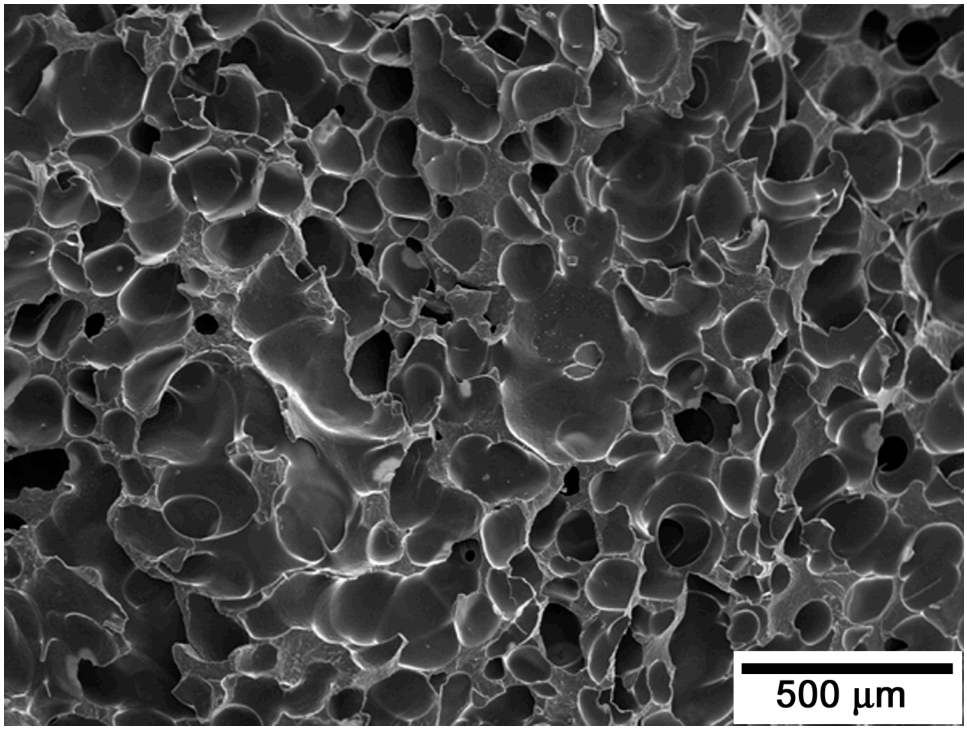


**Figure 3.11:** Scanning electron micrograph of PPNC-N1 foam extrudate.

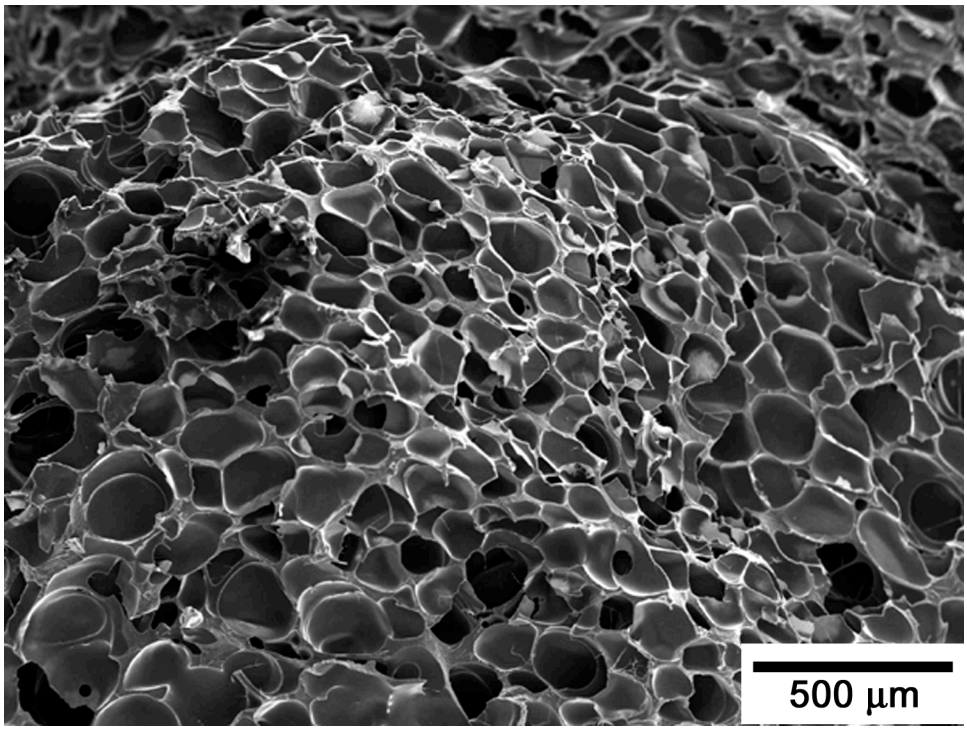


**Figure 3.12:** Scanning electron micrograph of PPNC-S1 foam extrudate.

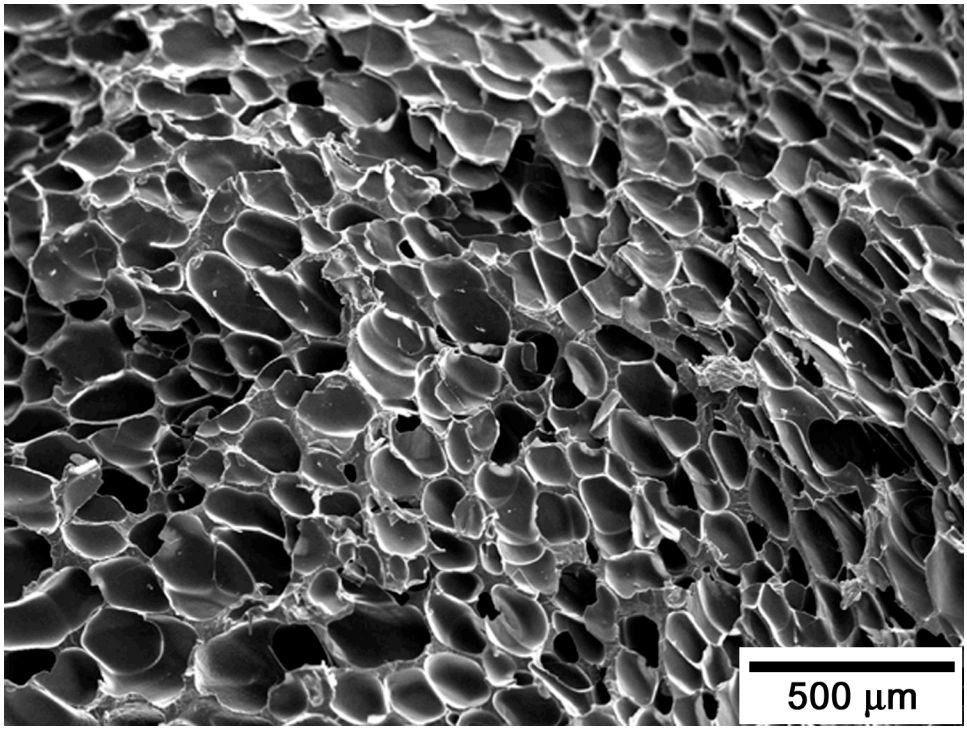


**Figure 3.13:** Scanning electron micrograph of PPNC-S2 foam extrudate.

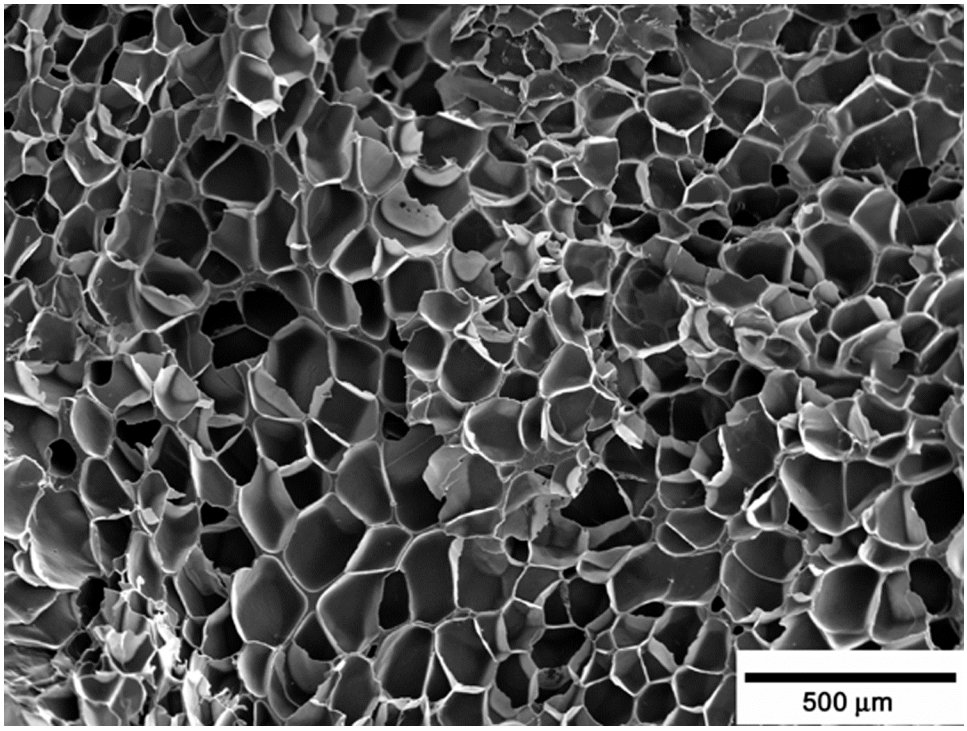


**Figure 3.14:** Scanning electron micrograph of PPNC-S6 foam extrudate.

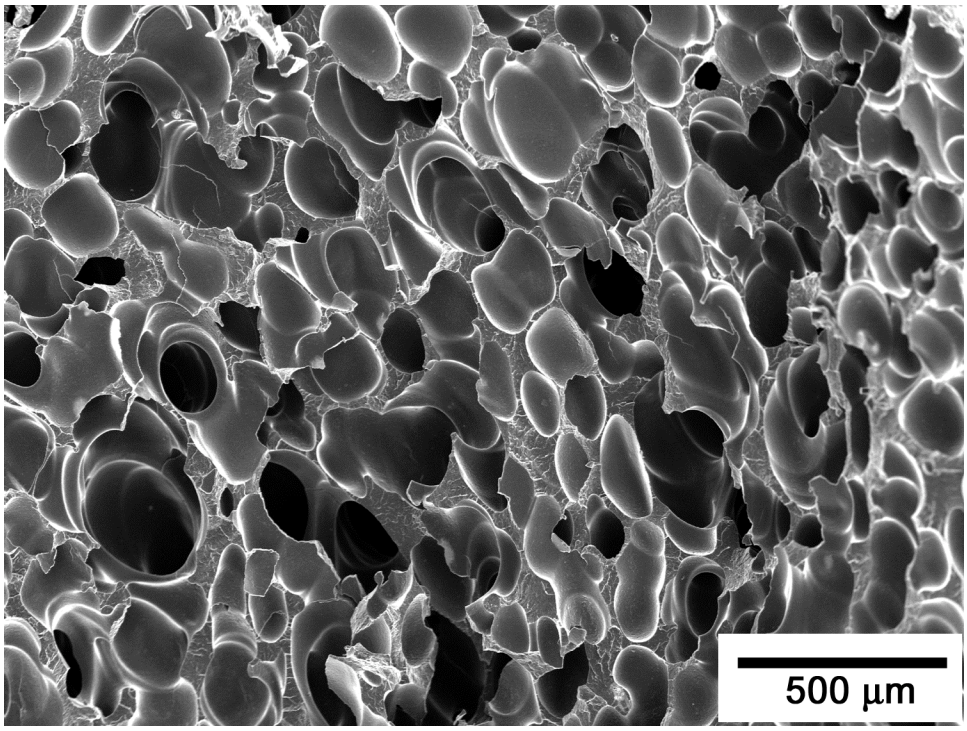


**Figure 3.15:** Scanning electron micrograph of L80B20 foam extrudate.

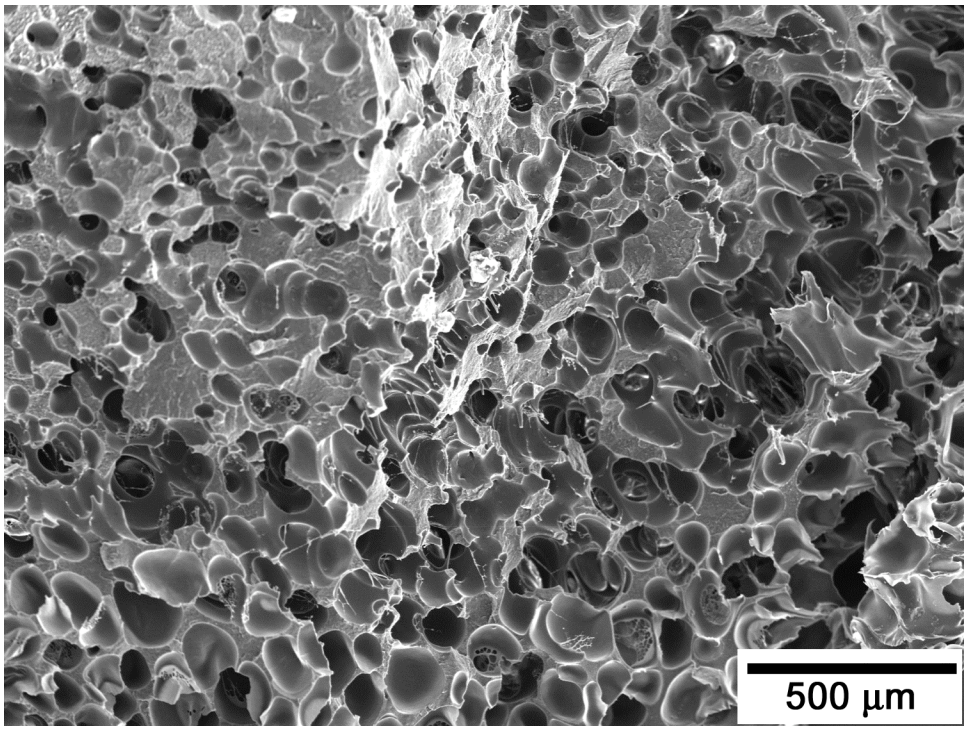


**Figure 3.16:** Scanning electron micrograph of TPO foam extrudate.

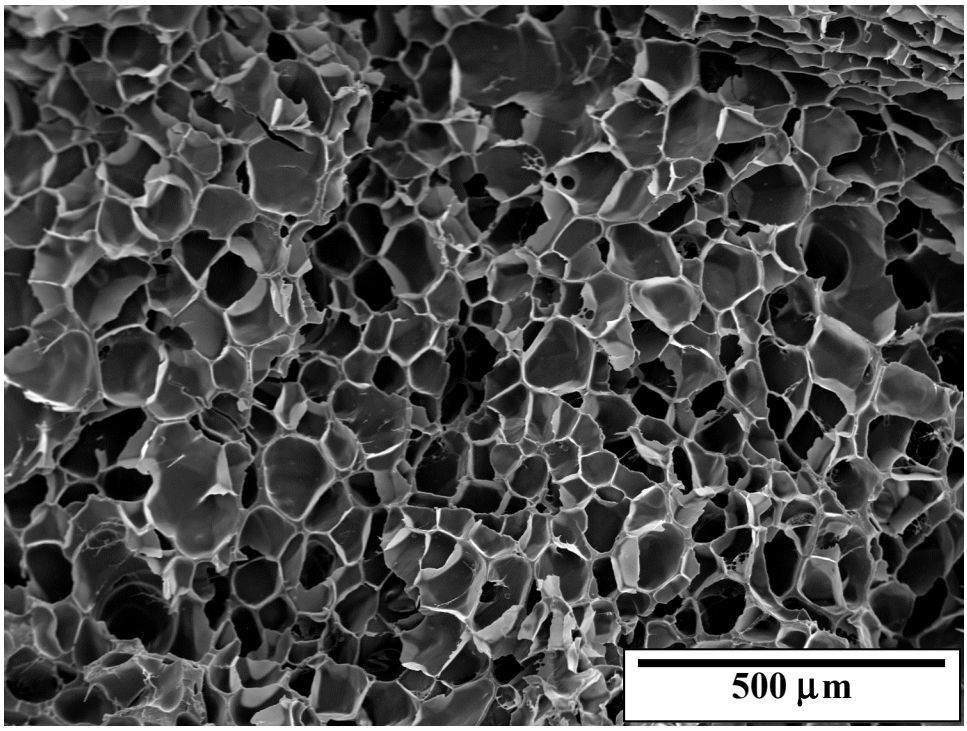


**Figure 3.17:** Scanning electron micrograph of TPONC foam extrudate.

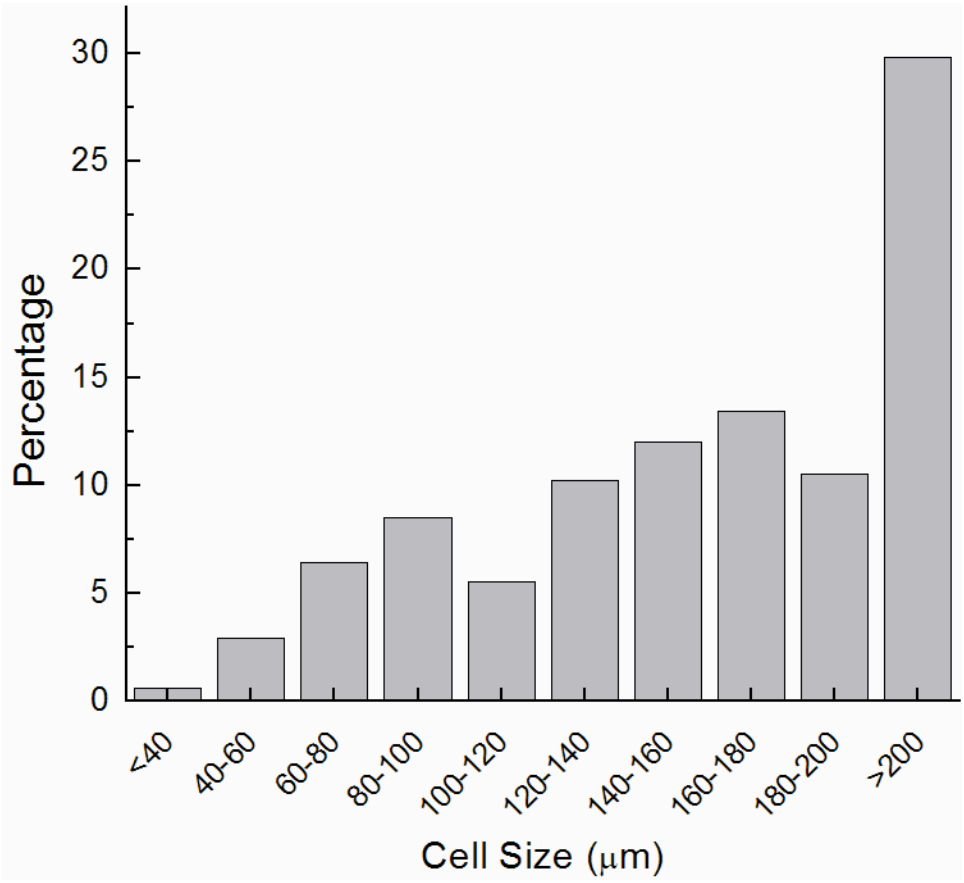


**Figure 3.18:** Cell size distribution of PPNC-N2 foam.

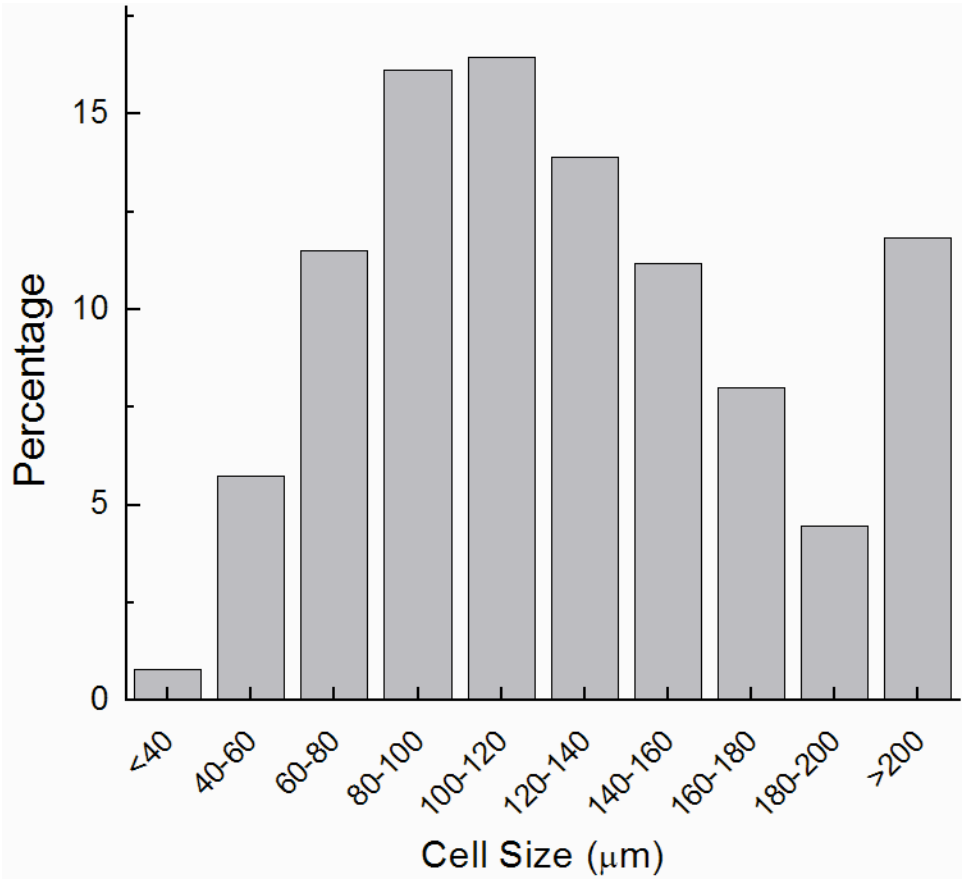


**Figure 3.19:** Cell size distribution of PPNC-N1 foam.

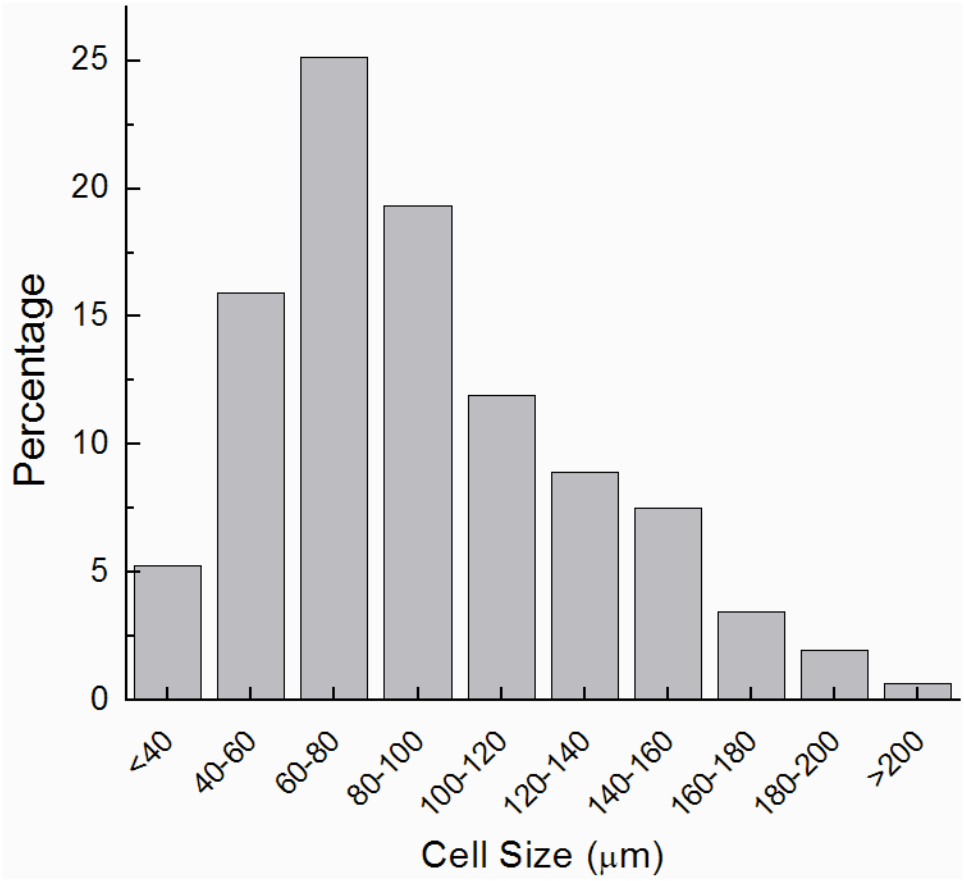


**Figure 3.20:** Cell size distribution of PPNC-S1 foam.

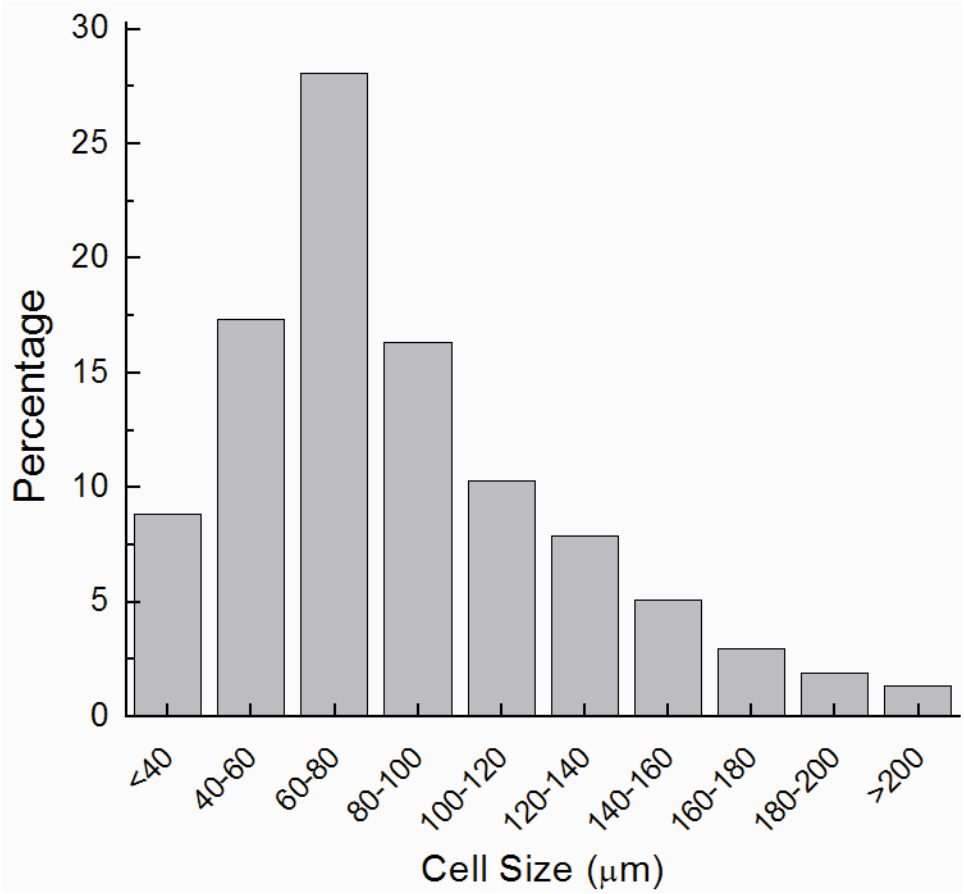


**Figure 3.21:** Cell size distribution of PPNC-S2 foam.

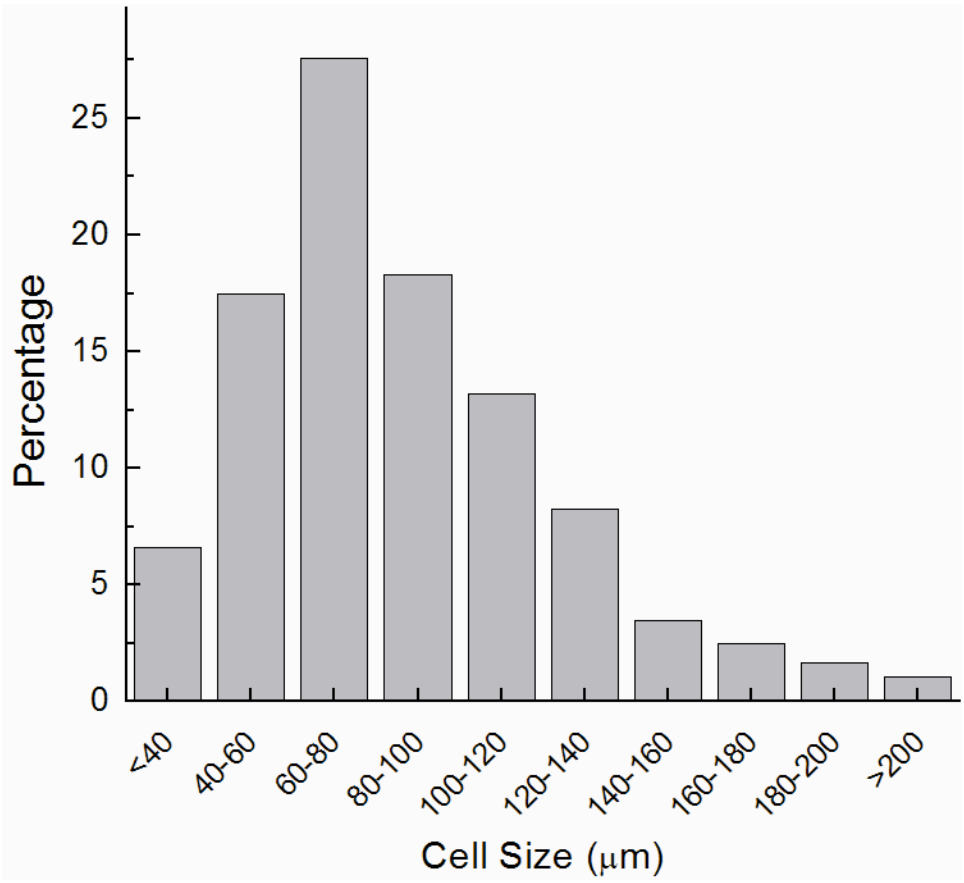


**Figure 3.22:** Cell size distribution of PPNC-S6 foam.

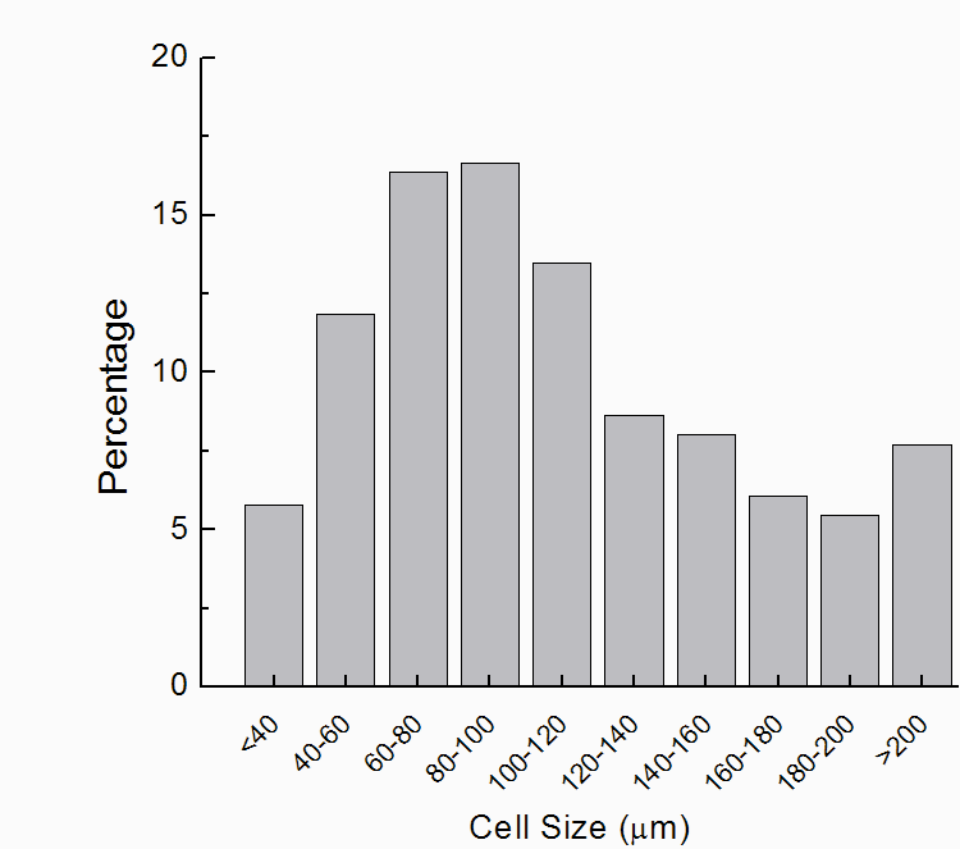


**Figure 3.23:** Cell size distribution of L80B20 foam.

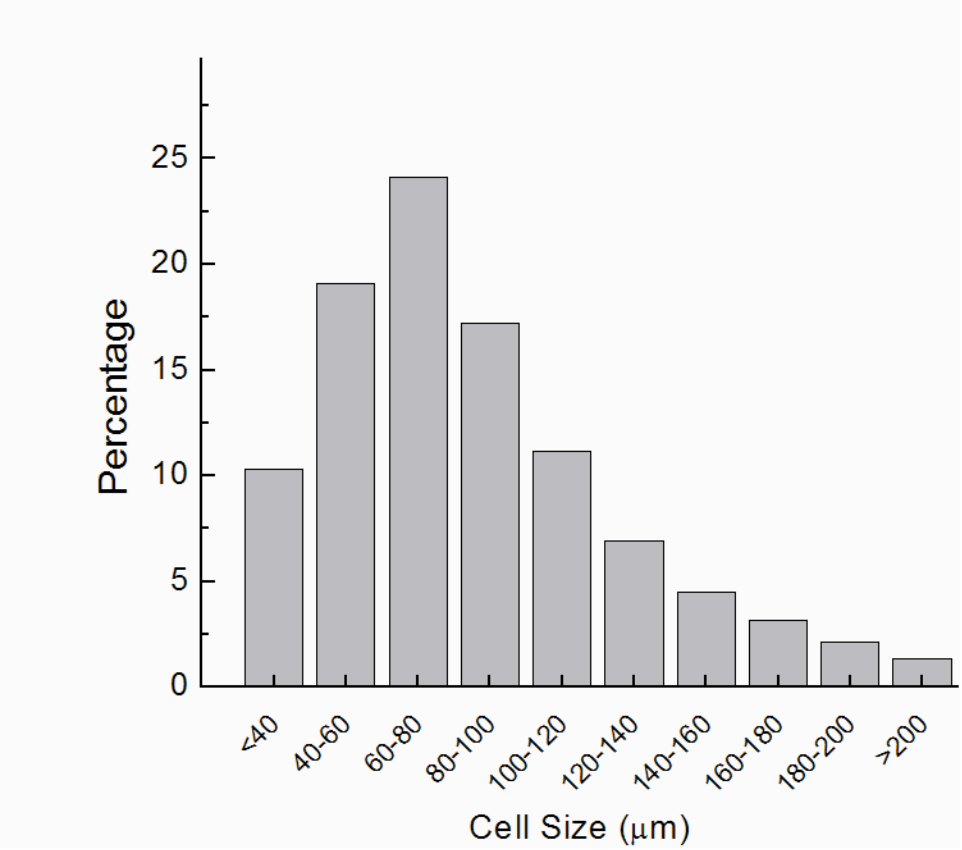


**Figure 3.24:** Cell size distribution of TPONC foam.

# 4. THE USE OF SILANE COUPLING AGENTS IN POLYPROPYLENE CLAY NANOCOMPOSITES

## 4.1. Introduction

Strain hardening, as established in Chapter 3, is a very important rheological property of polymers for foaming applications. However, absence of this property from linear PP has largely restricted the use of such a potential polymer in the field of foaming technology. We have successfully shown, in Chapter 3, that addition of suitable nanoclay and compatibilizer to linear PP can result in significant strain hardening characteristics under uniaxial extensional flow, which in turn led to significant improvement in foam quality.

Strain hardening in the nanocomposite melts is analogous to that reported for blends containing small amounts of crosslinked polymer. Blends of linear polypropylene with small amounts of chemically crosslinked polymers contain trapped entanglements on chain segments between crosslinks or junctions which respond to stretching differently from entanglements on chain segments in the bulk [152, 153]. Linkages or interactions between the clay surface or edge and the maleated polymer can form a network of "physical crosslinks" or anchor points between which entanglements may be trapped to produce similar effect. However, organically modified nanoclays and the compatibilizer has mainly electrostatic or hydrogen bonding type interactions [154], which are weaker forces of attraction. Hence, if these weaker forces of attraction can be replaced with covalent bonds then one can expect a significant increase in the strain hardening behavior of these PP nanocomposites. With the objective of producing PP nanocomposite foams with even smaller cell sizes compared to PPNC-S6 foams, by an improvement in the strain hardening characteristics, additional treatment of the nanoclays was investigated.

Over the past few decades, extensive research has been done on the use of montmorillonite clay as nanofiller to prepare polymer nanocomposites. The potential for significant improvements in various mechanical, barrier and rheological properties [69, 73-75, 88, 155, 156] upon the used of layered silicates in various polymer matrices has stimulated the growth of polymer nanocomposites. The extent of increment in these properties was attributed not only to dispersion of these nanolayers but also to the strong polymer-clay interactions [157-160]. However attempts to disperse the clay in non-polar systems like polypropylene still remain a challenge. This is primarily due to absence of favorable interfacial interactions between the nanoclay and non-polar polymers like polypropylene. In order to increase interfacial interactions between the two, functionalized polyolefin oligomers (compatibilizers) are commonly used [78, 86, 87, 89-91, 161, 162], where the polar functionality can favorably interact with the clay surface and the oligomers can interact with the bulk matrix. In order to achieve high levels of interaction between the clay and the polymer, a high level of maleic anhydride grafting is required, which causes chain scission in polypropylene [133] and results in poor physical and mechanical properties of the resulting nanocomposites.

Since montmorillonites has exchangeable interlayer cations and shows Bronsted and Lewis acidity, the most commonly accepted way to improve the polymer-clay interaction was to treat the nanoclays with various cationic surfactants [77-81]. Alternatively, due to the presence of hydroxyl groups on the edges of the clay platelets and due to active sites on the surface of the clay platelets, these nanoclays have also been treated with various silane-coupling agents to improve polymer-clay interaction [160, 163-169]. With the use of silated clays, researchers have shown significant improvements in clay dispersion in the polymer matrix [164, 170, 171], resulting in improvements in various mechanical [166, 172, 173] and rheological properties [174,

175]. However, none of the work reported till date discusses changes in extensional rheology characteristics by the use of silane treated nanoclays.

The properties and effects of silanes are determined by their molecular structures, generally represented as shown in Figure 4.1. The silicon at the center has an organofunctional group (Y) at one end and hydrolysable groups (most commonly alkoxy groups) on the other end. A judicious selection of the silane-coupling agent can act as a bridge between the polymer and the filler, where the alkoxy groups (after hydrolyzing) can link with the hydroxyl groups at the edges of the clay or with the active sites on the clay surface and the organofunctional group, Y, can interact with the polymer. The latter interaction can be in the form of covalent bonding or the formation of interpenetrating networks [176] for non-reactive systems like polypropylene. Depending upon the molecular structure of the silane coupling agents, it can end up either being inside the layered clay galleries [83, 165] resulting in an increase in clay basal spacing or react mainly with the edge hydroxyl groups [135, 165, 177, 178]. Shanmugharaj et al. [165] studied the influence of dispersing medium, used during the silation procedure, on the grafting of montmorillonite clays and reported that with the increase in solvent surface energy, the possibility of intercalation of silane molecules within the clay galleries increases. The presence of silane molecules within the clay galleries could provide greater interaction between the polymer and the clay, resulting in better dispersion and improved mechanical properties.

In this work, we have investigated the effects of increased interaction using carefully chosen silane coupling agents on the dispersion of nanoclays in linear polypropylene nanocomposites and the associated improvements in strain hardening in uniaxial extensional rheology of the polymer melt. In order to replace the weaker force of interaction (hydrogen bonding) between the compatibilizer and the nanoclay with a stronger covalent bond, the

organoclays were additionally treated with carefully chosen amino silanes. This selection was made based on the fact that amines present on the silane treated clays can react with the anhydride group of the PP-g-MA [179-183], forming an amide or imide linkage as per the reaction scheme shown in Figure 4.2. Lu et al. [181] investigated the reaction between PP-g-MA and amines by melt mixing them in various proportions in an extruder. The study suggested that the reaction between the two was very fast and was completed within 90s which was supported by FTIR analysis. Song et al. [183] studied the reaction between different amines (primary, secondary and tertiary amines) and anhydride group in polymeric systems and reported rapid formation of the imide linkage between the polymer and the amines. Increased interaction between the compatibilizer and the silated clay would further slow the relaxation of stretch in the polymer chains trapped between particles along the direction of flow, under uniaxial extensional flow at melt state, compared to the unsilated polypropylene nanocomposite system.

## 4.2. Materials and Experimental Procedures

Three different amino silanes were used for this study:

a) N-aminoethyl-Aza-2,2,4-trimethylsilacyclopentane (Diamino monomethoxy-Silane)

b) N-(2-aminoethyl)-3-aminopropylmethyldimethoxysilane (Diamino dimethoxy-Silane)

c) N-(2-aminoethyl)-3-aminopropyltrimethoxysilane (Diamino trimethoxy-Silane)

d) Phenyl trimethoxy silane.

The chemical structures of all the silanes are presented in Figure 4.3. The main differences among the three amino silanes are in the number of hydroxyl groups, which could be significant if poly-condensation of silanes were more likely to occur with the large number of hydroxyl groups. However, since the silation reaction is carried out under constant stirring and

also due to small amounts of silane used for the clay treatment chances of poly-condensation of silanes is less likely. Phenyl trimethoxy silane is used as a control silane coupling agent, as it does not have amine functionality. The methoxy groups of all the silanes get hydrolyzed in presence of moisture and can then follow the reaction scheme as shown in Figure 4.2 (a similar reaction scheme has also been proposed by Zheng et al. [184] and Nygard et al. [185]). However, the monomethoxy-silane follows a ring opening mechanism during the hydrolysis step as shown in Figure 4.3 and then follows the usual silane reaction scheme. The detail of the silation procedure is laid out in Chapter 2.

Two different organically modified montmorillonite clays (I.44P and I.30P) were used for the silane treatment. The silated clays were then used to prepare nanocomposites with 85 wt% linear PP, 12 wt% PO 1015 as the compatibilizer and 3 wt% of nanoclay, the details of which are presented in Table 4.1. The various techniques used in this section for characterization of nanoclays and nanocomposites are: XRD, TEM, TGA, BET, and uniaxial extensional rheology. The details of all the experimental procedures are presented in section 2.

## 4.3. Results and Discussion

### 4.3.1. Characterization of Silated Clays

Thermo-gravimetric analysis, X-ray diffraction studies, and BET surface area measurements were used to characterize the various silane treated organoclays. The information from these techniques was then used to predict whether silation of the organoclays resulted in edge grafting or face grafting.

#### 4.3.1.1. Thermo-gravimetric analysis

Thermo-gravimetric analysis was used to estimate the organic content in the organoclays, silated and unsilated. The TGA weight loss profile for silated and unsilated I.44P is presented in Figure 4.4 and the same for I.30P clays are presented in Figure 4.5. To begin with, unsilated I.44P has 35 wt% of organic content while I.30P has 24 wt% of organic content, however, they both have same molecular equivalent of surfactant inside the clay galleries. The weight loss profile (up to 500°C) for silated I.44P organoclay shows negligible change in the amount of organic content after silation irrespective of the silane used, whereas the same for I.30P organoclays, there is an increase in the organic content after silation (3.5 wt% for mono-silation case and 7.3 wt% for diamino dimethoxy-silation case). This indicates that the silane molecules have most probably intercalated inside the clay galleries for I.30P system whereas insignificant change in the organic content of silated I.44P system indicated that the silane molecules are most grafted on the edges. In order to further substantiate the grafting sites of the silane molecules in the two organoclay system, BET surface area measurements and XRD was carried out.

#### 4.3.1.2. BET surface area measurements

The nanoclays before and after silation were analyzed for their total surface area using BET surface area measurements. The total BET surface area of sodium montmorillonite clays is in the range of 43 $m^2/g$ to 50 $m^2/g$ [186-188]. It has been reported by He et al. [189] that with progressive increase in adsorption of hexadecyltrimethyl ammonium surfactant inside the clay galleries, the BET specific surface area, measured by nitrogen adsorption, of the resulting organoclay decreases progressively (Figure 4.6). The BET specific surface area experimental results for all the silated and unsilated organoclays are tabulated in Table 4.2. The BET specific

surface area of both the organoclays, I.30P and I.44P, is around 10 $m^2/g$ after surfactant treatment, thus indicating that both these nanoclays are cationically exchanged with similar molar equivalent of the cationic surfactant. A drop in BET surface area, from sodium montmorillonite to organically modified montmorillonite, also indicates that a fraction of the clay surface is occupied by bulkier ions. When I.44P was further treated with different silane coupling agents, there was no significant drop in the BET surface area irrespective of the silane used, indicating that silation of the clay has mainly occurred at the edges of the nanoclay platelets. However, there is a significant drop in the BET surface area of the silane treated I.30P nanoclays, indicating that silane coupling has occurred both at the edges and the faces of the nanoclay platelets. This is probably due to different molecular structure and subsequently different molecular conformations of the surfactants used in the two nanoclays, even though both I.30P and I.44P are intercalated with same molar equivalents of the organic cation. Further, I.30P has 24 wt% of surfactant while I.44P has 35 wt% of surfactant. Hence due to densely packed conformation of I.44P, the silane coupling reaction happens predominantly at the edges while that for I.30P is both at the edges and the faces.

The difference between surface area of diamino monomethoxy-silane treated I.30P and diamino dimethoxy-silane treated I.30P could be explain by the fact that in case of diamino dimethoxy-silane there are two methoxy groups that can graft to neighboring sites thereby reducing the surface area available for nitrogen adsorption. Also due to the cyclic structure of the diamino monomethoxy silane, the intercalation of the silane molecule might be sterically hindered. However, there is no further drop in the surface area between diamino dimethoxy-silane treated and diamino trimethoxy-silane treated I.30P. This is probably because due to the tetrahedral conformation of the three methoxy groups on the silane atom making it sterically

difficult to adsorb at three neighboring sites. A very small reduction in the surface area of the phenyl trimethoxy silane could be explained by the fact that the bulky nature of the phenyl group makes it difficult for the silane molecule to enter the galleries [135].

#### 4.3.1.3. X-ray diffraction study

X-Ray diffraction studies were conducted on these silane treated clays for the characterization of their morphology. The analysis of TGA and BET surface area results indicated that silation of I.44P clay resulted in edge grafting while that of I.30P clay resulted in face grafting. This should result in an increase in d-spacing of I.30P nanoclay post silation and the same for I.44P clay system should remain unchanged. The XRD patterns of silated I.30P clay and silated I.44P clay are presented in Figure 4.7 and the corresponding d-spacings are presented in Table 4.3. From the XRD pattern of the treated I.30P clay system, it is evident that the d-spacing for all the amino silated clays have increased compared to the unsilated I.30P except phenyl trimethoxy silane. This confirms that the amino silane molecules have resulted in face grafting while phenyl trimethoxy silane is predominantly face grafted. However, the d-spacing for I.44P clays remain unchanged after silation, indicating no possible intercalation of the silane molecules inside the clay galleries and the silane molecules have been grafted to the edges of the clay.

If the proposed hypothesis of stronger interaction between nanoclay and the compatibilizer resulting in higher strain hardening characteristics is true, then nanocomposites derived from amino silane treated nanoclays would result in greater strain hardening behavior compared to untreated or phenyl trimethoxy treated nanoclay. Furthermore, nanocomposites prepared using amino silated I.30P nanoclays should show even higher strain hardening

characteristics compared to those prepared from amino silated I.44P nanoclays, due to greater number of sites for interaction with PP-g-MA.

### 4.3.2. Characterization of Polypropylene – Silated Clay Nanocomposites

#### 4.3.2.1. Structural characterization

Various linear PP nanocomposites were prepared using 3 wt% of silated I.30P and I.44P organoclays using PP-g-MA1 as the compatibilizer. The objective here is to study the effect of different silation on the morphology and strain hardening behavior of the nanocomposites.

The X-ray diffraction pattern for various PP nanocomposites derived from silated I.30P and I.44P nanoclays are presented in Figure 4.8 and corresponding d-spacing in Table 4.3. The XRD pattern of silated I.44P nanocomposites shows negligible change in d-spacing and the extent of dispersion (evident from the distinct peak in the XRD pattern) due to silation of the organoclays. The TEM micrographs presented in Figure 4.9 also shows that nanocomposite prepared from untreated I.44P as well as diamino dimethoxy silane treated I.44P have intercalated structure with comparable thickness of clay stacks. This was expected because the silane coupling has primarily occurred at the edges of the I.44P nanoclays. However the same is not true for nanocomposites prepared form silated I.30P clay system. All the amino silane treated I.30P clay nanocomposites showed an increase in d-spacing, indicating greater polymer intercalation compared to untreated I.30P. The d-spacing for phenyl trimethoxy silated I.30P clay nanocomposites is comparable to the unsilated I.30P clay. Also the XRD patterns of the nanocomposites prepared from amino silane treated I.30P lacks distinct peaks, an indication of random well dispersed clay platelets as compared to ordered clay stacks in case of untreated I.30P and phenyl trimethoxy silane treated I.30P system. This is also evident from the TEM

micrographs for untreated I.30P and diamino dimethoxy silane treated I.30P nanocomposites presented in Figure 4.10. Hence, the face grafting of the amino silanes in I.30P clay system resulted in greater intercalation of the polymer chains leading to better dispersion, as opposed to the edge grafting of amino silanes in I.44P clay system, which showed no appreciable change in the extent of polymer intercalation or dispersion of nanoplatelets.

#### 4.3.2.2. Uniaxial Extensional Rheology

The melt extensional viscosity transients for the linear PP nanocomposites prepared from various I.30P nanoclays and I.44P nanoclays are presented in Figures 4.11-4.13. The melt extensional viscosity transients for phenyl trimethoxy silated I.30P nanocomposites along with unsilated I.30P nanocomposites are presented in Figure 4.11. As expected, the transient melt extensional viscosity data of PP nanocomposites prepared with phenyl trimethoxy silane treated I.30P nanoclay is similar to that of untreated I.30P nanoclay, indicating no improvement in the strain hardening behavior. This is because presence of an additional phenyl group attached to the clay surface does not change the nature of interaction between the compatibilizer and the clay. However, as shown in Figures 4.12 and 4.13, all the nanocomposites prepared using amino silane treated I.30P and I.44P shows a significant increase in the strain hardening behavior compared to the unsilated system clay system. This is because the weaker hydrogen bonds between the clay and the compatibilizer are now replaced with much stronger covalent bonds, which can help orient the polymer chains to a greater extent and thus resulting in significant increase in strain hardening characteristics. Moreover, there is no significant difference between the strain hardening characteristics of clays treated with amino silanes with one or more hydrolysable groups. This proves that the increase in polymer clay interaction is primarily due to the presence

of amine functionality on the silated clays. This also indicates that poly-condensation of the silanes does not appear to be significant.

A comparison between amino silane treated I.30P and I.44P nanocomposites indicates that I.30P system shows greater increase in strain hardening behavior. This is because, in case of silated I.30P clays the silane molecules are present both on the edges as well as on the faces of the nanoclay, which provides greater number of interaction sites between the polymer and the clay surface as opposed to only edge functionalization in case of silated I.44P system. In order to verify that the samples were stable during these tests and that the strain hardening data is not an artifact of the continuously changing structure of the nanocomposite, dynamic time sweep tests were conducted on these samples. The time sweep data (Figure 4.14) shows that the storage modulus of these nanocomposite melts remained unchanged over a period of 1 hour, confirming that the samples were stable over an hour.

For a quantitative evaluation of the strain hardening behavior of these nanocomposites, the strain hardening parameters are calculated using equation 3.1, for a Hencky strain of 2.25, and are presented in Figures 4.15-4.16. The choice of Hencky strain of 2.25 was done so as to compare the strain hardening behavior of all the nanocomposites at the same strain and for few nanocomposites, maximum achievable Hencky strain was 2.25. From the strain hardening data for I.44P clay system (Figure 4.15), the significant change in strain hardening behavior of nanocomposites prepared using amino silane treated I.44P is clearly reflected. However, it seems as if there is not much of an improvement in strain hardening behavior of the I.30P system after silation (Figure-4.16), even though the melt elongational viscosity transients presented in Figure 4.12 says otherwise. A closer look at the strain hardening data indicates that the deviation from the linear viscoelastic curve starts at a higher strain for amino silane treated I.30P system and

continue to show an increase in the extensional viscosity under uniaxial extensional flow up to the maximum value of Hencky strain used during the test, compared to unsilated I.30P nanocomposites where the extensional viscosity starts to drop after a Hencky strain of 2.25. Figure 4.16 also shows the strain hardening parameter of nanocomposites containing amino silane treated I.30P clays at higher values of Hencky strain. It is evident from Figure 4.16 that the strain hardening parameter (at $\varepsilon_H = 2.9$) of amino silated I30P nanocomposites is greater than that measured at $\varepsilon_H = 2.25$ at all strain rates tested. While all other nanocomposites (including silated I.44P system) shows a maximum value of extensional viscosity close to a strain of 2.25, amino silane treated I.30P nanocomposites continues to show an increase in extensional viscosity up to the maximum Hencky strain tested. This clearly demonstrates the superiority of the amino silane treated I.30P nanocomposites over silated I.44P clay nanocomposites in withstanding the uniaxial stretching force up to a larger Hencky strain at all rates tested. Another important observation of these nanocomposites is the nature of change in the strain hardening parameter with increase in strain rates. The I.44P system even after silation shows a drop in strain hardening parameter with increase in strain rates (Type – 2 strain hardening behavior) while the amino silated I.30P system is able to maintain its strain hardening characteristics with increase in strain rates (Type – 1 strain hardening behavior) (Figures 4.15-4.16). Since the instrument used to measure the extensional viscosity transients under uniaxial extensional flow, has a testing limitation at higher strain rates, one can assume that amino silated I.30P nanocomposites will continue to show strain hardening properties even at higher strain rates as opposed to amino silated I.44P nanocomposites. This allows us to study the effect of type of strain hardening behavior on foamability of polymer system.

#### 4.3.2.3. Effect of solvent used during silation on final PP/clay nanocomposite property

In order to study the influence of solvent surface energy on the coupling of the silane molecule on the organoclay, the three different solvent systems were used to silate I.44P clay using diamino dimethoxy-silane. They are:

(a) A mixture of 80 wt% methanol and 20 wt% de-ionized water,

(b) A mixture of 80 wt% methanol and 20 wt% de-ionized water, and

(c) De-ionized water.

The resulting diamino dimethoxy-silated I.44P clays were then used to prepare PP/clay nanocomposites with 3 wt% clay and 12 wt% PP-g-MA1. These nanocomposites were then tested for their strain hardening behavior under uniaxial extensional flow. The melt extensional viscosity data for the three cases are presented in Figure 4.17. It can be seen from the figure that silated clays synthesized using different solvent system has negligible effect on the strain hardening behavior of the resulting I.44P clay nanocomposites, indicating that the silane grafting in still predominantly on the edges of the clay. Hence, the choice of solvents, depending on solvent surface energy, for silation does not influence the grafting location of silane molecules for our system. This primary objective of this experiment was based on industrial interests. Since aqueous suspension of sodium montmorillonite is used for surfactant system, hence the moist clay cake obtained after surfactant treatment can directly be used for further silane treatment.

## 4.4. Conclusions

Results presented in this section reveals that carefully chosen silane-coupling agents can significantly improve the interfacial interactions between the nanolayer and the compatibilizer. Depending on the precursor nanoclays, the silane treatment can predominantly result in either face or edge grafting. Since the available volume within the clay galleries in greater in I.30P organoclays due to lower organic content (wt%) compared to I.44P clay, former system results in face grafted silated clay while the later results in edge grafting of the silane molecules. This is been convincingly proven by various characterization techniques. The linear PP nanocomposites prepared using amino silane treated nanoclays resulted in significant increase in strain hardening behavior under uniaxial extensional flow compared to the unsilated clay nanocomposite, irrespective of the organoclays used. Phenyl trimethoxy silated I.30P, used as control, showed no improvement in strain hardening behavior compared to the unsilated I.30P. Further, since I.30P resulted in face grafted silated clay, the resulting nanocomposites showed greater strain hardening, up to higher Hencky strains, compared to silated I.44P clays. This is due to greater number of interaction points available on the silated I.30P clay because of face grafting as opposed to edge grafting of the silated I.44P clay system. Another critical observation was the nature of change in strain hardening behavior with the change in strain rate. Silate I.30P nanocomposites resulted in more LDPE type strain hardening behavior that remain unchanged with strain rates while silated I.44P system behaved more like blends of linear and branched PP. These results demonstrate the effect of polymer-clay interaction on strain hardening behavior of nanocomposites under uniaxial extensional flow. It will further be shown that these nanocomposites with superior strain hardening property can result in closed cell foams with even small size and greater cell densities compared to those obtained by using the unsilated clays.

| Specimen | Clay treatment |
|---|---|
| PPNC-S3 | Diamino monomethoxy-silane treated I.30P |
| PPNC-S4 | Diamino dimethoxy-silane treated I.30P |
| PPNC-S5 | Diamino trimethoxy-silane treated I.30P |
| PPNC-S10 | Phenyl trimethoxy silane treated I.30P |
| PPNC-S11 | Unsilated I.30P |
| PPNC-S7 | Diamino dimethoxy-silane treated I.44P |
| PPNC-S12 | Diamino monomethoxy-silane treated I.44P |

**Table 4.1:** Formulation details of linear PP/ clay nanocomposites with 85 wt% Profax 6523, 12 wt% of PO 1015, and 3 wt% to treated clays.

| Treatment | Surface Area ($m^2/g$) | |
|---|---|---|
| | **I.30P** | **I.44P** |
| No silane treatment | 9.51 | 9.8 |
| Diamino monomethoxy-silane | 6.63 | 10.13 |
| Diamino dimethoxy-silane | 3.82 | 9.12 |
| Diamino trimethoxy-silane | 3.67 | 9.31 |
| Phenyl trimethoxy silane | 7.71 | 9.25 |

**Table 4.2:** BET surface area measurements of silane treated nanoclays.

| Treatment | I.30P | | I.44P | |
|---|---|---|---|---|
| | Clays | PPNCs | Clays | PPNCs |
| No silane treatment | 2.34 | 2.95 | 2.58 | 3.16 |
| Diamino monomethoxy-silane | 2.76 | 3.33 | 2.54 | 2.99 |
| Diamino dimethoxy-silane | 3.21 | 3.33 | 2.54 | 3.33 |
| Diamino trimethoxy-silane | 3.1 | 3.16 | -- | -- |
| Phenyl trimethoxy silane | 3.21 | 2.27 | -- | -- |

**Table 4.3:** Basal spacing (d-spacing) of various treated nanoclays and their corresponding nanocomposites prepared using 85 wt% linear PP and 12 wt% PO 1015.

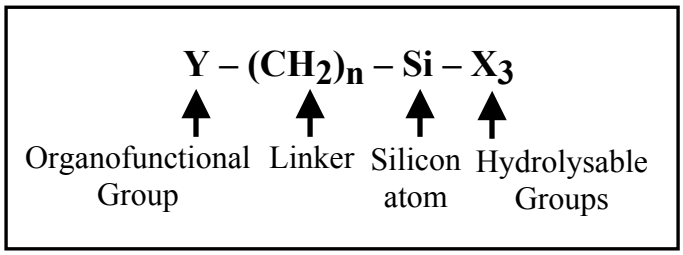


**Figure 4.1:** General structure of a silane coupling agent.

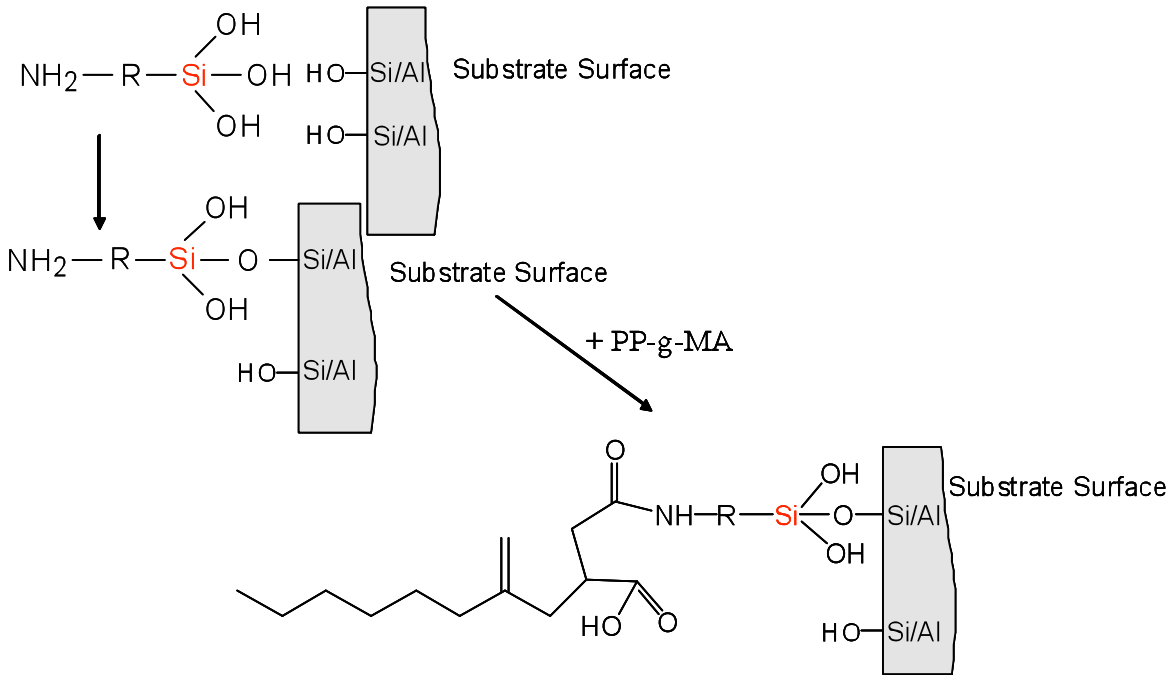


**Figure 4.2:** Reaction scheme between silane treated clays and maleic anhydride grafted polypropylene.

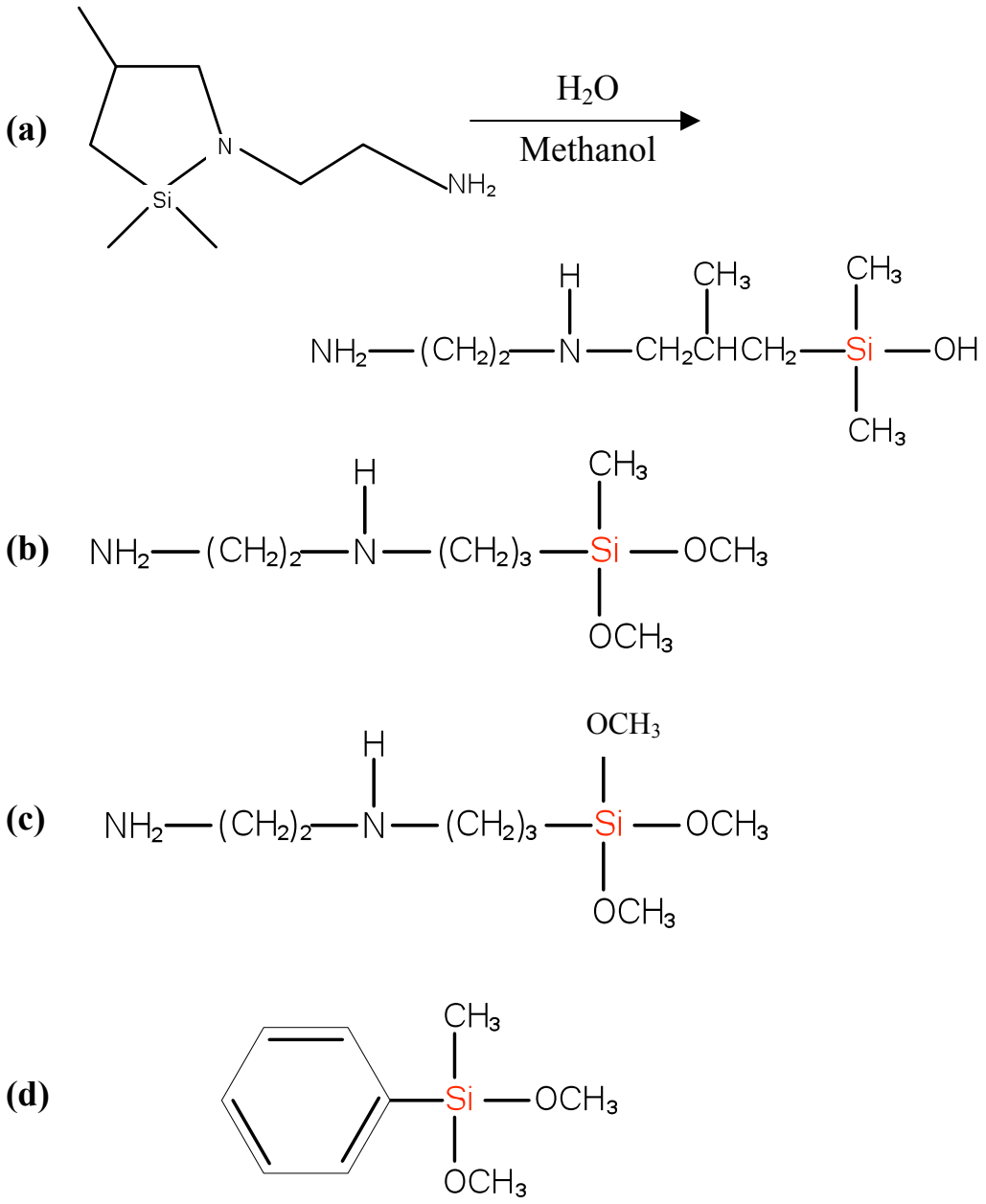


**Figure 4.3:** Chemical structure of silane coupling agents (a) Diamino monomethoxy-silane, (b) diamino dimethoxy-silane, (c) diamino trimethoxy-silane, and (d) Phenyl trimethoxy silane. The ring opening hydrolysis of diamino monomethoxy-silane is also shown along with its chemical structure.

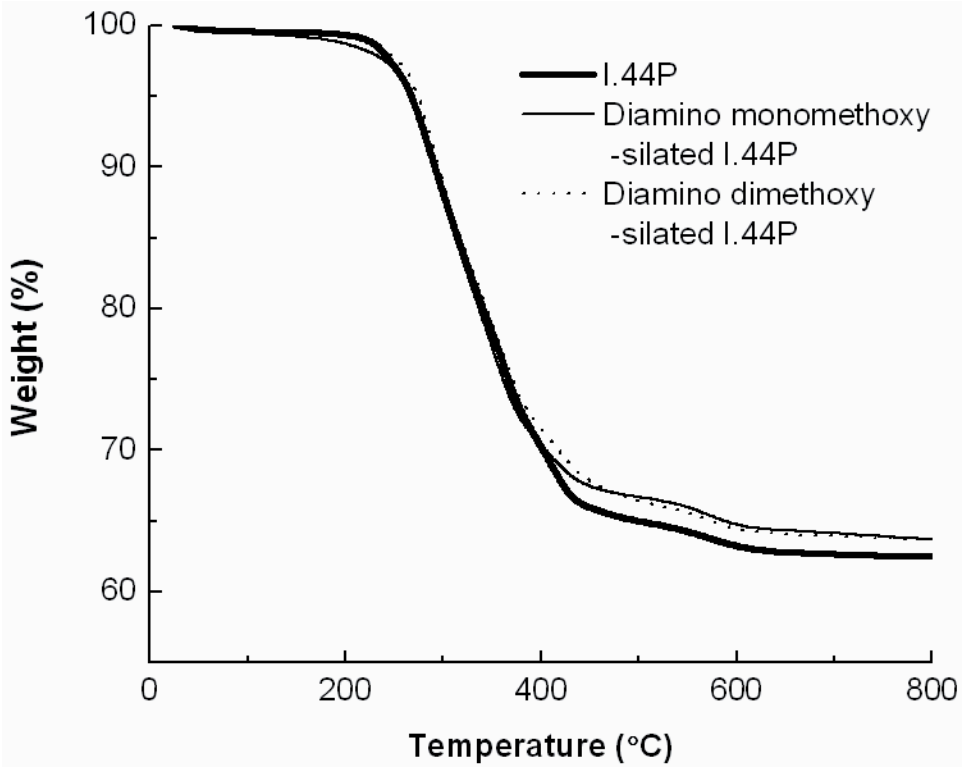


**Figure 4.4:** TGA profile of various silane treated I.44P clays.

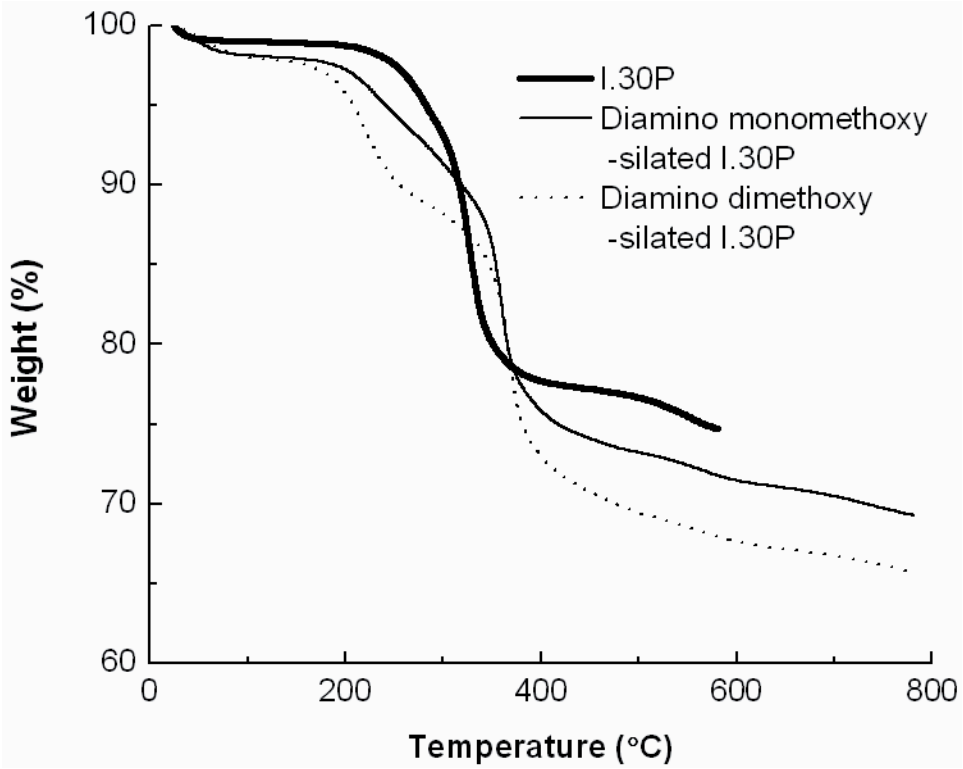


**Figure 4.5:** TGA profile of silane treated I30P clays.

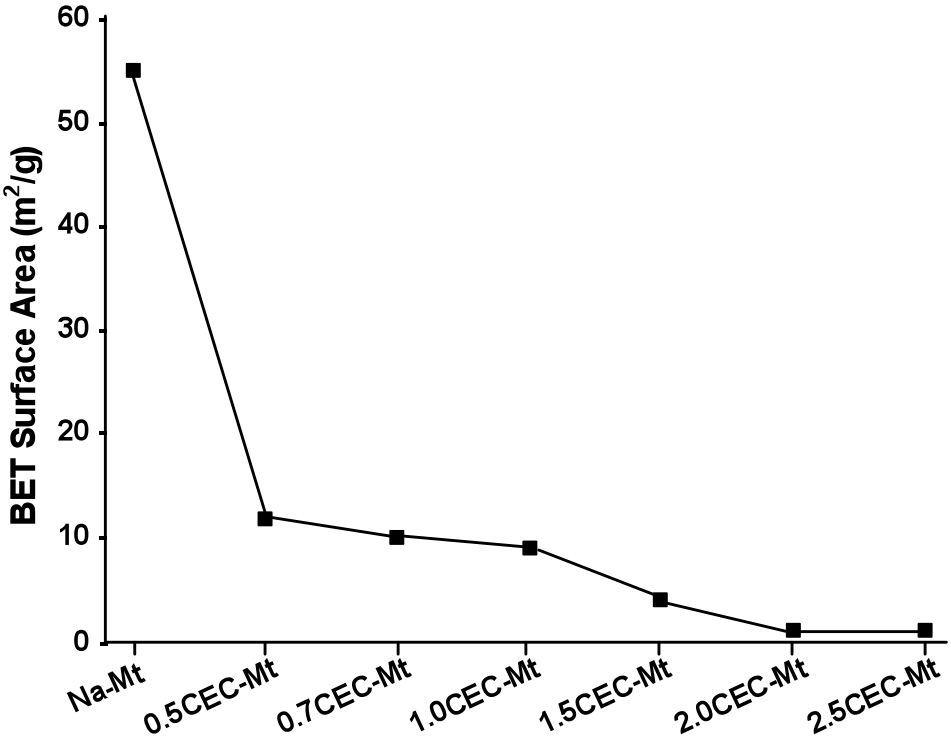


**Figure 4.6:** BET surface area data from He et al. [189] on reduction in surface area due to surfactant adsorption.

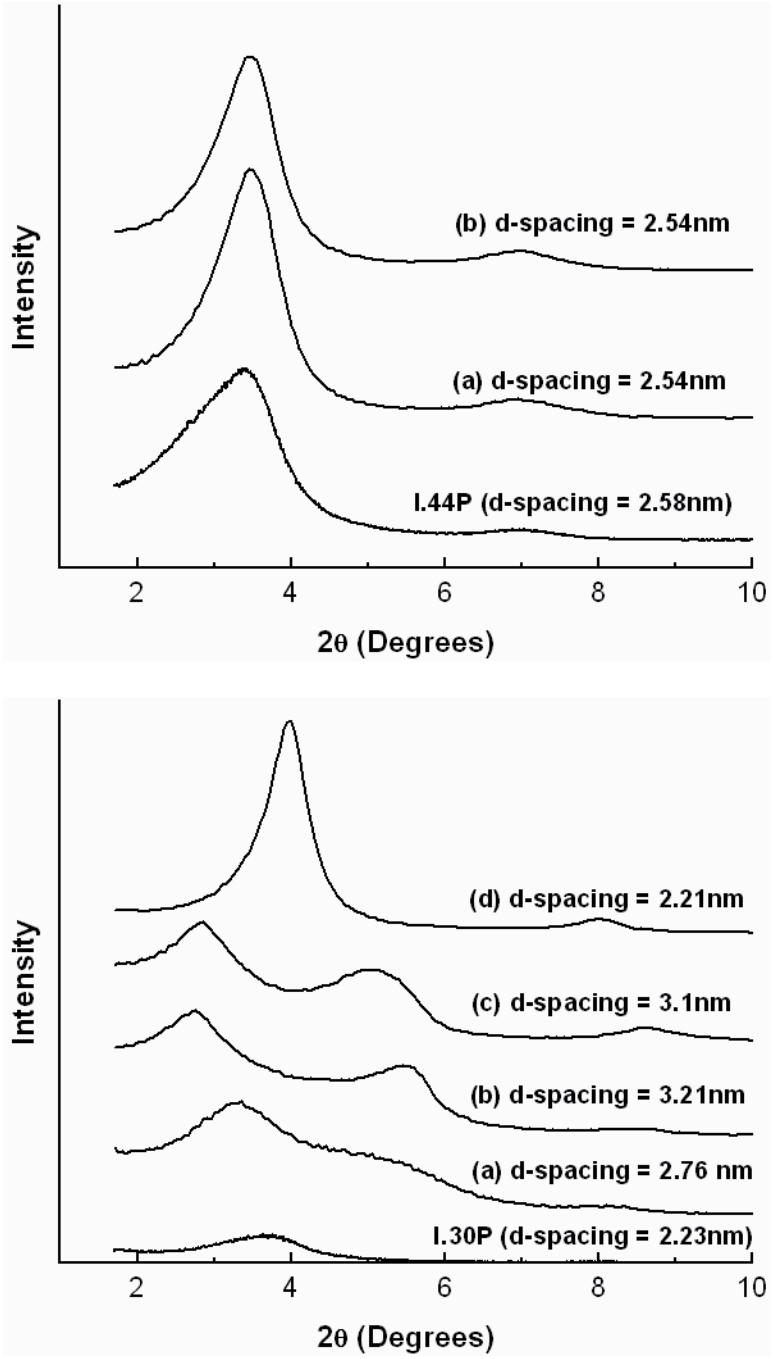


**Figure 4.7:** X-ray diffraction pattern of silane treated I.44P clays (top) and silane treated I.30P clays (bottom). The treatment of clays is represented as (a): Diamino monomethoxy-silated clay, (b) Diamino dimethoxy-silated clay, (c) diamino trimethoxy-silated clay, and (d) Phenyl trimethoxy silated clay. The d-spacing of the corresponding organoclays are presented alongside the XRD curve.

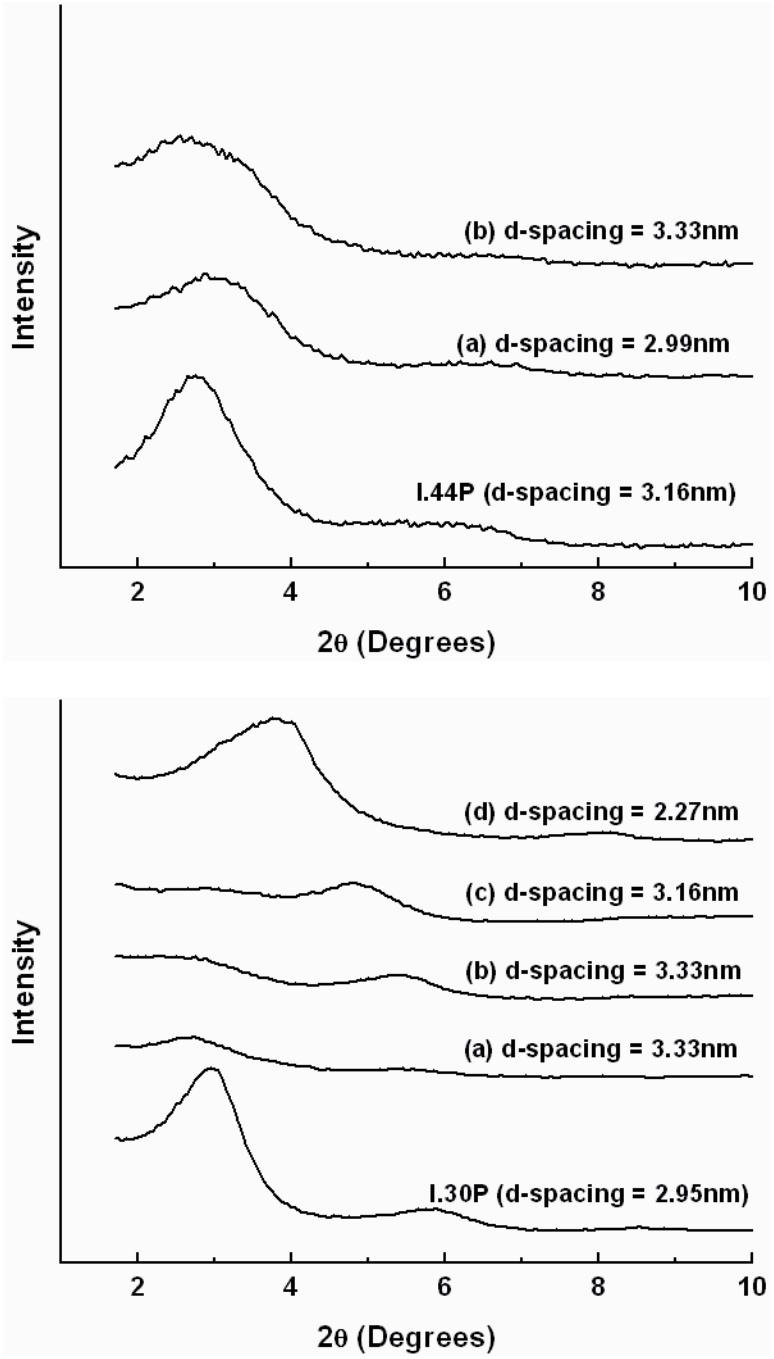


**Figure 4.8:** X-ray diffraction pattern of linear PP nanocomposites with silane treated I.44P clays (top) and silane treated I.30P clays (bottom). The treatment of clays is represented as (a): Diamino monomethoxy-silated clay, (b) Diamino dimethoxy-silated clay, (c) diamino trimethoxy-silated clay, and (d) Phenyl trimethoxy silated clay. The d-spacing of the corresponding organoclays are presented alongside the XRD curve.

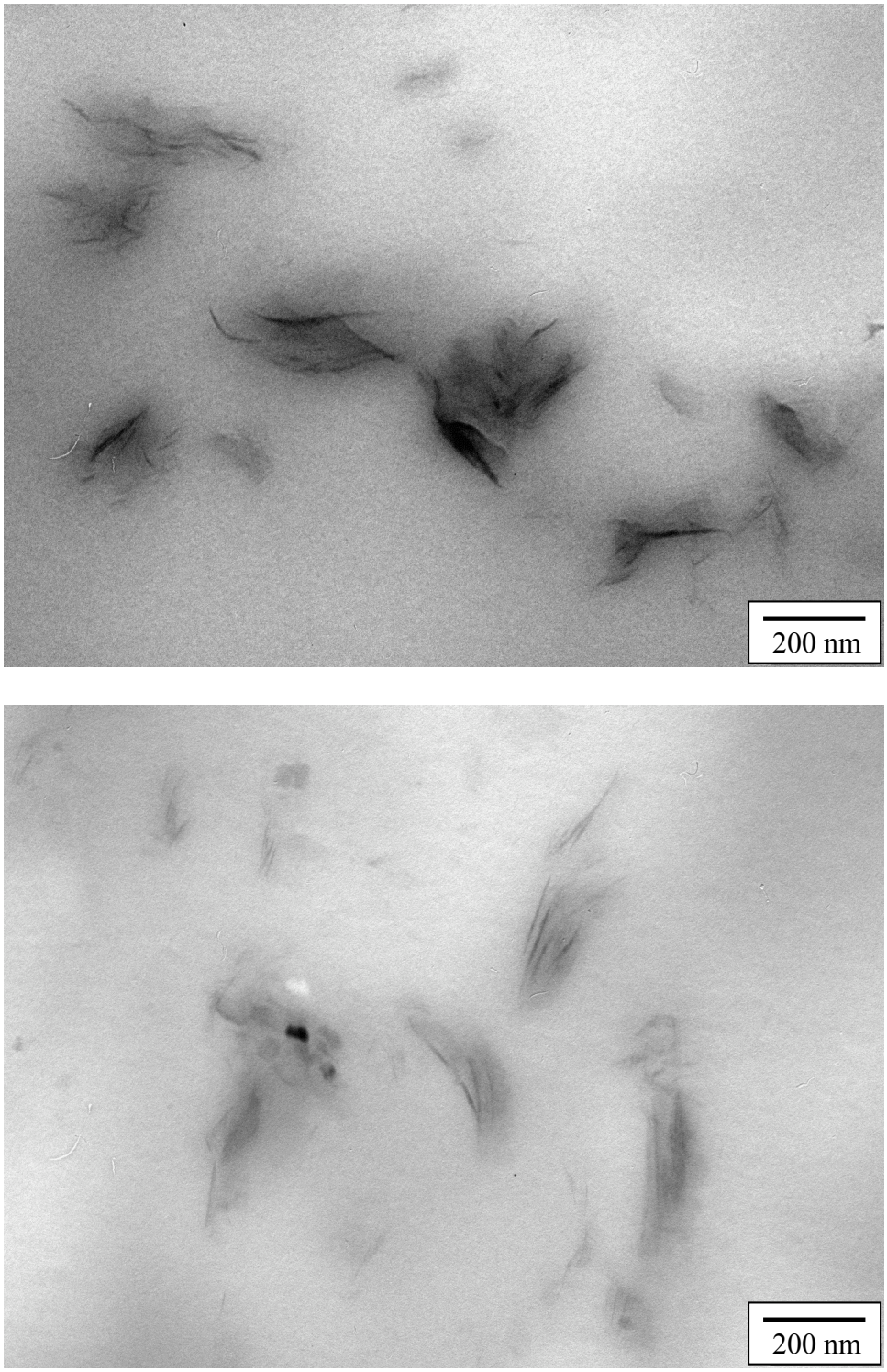


**Figure 4.9:** TEM micrographs of linear PP nanocomposites with untreated I.44P clay (PPNC-S6) (top) and with diamino dimethoxy silane treated I.44P clay (PPNC-S7) (bottom).

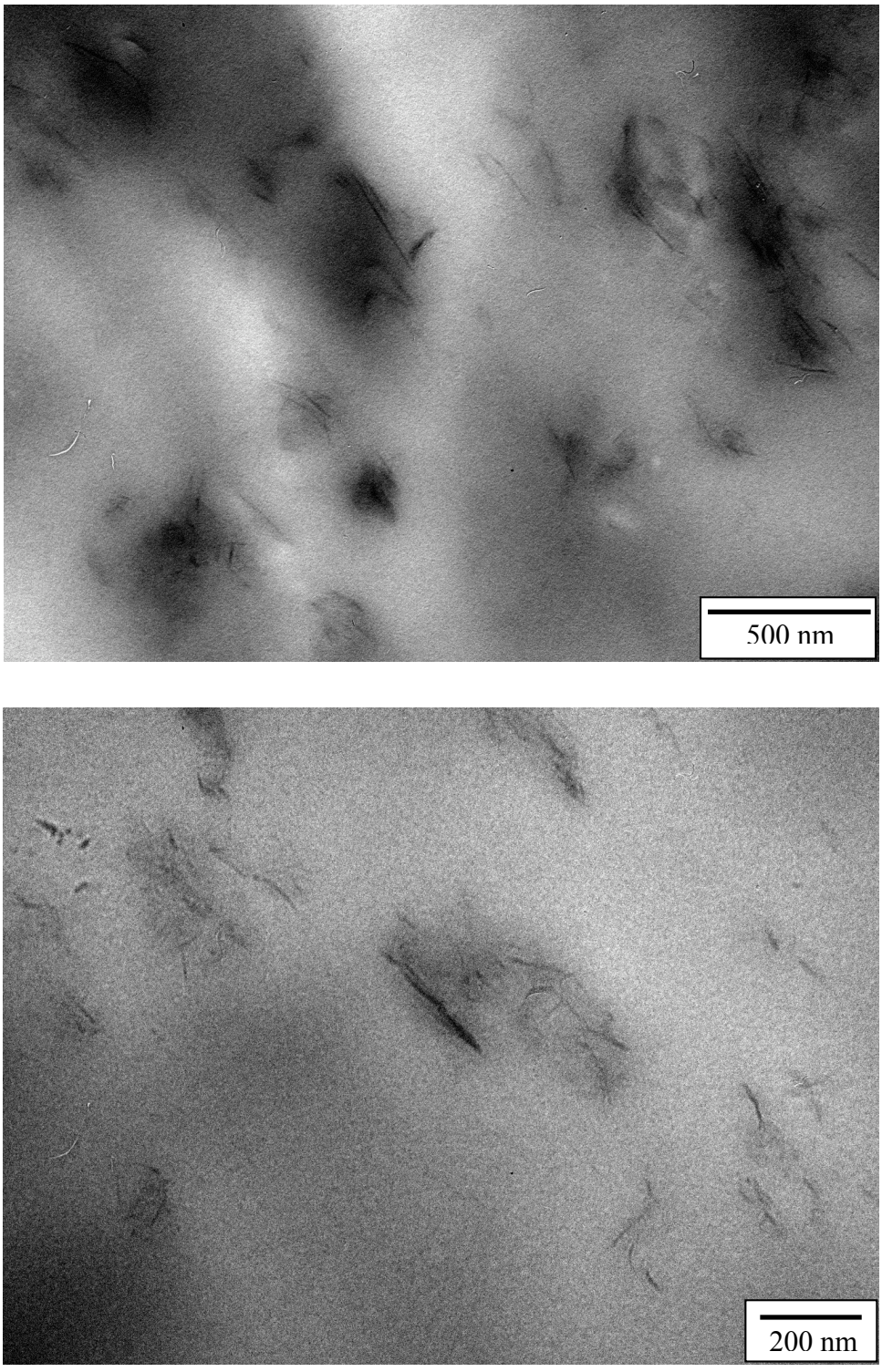


**Figure 4.10:** TEM micrographs of linear PP nanocomposites with untreated I.30P clay (PPNC-S11) (top) and with diamino dimethoxy silane treated I.30P clay (PPNC-S4) (bottom).

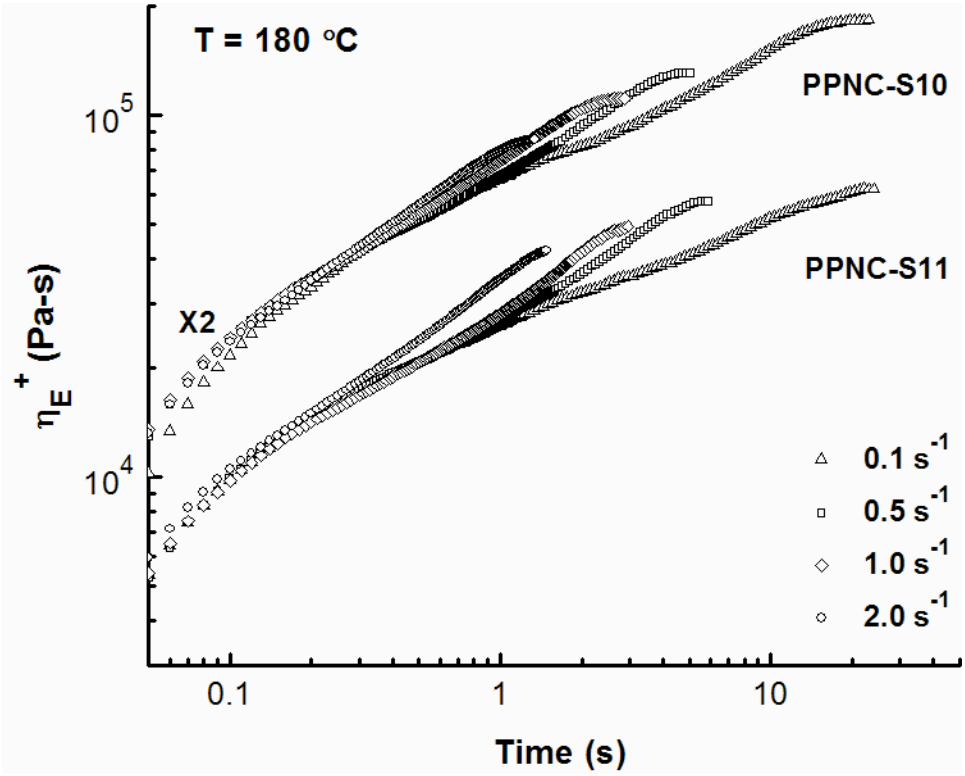


**Figure 4.11:** A comparison of melt extensional viscosity of PPNC-S10 (phenyl trimethoxy silated I.30P) and PPNC-S11 (unsilated I.30P) nanocomposites under uniaxial extensional flow.

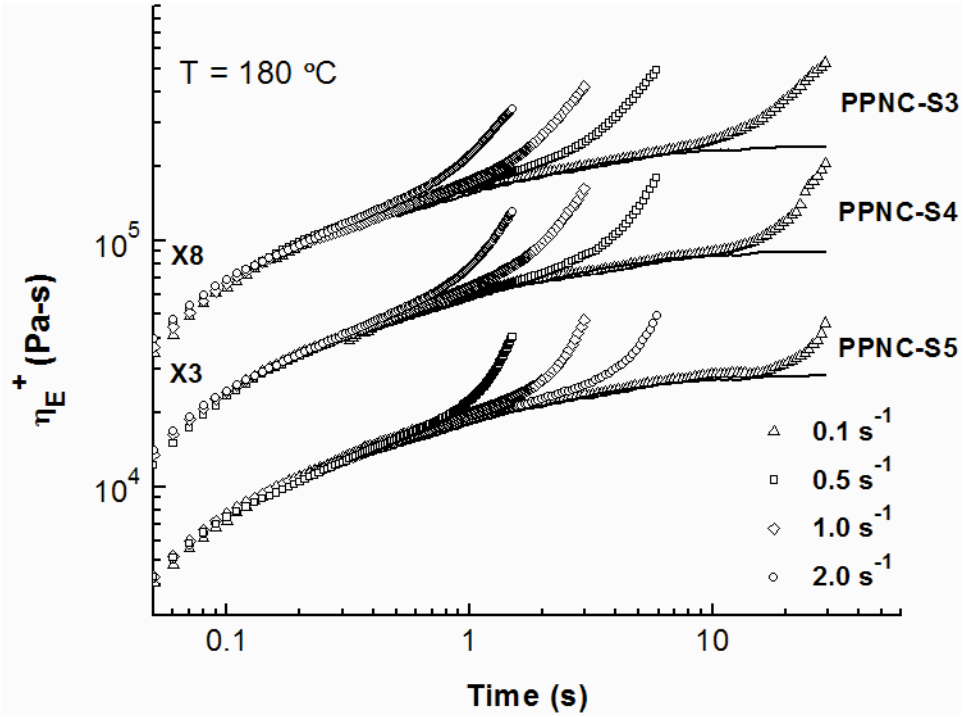


**Figure 4.12:** Effect of amino silane treatment of I.30P clay on the melt extensional viscosity of linear PP nanocomposites under uniaxial extensional flow. The number of hydrolysable groups has negligible effect on the strain hardening behavior of the nanocomposites.

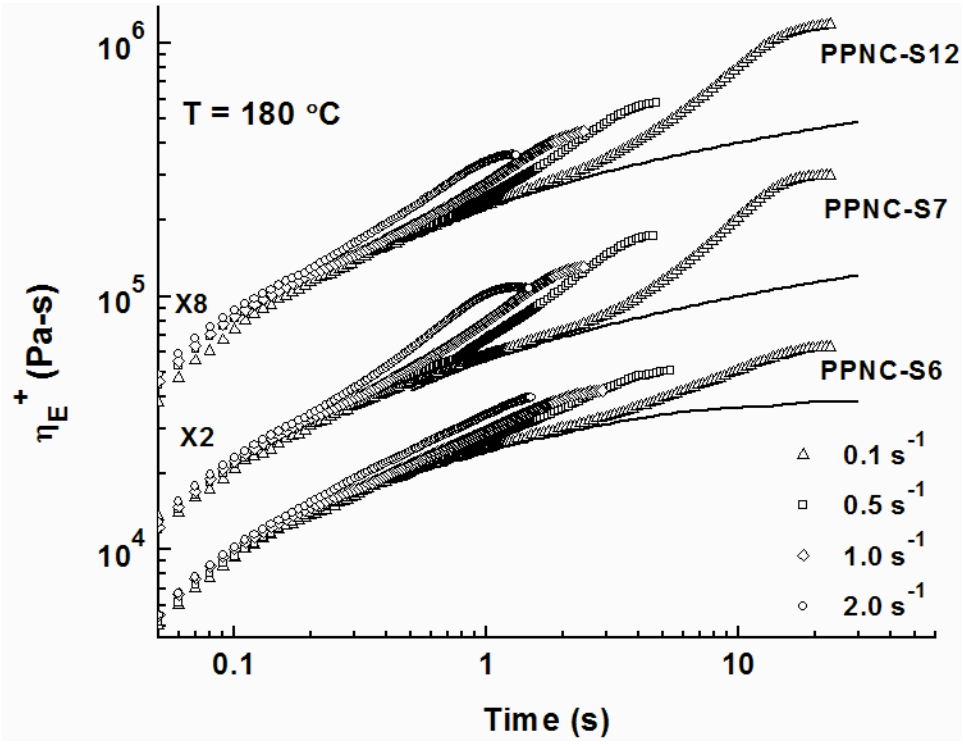


**Figure 4.13:** Effect of amino silane treatment of I.44P clay on the melt extensional viscosity of linear PP nanocomposites under uniaxial extensional flow.

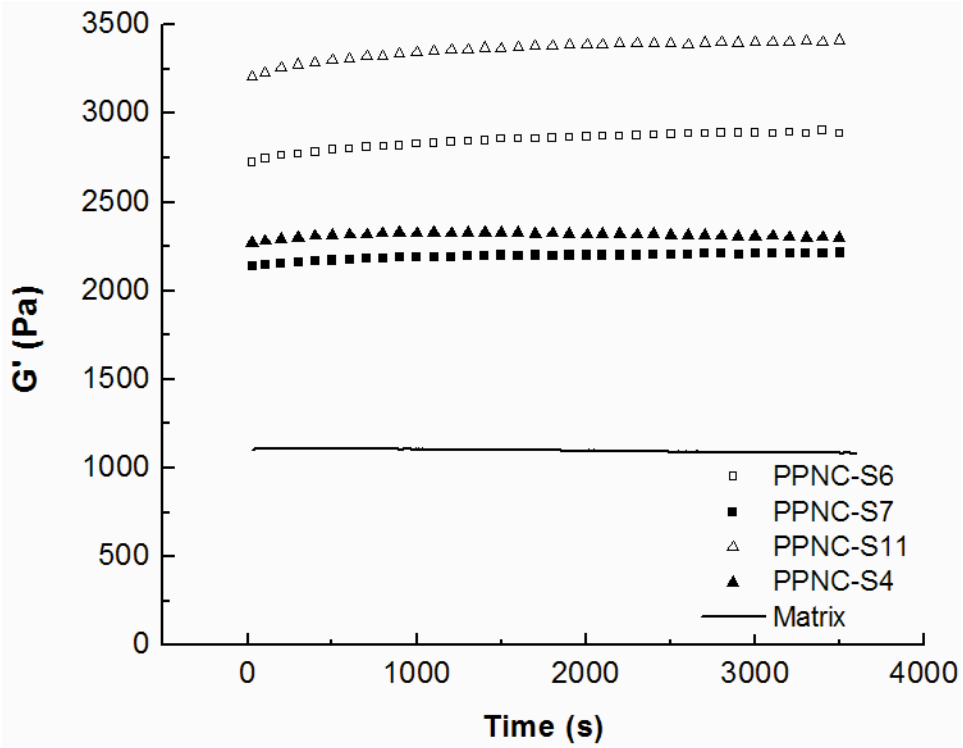


**Figure 4.14:** Dynamic time sweep test at 180°C for various PP nanocomposites along with its matrix (PP+compatibilizer).

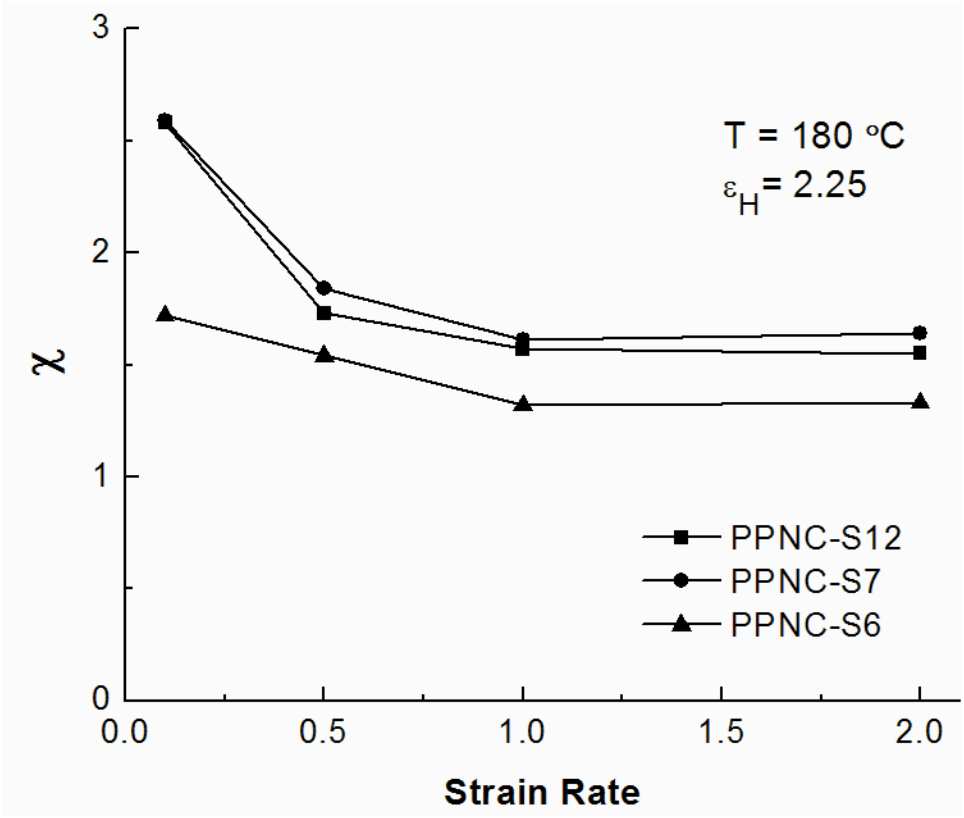


**Figure 4.15:** Variation of strain hardening parameter with strain rate for PPNCs prepared with silated I.44P clays.

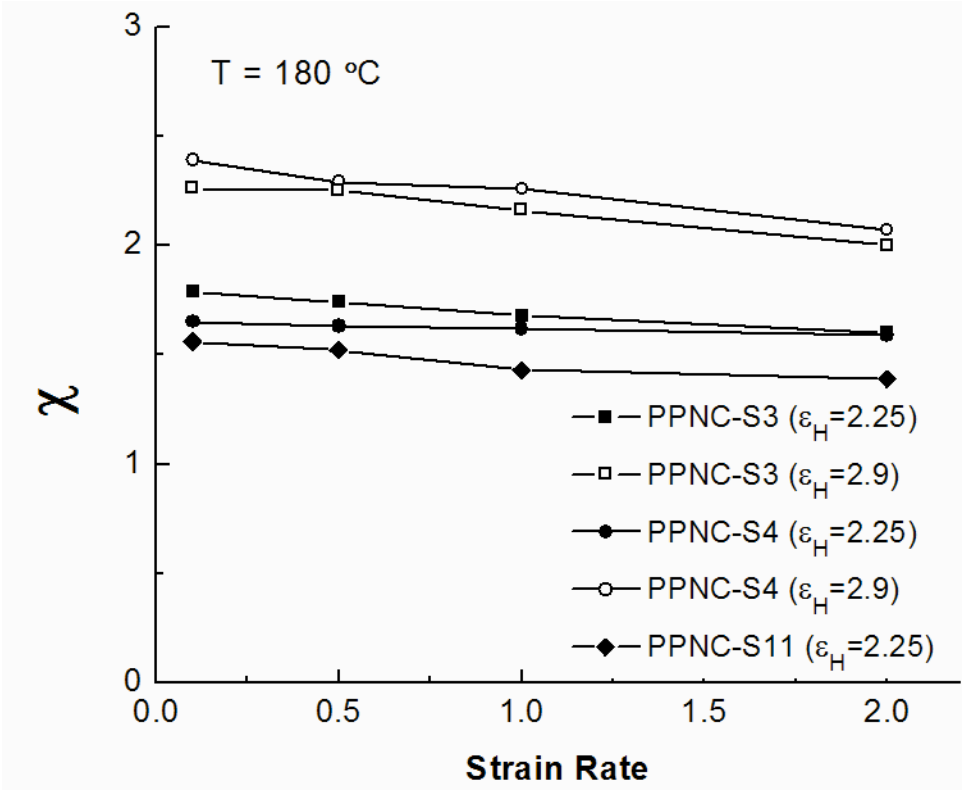


**Figure 4.16:** Variation of strain hardening parameter with strain rate for PPNCs prepared with silated I.30P clays. Open symbols are for Hencky strain = 2.9 and closed symbols are for Hencky strain = 2.25.

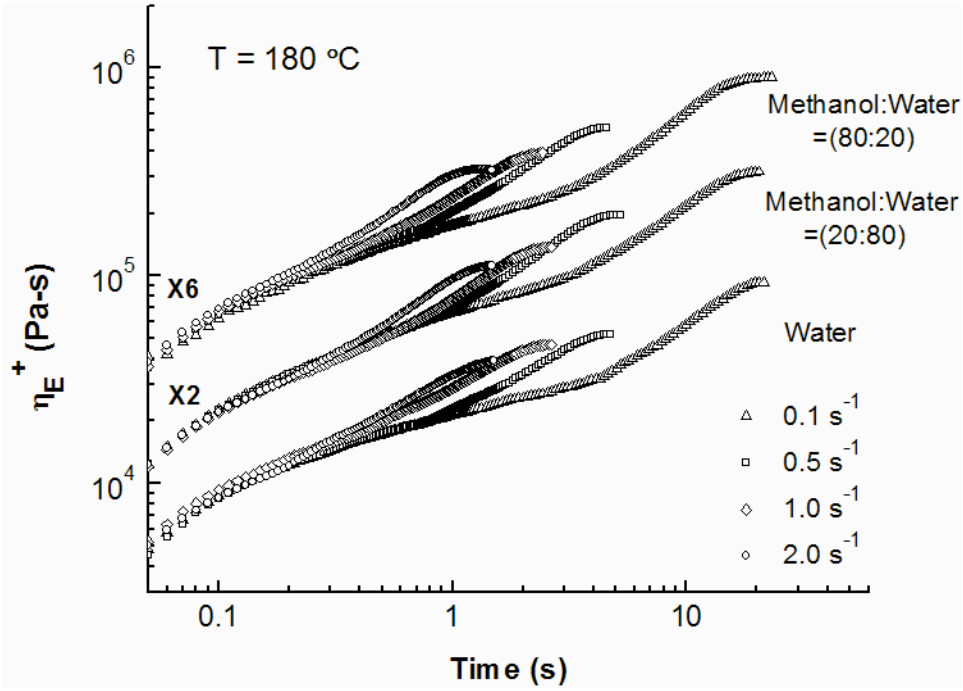


**Figure 4.17:** Effect of solvent used for silation process on melt extensional viscosity of PPNC-S7 nanocomposites.

# 5. CONTINUOUS FOAMING OF POLYPROPYLENE CLAY NANOCOMPOSITES HAVING DIFFERENT STRAIN HARDENING CHARACTERISTICS

## 5.1. Introduction

It is well established, as well as demonstrated in Chapter 3 that small cell and high cell density closed cell polymer foams can be produced only with melts showing strain hardening under uniaxial extensional flow [58, 100, 105, 106]. Linear PP displays lack of strain hardening under uniaxial extensional flow, hence foaming of linear PP, even in the presence of nanoparticles, have led to inferior quality foams [41, 42, 48, 121, 125]. Owing to its unique physical and mechanical properties along with its recyclability and affordability, linear PP foams can serve as an immediate replacement to market dominating polyurethane or polystyrene foams. TPOs, a blend of linear PP and an elastomer, have all the required properties necessary to replace the non-recycling polyurethane foams from automotive industry. Since linear PP is a major component of these TPOs, foaming of such materials has also been largely restricted due to its weak tensile melt strength. Various approaches have been adopted to increase the tensile melt strength of linear PP, for example, long chain branching [48, 58, 59, 116], cross-linking [44, 111, 112, 190] to eventually improve its foamability, but these approaches have strong impact on economy of foam production. As presented in Chapter 3, the novel approach of using organically modified montmorillonite nanoclays and high molecular weight PP-g-MA as the compatibilizer resulted in significant increase in the melt strain hardening behavior of linear PP nanocomposites. These strain hardening nanocomposites were tested for foaming performance and was compared with a blend of linear and branched PP. The results indicated that, even though both showed significant melt strain hardening under uniaxial elongational flow, due to

the presence of nanoparticles, serving as both strain hardening promoter and heterogeneous nucleating agent, linear PP nanocomposites resulted in foams with much smaller cell size and higher cell densities compared to the blend. The objective of this work is to study the extent and nature of melt strain hardening on the final foam properties.

As presented in Chapter 4, linear PP/clay nanocomposites prepared using an amino silane treated organoclays led to significant improvements in melt strain hardening under uniaxial extensional flow. This novel approach for improvements in strain hardening provided an opportunity to evaluate the effects and nature of strain hardening on foamability of linear PP.

The nature of strain hardening of polymer melts can be classified into two types. In one type (labeled Type – 1 here), the strain hardening increases or remains constant with increasing strain rate, e.g. branched polypropylene and low density polyethylene [191, 192]. In the other type (labeled Type - 2 here) strain hardening decreases with increasing strain rate, e.g. blends of linear and branched polypropylene [58, 116]. Stange et. al. [116] found that blends containing up to 50 wt% of long chain branched PP with linear PP showed a drop in strain hardening with increase in strain rates. This type of dependence of strain hardening on strain rates is also observed for metallocene-catalyzed ethylene–α olefin random copolymers with "sparse long-chain branching' [193] and with sparse long-chain branched PP [194].

Spitael and Macosko [59] have reported that larger cell sizes were obtained upon extrusion foaming tree-type branched PP (using carbon dioxide as the physical blowing agent) than with blends that displayed strain hardening decreasing with increasing strain rates. They attributed this to poorer crystallizability of the highly branched polypropylene. Results presented in Chapter 2, also show that crystallization kinetics indeed plays a significant role in the continuous foaming process of polypropylene, a semi-crystalline polymer. A slowly crystallizing

polymer allows the cells to develop before crystals starts growing compared to the polymer melt that crystallizes at a faster rate. Hence, in order to study the effect of strain hardening type or extent of strain hardening, it must be ensured that the crystallization kinetics of the polymers studied are comparable. Since the strain rate at which the foam cells are growing during foaming process is not well known, an attempt is made here to study the effect of change in strain hardening with strain rates on foamability of polymers.

In Chapter 2, the best PP nanocomposite foams produced in a continuous extrusion process using a CBA had an average cell size of 6.7 mm with an average cell density of $1.3x10^6$ cells/cc. The objectives of this work are to compare foams produced by extrusion with a chemical blowing agent from two different polypropylene nanocomposites with different types of strain hardening characteristic.

## 5.2. Materials and Experimental Procedures

Three different nanocomposites were used for this study, PPNC-S4, PPNC-S6 and PPNC-S7, all having 3 wt% of different organically treated montmorillonite clays and 12 wt% of the same compatibilizer, PP-g-MA (Exxelor PO 1015). PPNC-S6 is prepared with I.44P organoclay while PPNC-S7 is prepared with diamino dimethoxy silane treated I.44P and PPNC-S4 was prepared with diamino dimethoxy silane treated I.30P. These nanocomposites were characterized in detail and the results are presented in Chapter 3 and 4. These nanocomposites were foamed in a single screw extruder using 3 wt% of the CBA. PPNC-S6 was foamed using a 2mm diameter die with L/D = 15 while the other two nanocomposites were foamed using a higher L/D = 20. The first three temperature zones were maintained at the same temperature for all the three nanocomposites (180 ºC, 200 ºC and 175 ºC respectively), however the die exit

temperature was maintained at 15 ºC above the crystallization temperature for PPNC-S4 and PPNC-S7 while the same for extruding PPNC-S6 foam was maintained at 35 ºC above the crystallization temperature. This was done so as to maintain an overall constant pressure drop (~ 4000psi) across the die. The resulting foam extrudates were characterized for the foam cellular structure using SEM. The details of all the procedures are presented in Chapter 2.

## 5.3. Results and Discussion

Nonisothermal crystallization exotherms obtained from cooling ramps in DSC tests have been compared for PPNC-S4, PPNC-S6 and PPNC-S7 in Figure 5.1. The DSC exotherms show that the nature of crystallization (crystallization temperature and the rate of crystallization) is similar for all the three PP/clay nanocomposites; hence any changes in the foaming behavior of these nanocomposites cannot be attributed to differences in crystallization behavior.

The nanocomposites studied in this section had two different type of strain hardening behavior. PPNC-S4 showed more like Type – 1 strain hardening, while PPNC-S6 and PPNC-S7 had Type – 2 strain hardening characteristics, with PPNC-S7 having greater strain hardening parameter than PPNC-S6. These are presented in details in Chapter 4. The thermal characteristics of these nanocomposites are comparable which is in contrast to different blends of linear and branched PP. In blends of linear and branched PP, as the proportion of linear PP is increased, the strain hardening characteristics changes from Type – 1 to Type – 2. Naguib and coworkers [195] have studied the effect of blends of linear and branched PP on foamability. The crystallization temperature of the blend increases with the increase in branched resin and they reported that the optimum temperature for producing foams with maximum volume expansion ratio decreases with increase in branched resin. In this work, we have successfully prepared nanocomposites

with different strain hardening characteristics while keeping the thermal characteristics comparable, in order to study the effect of different type and extent of strain hardening characteristics on foaming.

Various theoretical and experimental studies [196-199] have shown the evolution of foam cell size with time. Figure 5.2 shows the nature of the foam cell evolution with time. Cell size growth with time profile indicates that the strain rates (slope of the curve) experienced by smaller cells are much higher than the rates at which the strain hardening measurements are conducted. For an extrusion foaming set-up, the highest strain rates are generally experienced within the diverging section of the die, represented as Zone I. Immediately after the foam extrudate exits the die region, the polymer starts to crystallize and arrest further growth of cell size. This is represented as Zone II in Figure 5.1. Hence, in order to produce foams with cell sizes in the range of microcellular regime, the polymer melt should show strain hardening behavior at higher strain rates. With the nature of Type – 1 strain hardening behavior, it is possible that the polymer melt would show higher strain hardening behavior inside the die region (zone I) compared to Type – 2 polymer melt. This would result in more controlled and smaller cell size at the end of zone I for Type – 1 strain hardening melt compared to Type – II melt. Since the nanocomposites studied in this section are based on same compatibilizer and linear PP, time taken for the melt to crystallize after exiting zone I would be similar which is also evident from the DSC exotherms presented in Figure 5.1. Based on this hypothesis, it should be expected that PPNC-S4 should result in foams with smallest possible cell size within the limitation of the experimental conditions.

The SEM images for the cellular structures of polypropylene-clay nanocomposite foam samples are shown in Figures 5.3 – 5.5, and the cell size distributions are presented in Figures

5.6 – 5.8. A comparison between the SEM micrographs of PPNC-S6 and PPNC-S7 shows that, PPNC-S7 results in foams with smaller cells and greater cell density as compared to PPNC-S6. The average cell size and cell density of PPNC-S6 foam is 87.9 μm and $1.2x10^6$ cell/$cm^3$ respectively while that for PPNC-S7 foam is 60.98 μm and $2.7x10^6$ cells/$cm^3$. Even though both these nanocomposites have same amount of nanoclays and Type – 2 strain hardening characteristics, PPNC-S7 shows higher strain hardening behavior, thereby resulting in foams with smaller cell size and higher cell density. This is presumably due to greater strain hardening parameter of PPNC-S7 compared to PPNC-S6, in the range of strain rates encountered during cell growth, arrested the growth of foam cells and restricted the cell size to lower values.

In order to compare the effect of strain hardening type, SEM images of PPNC-S4 and PPNC-S7 foams are compared. Both have similar strain hardening parameter in the range of strain rates tested, however PPNC-S7 shows a gradual drop in the strain hardening parameter with increase in strain rates, while PPNC-S4 shows an almost constant strain hardening parameter. The average cell size and cell density of PPNC-S4 nanocomposite foam is 37.09μm and $6.2x10^6$ cells/$cm^3$ respectively. This shows that polymer melts with higher strain hardening parameter along with Type – 1 nature of the strain hardening behavior can lead to closed cell foams with smaller cell sizes and higher cell densities compared to Type – 2 melts. Since, the strain rate of a growing bubble or cell is inversely proportional to its size, hence in order to arrest the growth of cell size, strain hardening of polymer melts under uniaxial extensional flow at higher rates is more important for foaming applications. This behavior is also reflected from the cell size distributions presented in Figures 5.4 – 5.6. PPNC-S4 has maximum fraction of cells in the range of 20 – 40 μm while the same for PPNC-S7 is in the range of 40 – 60 μm. A summary

of all the foam results is presented in Figure 5.8, which clearly shows superior foam characteristics of Type – 1 strain hardening melt.

## 5.4. Conclusions

The importance of effect of extent and nature of strain hardening behavior on foamability of polypropylene/clay nanocomposites was studied in this section. Nanocomposites with different types of strain hardening behavior were tested for foam evaluation. A comparison of foam quality (average cell size and cell density) produced by nanocomposites prepared by silated and un-silated organoclays was presented in this section. The polymer melt that shows significant strain hardening at the lowest strain rate but has very little strain hardening at the higher strain rates (Type – 2) resulted in foams with cell sizes that are larger than polymer melts displaying a steady strain hardening at all rates (Type – 1), indicating that the cell growth is arrested at a smaller cell size in the presence of Type – 1 strain hardening than in the presence of Type – 2 strain hardening.

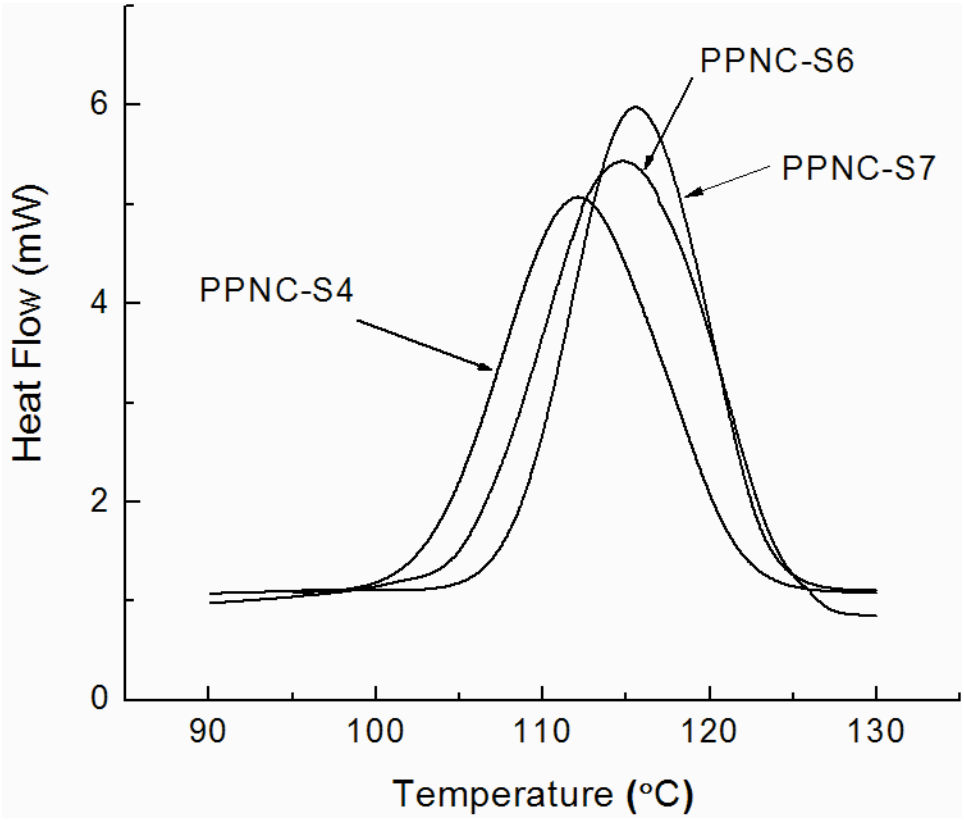


**Figure 5.1:** Non-isothermal crystallization exotherm for linear PP/clay nanocomposites prepared using 85 wt% linear PP, 12 wt% PO 1015 and 3 wt% of different treated organoclays.

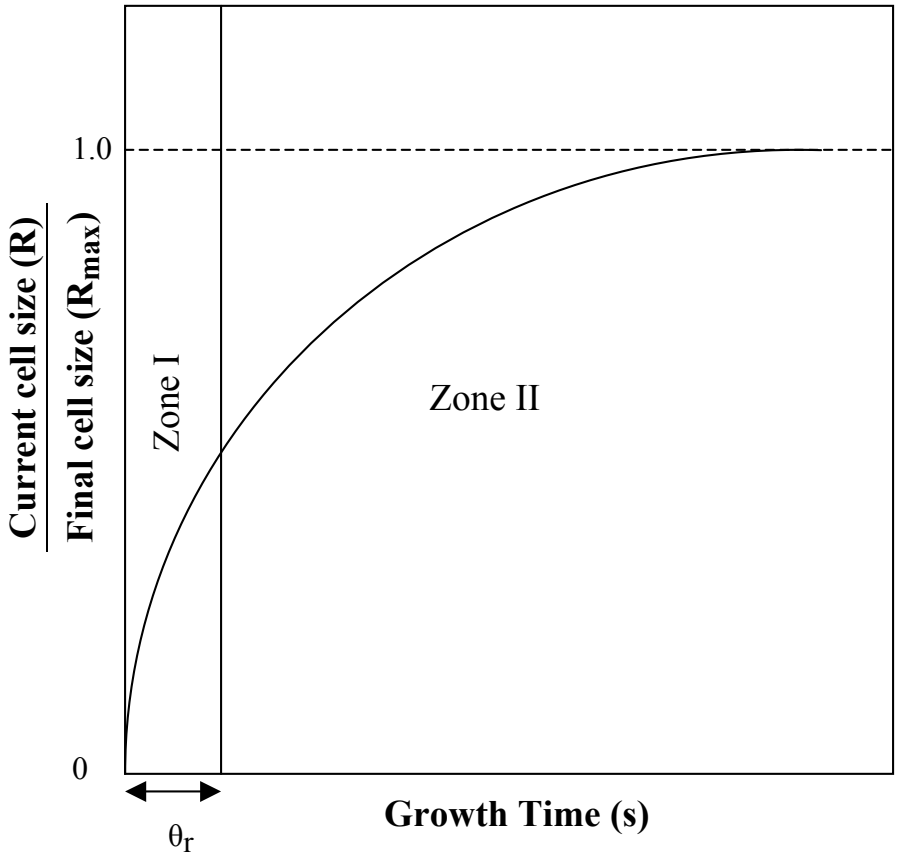


**Figure 5.2:** Evolution of cell size as a function of time demonstrated by various theoretical and experimental work [196-199]. ($\theta_r$ represents the residence time in the die)

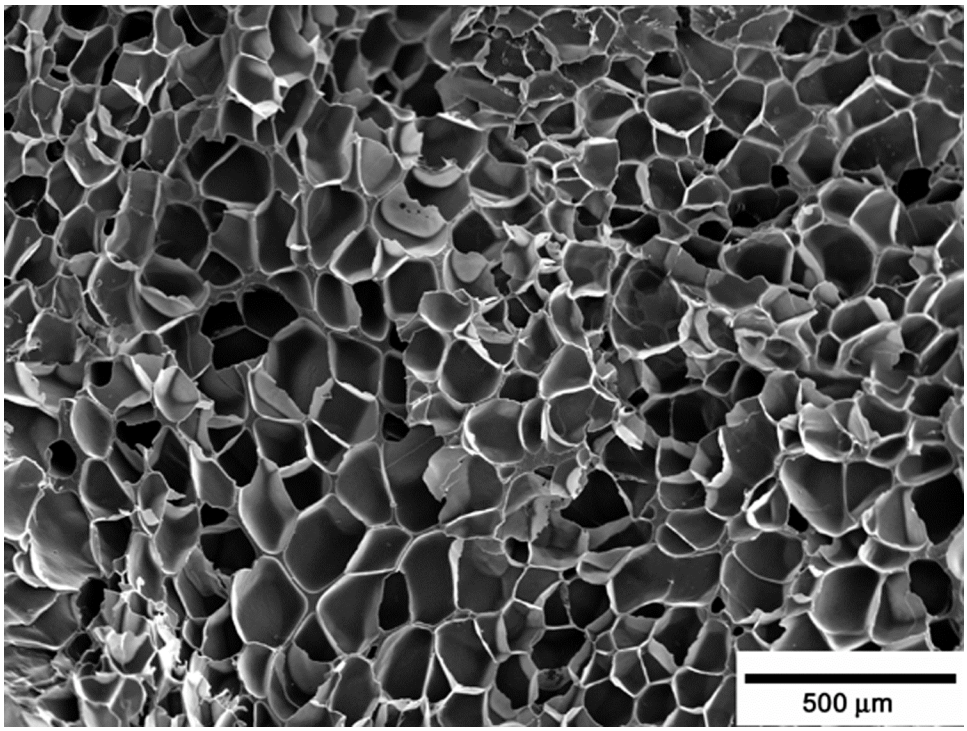


**Figure 5.3:** Scanning electron micrograph of PPNC-S6 (prepared using 3 wt% of unsilated I.44P) foam extrudate.

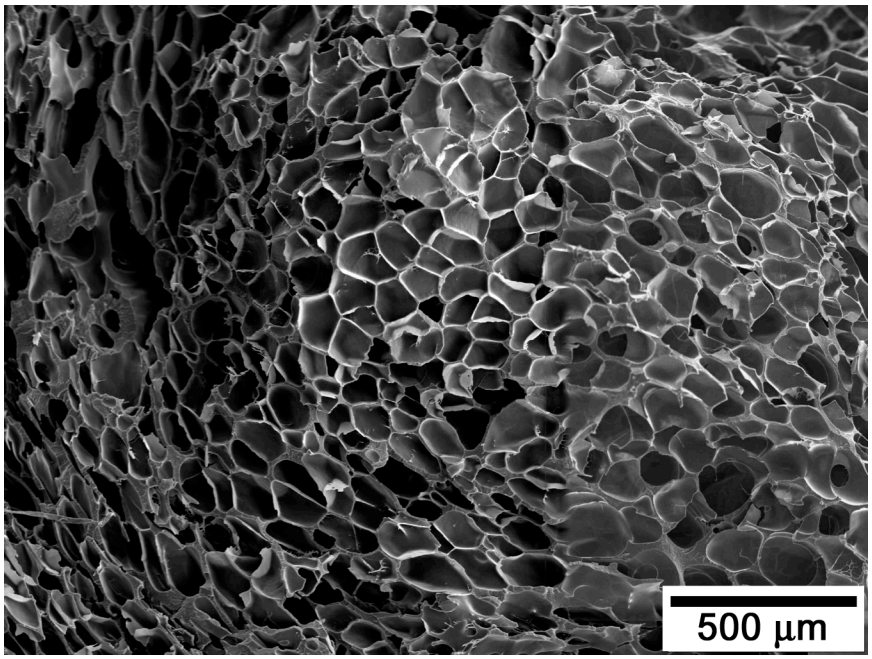


**Figure 5.4:** Scanning electron micrograph of PPNC-S7 (prepared using 3 wt% of diamino dimethoxy silane treated I.44P organoclay) foam extrudate.

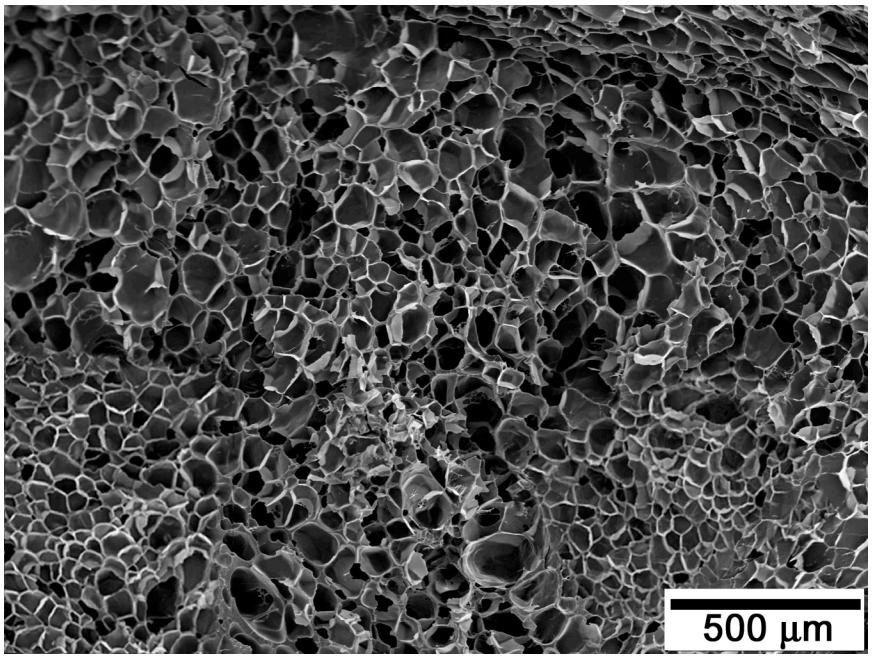


**Figure 5.5:** Scanning electron micrograph of PPNC-S4 (prepared using 3 wt% of diamino dimethoxy silane treated I.30P organoclay) foam extrudate.

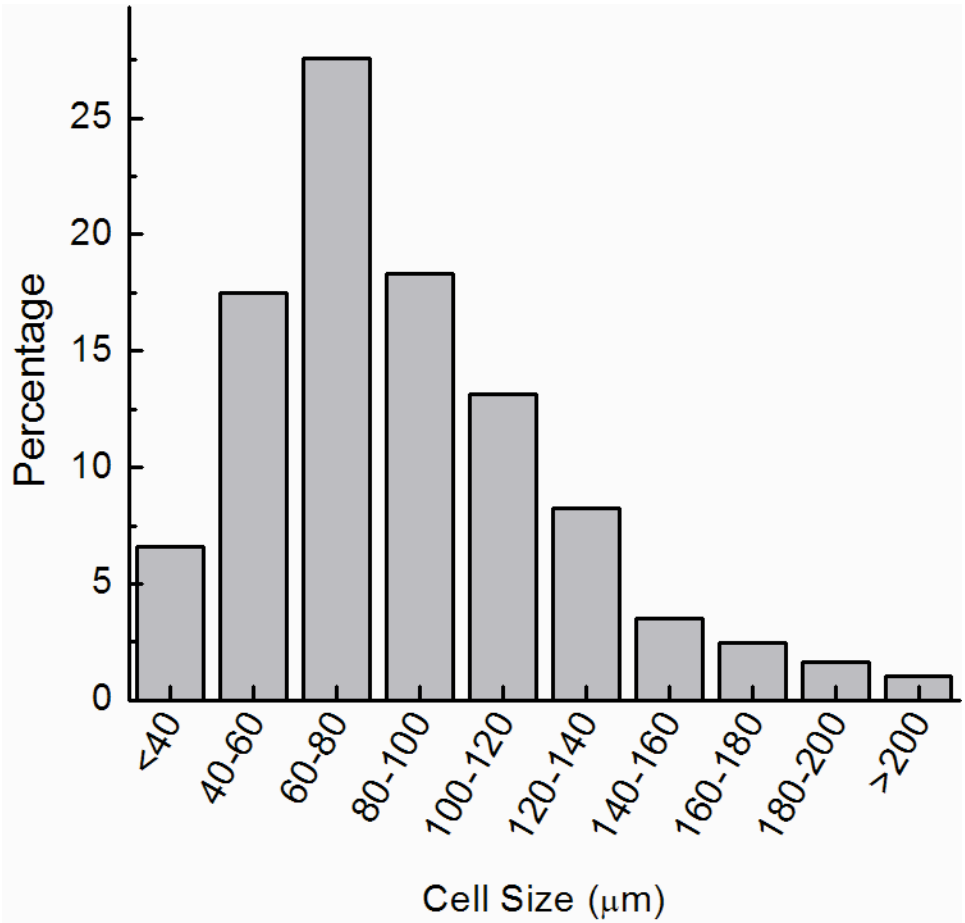


**Figure 5.6:** Cell size distribution of PPNC-S6 foam.

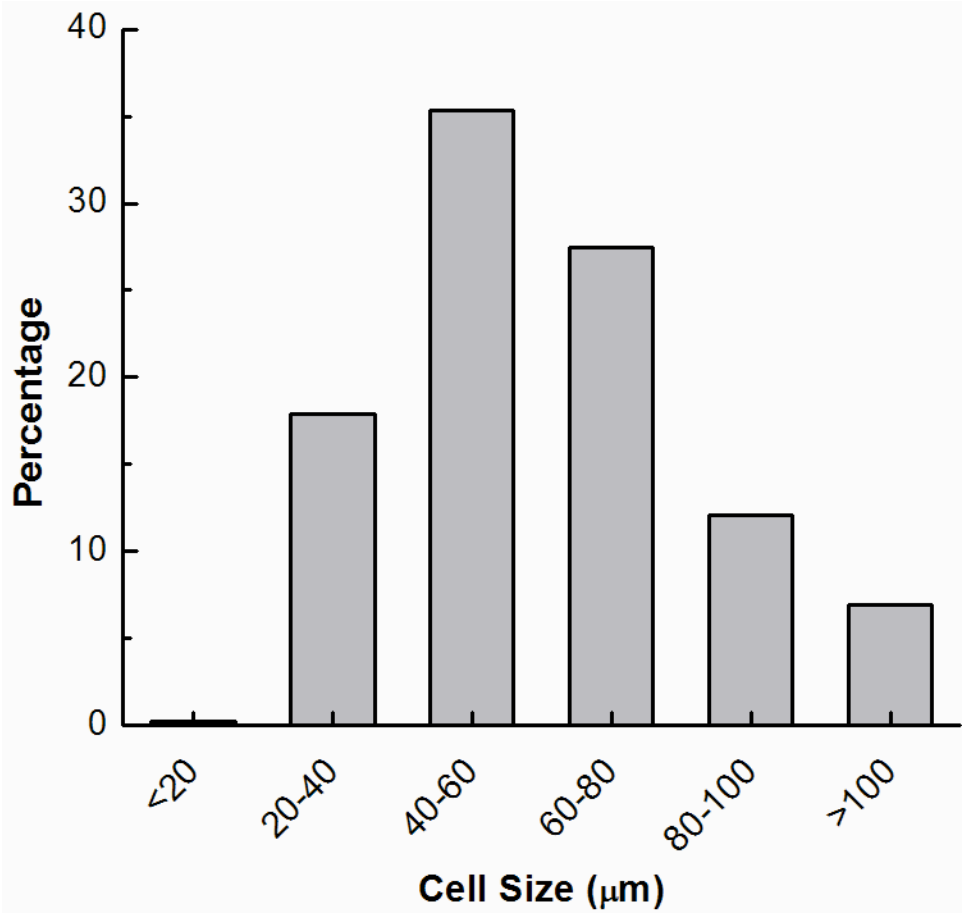


**Figure 5.7:** Cell size distribution of PPNC-S7 foam.

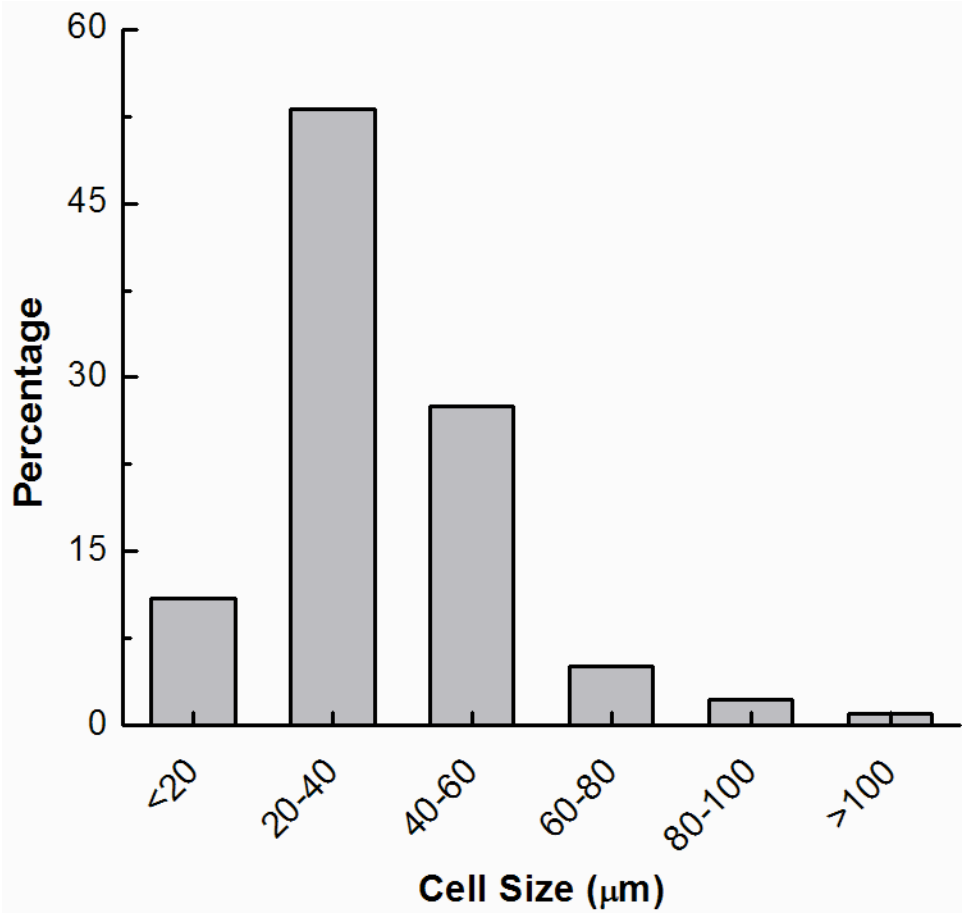


**Figure 5.8:** Cell size distribution of PPNC-S4 foam.

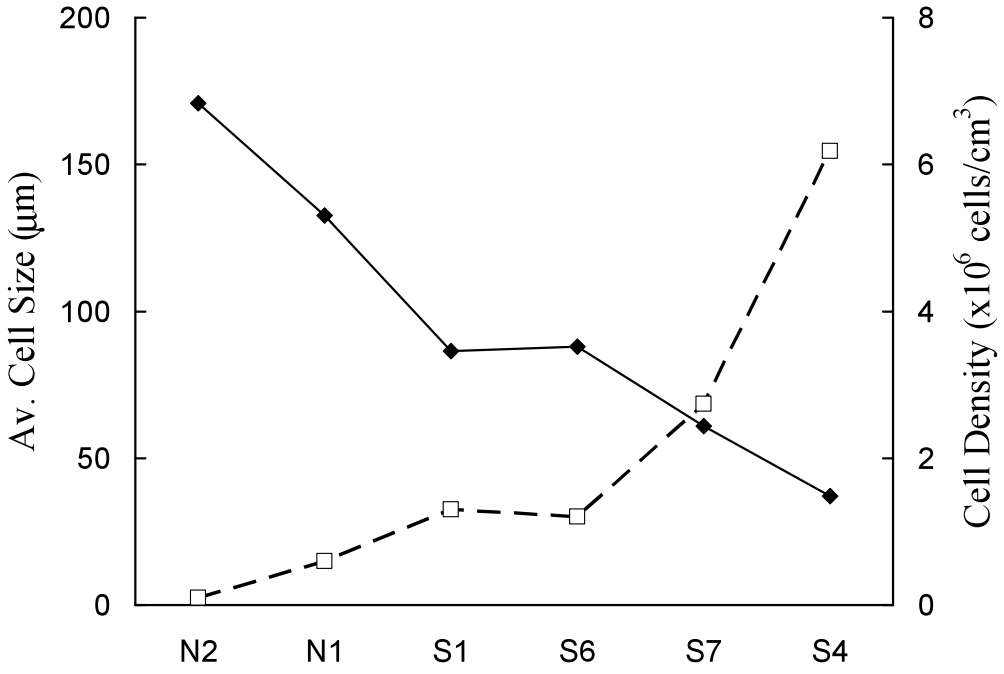


**Figure 5.9:** Progressive decrease in cell size and increase in cell density as a function of material property of linear PP/clay nanocomposite.

# 6. EFFECT OF COMPATIBILIZER PROPERTIES ON STRAIN HARDENING BEHAVIOR OF POLYPROPYLENE CLAY NANOCOMPOSITES

## 6.1. Introduction

Polymer nanocomposite is a field of research that has been studied in great detail over the past two decades. Interest in polymer nanocomposites has been results of improvements in their various physical and mechanical properties due to the addition of a small amount of anisotropic nanoparticles in the polymer matrix [73, 74]. Amongst all nanofillers, nanoclays are most widely studied probably because of its availability and cost.

Polymer/layered silicate (PLS) nanocomposites are synthesized by dispersing nano silicate layers in the polymer matrix. In order to achieve better dispersion of these nanolayers, the naturally occurring montmorillonite has to be organically modified to synthesize polymer compatible nanoclay. In order to facilitate the interaction between the hydrophilic clay layers and hydrophobic polymers, the galleries of the clay tactoids are intercalated with long chain alkyl ammonium surfactants [77-81].

Even with the organic functionalization of montmorillonites, the intercalation of hydrophobic polypropylene in the organically modified montmorillonites is difficult and is generally facilitated by the use of less hydrophobic compatibilizers. These compatibilizers are, in general, polypropylene functionalized by grafting hydroxyl groups or more commonly maleic anhydride groups at the ends of the polyolefin chains [78, 86, 87]. Okada et al. [88] were the first to demonstrate the use of polypropylene-grafted maleic anhydride (PP-g-MA) as a compatibilizer to synthesize PP-clay nanocomposites. Since then the importance of such polar compatibilizers for the use in non-polar clay nanocomposite preparation is well demonstrated by

various researchers [86, 89-94]. The effect of maleic anhydride content and molecular weight of the PP-g-MA on the dispersion of nanoclays in polypropylene nanocomposites have been studied thoroughly by various researchers [136, 200-203]. Both these factors along with the loading of the compatibilizer significantly affect the extent of polymer intercalation and subsequent improvement in various physical and mechanical properties. Marchant and Jayaraman [136] reported that optimum loading of the compatibilizer and higher maleic anhydride content resulted in exfoliated structure of PP nanocomposites. The effect of molecular weight, maleic anhydride content and loading of PP-g-MA was investigated by Wang et al. [161, 204]. They reported that compatibilizers with lower melt flow index (higher molecular weight) leads to better dispersion of the clay layers in the PP matrix. It is well established that state of dispersion of these nanoparticles significantly affect the rheological properties in shear flow [69-71, 74, 78], however very limited research has been done on the effect of PP-g-MA material properties on extensional rheology of polypropylene nanocomposites.

It has been well established that maleation of linear polypropylene leads to reduction in the molecular weight of the resulting PP-g-MA due to chain scission [205]. The grafting process of maleic anhydride (MA) groups onto polypropylene follows a free radical mechanism, in presence of organic peroxide [206, 207]. Due to the complexity of the grafting mechanism, two different grafting mechanisms have been proposed in the literature; one where the MA groups are distributed along the length of the PP chain as succinic anhydride units [208, 209], and other where the MA groups are grafted only at the polypropylene chain-ends [210-212]. Sclavons et al. [212] have recently validated the later mechanism of MA grafting at the chain-ends of polypropylene by thorough FTIR studies. Further in their study they have mentioned that apart from being grafted at the chain-ends, MA groups are present in a cluster of more than one unit.

The objective of this research is to understand or even propose a plausible explanation that can help understand the role of compatibilizer in the strain hardening mechanism of linear polypropylene/clay nanocomposites.

## 6.2. Materials and Experimental Procedures

Several compatibilizers were selected in order to understand the effect of molecular details of PP-g-MA on the strain hardening of the resulting PP/clay nanocomposites. The variables that led to the selection of these compatibilizers were molecular weight, maleic anhydride content and the molecular structure of the resulting PP-g-MA. Maleic anhydride can be grafted either on PP homopolymer or a copolymer. Based on these factors the various compatibilizers used in this study were AC950, Exxelor PO 1015, Exxelor PO 1020, Bondyram 1001CN, and Bondyram 1001; the details of which are listed in Table 2.1 and the details of corresponding nanocomposites are tabulated in Table 6.1.

The nanocomposites were characterized for their structural morphology and for their rheological behavior in both shear and uniaxial extensional flow.

## 6.3. Results and Discussion

### 6.3.1. Uniaxial extensional rheology

The melt extensional viscosity curves presented in Figures 6.1-6.3 compares the effect of molecular weight and molecular structure of the PP-g-MA on strain hardening behavior of linear PP/clay nanocomposites. The strain hardening data suggests that certain minimum molecular weight is required below which strain hardening is not observed in PP/clay nanocomposites.

Strain hardening in branched polymer melts undergoing extensional flow has been attributed to slowly relaxing chain stretch by Larson and McLeish [213]. The dynamics of entanglements involving the branches is accounted for by a chain relaxation equation in addition to the dynamics of the main chain or backbone. Alternatively, strain hardening in the melt has been attributed to compression of the tube around the main chain which amounts to an increase in the entanglement density along the chain by Wagner et al. [214-218].

In cases where strain hardening in polymer melts has been achieved by partial crosslinking of the polymer chains, the phenomenon has been attributed to the trapped entanglements between crosslink junctions. Blends of linear polypropylene with small amounts of chemically crosslinked polymers contain trapped entanglements on chain segments between crosslinks or junctions which respond to stretching differently from entanglements and chain segments in the bulk – cf. Yamaguchi and Suzuki [153] and Yamaguchi [152]. Ogura et al. [190] have also indicated that this effect will be lost upon excessive crosslinking.

The mechanism of strain hardening in linear PP – clay nanocomposite melts appear to be analogous to that reported for blends containing small amounts of crosslinked polymers. Linkages or interactions between the clay surface or edge and the maleated polymer can form a network of "physical crosslinks" or anchor points between which entanglements may be trapped to produce a similar effect. In nanocomposites where the organoclay was used without additional treatment, hydrogen bonding between the hydroxyl groups of the organoclays and the maleic anhydride group of the compatibilizer holds the compatibilizer chains and the clay together. Since MA groups are primarily grafted as multiple clusters at the chain-ends, a maximum of four to six MA groups are available per chain for a maleated homopolymer [212]. However, in case

of a maleated PP-PE copolymer, there could be several MA groups all across the chain length, as shown in Figure 6.5.

Comparison of strain hardening data (Figure 6.1) for nanocomposites with compatibilizers having different molecular weight and therefore different chain lengths (PPNC-N2, PPNC-S6 and PPNC-S13) revealed that the length of compatibilizing polymer chain that is anchored at one or more clay surfaces is critical because it determines the number of trapped entanglements along the chains that bridge between clay surfaces or edges. Trapped entanglements and the chains which bridge between the clay edges or surfaces respond to stretch differently from chains and entanglements in the bulk polymer and produce strain hardening in the melt. However, a comparison between PPNC-S6 and PPNC-S13 suggests that beyond a sufficient molecular weight, a further increase in molecular weight do not translate to progressive increase in the strain hardening property of the nanocomposite prepared with organoclays without further treatment. This is despite the fact that PPNC-S6 has maleated copolymer that has greater number of MA groups along the chain that can interact with the organoclays. This is because, the strength of such interaction is still dictated by weaker hydrogen bonding, which limits further improvements in strain hardening.

A comparison between PPNC-S7 and PPNC-S14 (Figure 6.2) and PPNC-S16 and PPNC-S17 (Figure 6.3) is made to understand the effect of molecular structure of the PP-g-MA on the strain hardening of the nanocomposites. In this case, diamino dimethoxy silane grafted I.44P was used to prepare the nanocomposites. As mentioned in Chapter 4, the amino silanes grafted on the clay faces and/or edges can react with the maleic anhydride groups to replace the weaker forces of attraction with stronger chemical bonds. Chemical reactions between the silated clays and maleated PP-PE copolymer (PO 1015) resulted in nanocomposites with significant increase in

melt strain hardening compared to the unsilated clay nanocomposites. However, the same was not true with nanocomposites prepared with maleated PP homopolymer (PO1020). This could be due to the additional grafting of maleic anhydride on copolymer backbone or it could also be due to the difference in the molecular weight between the two compatibilizers. Strain hardening comparison between PPNC-S16 and PPNC-S17 shows that molecular weight or the chain length of the compatibilizer is more important than the molecular structure of the compatibilizer. PPNC-S16 is prepared from Bondyram 1001CN which is a propylene-ethylene copolymer while PPNC-S17 is prepared from Bondyram 1001 which is a homopolymer and both the Bondyram compatibilizers have comparable molecular weight (as MFR is same for both of them). This confirms that longer chain length results in greater number of trapped entanglements along the chains that bridge between clay surfaces and edges. The entangled polymer-clay structure when stretched under uniaxial extensional flow, forces the clay and the polymer chains to orient along the direction of the stretch. The orientation of the clay platelets has been confirmed by conducting TEM on a stretched specimen (Figure 6.6). Since the polymer chains are anchored to the clay edges and/or faces, the relaxation mechanism of the chain stretch would slow down increasing the chain stretch relaxation time.

To further understand the strain hardening mechanism, nanocomposites prepared using Bondyram 1001CN and Bondyram 1001 were studied. Strain hardening curves for PPNC-N3, PPNC-S15, PPNC-S16 and PPNC-S17 are presented in Figure 6.3 and 6.4. A comparison between PPNC-S16 and PPNC-N3 shows the effect of compatibilizer to nanoclays ratio on strain hardening. With the same compatibilizer and the clay being used in these two nanocomposites, as the ratio of compatibilizer to clay is increased from 4 to 7, strain hardening increases. This suggests that some minimum polymer-clay interaction is required for strain hardening to appear.

Shear rheology has been used to get a qualitative idea of extent of entanglement formed in various polypropylene clay nanocomposite systems. It has been well reported that with the increase in polymer-particle interaction, the low frequency plateau modulus also increases [74, 92, 155]. Figure 6.7 shows the variation of storage modulus (G') with frequency for various nanocomposites prepared using Bondyram 1001CN and Bondyram 1001 as the compatibilizer. A comparison between the matrix and the nanocomposites shows that with the addition of 3 wt% of nanoclays the low frequency storage modulus increases confirming the there indeed exists significant polymer-particle interaction. However, the low frequency plateau modulus cannot be seen from such plots. An alternative way to estimate the low frequency plateau modulus is by the use of van-Gurp Palmen (vGP) plots, a plot of phase angle ($\delta$) against the complex shear modulus ($G^*$). A minimum at low frequency region in the vGP plot is an estimate of low frequency plateau modulus of a polymer melt. For linear polymer melts or melts with high poly-dispersity index, the vGP plot generally shows a monotonic decrease in the phase angle [219, 220]. Figure 6.8 shows the vGP plot for linear PP/clay nanocomposites with Bondyram 1001CN and Bondyram 1001 as the compatibilizer. A prominent minimum is observed for PPNC-S15, PPNC-S16 and PPNC-S17 nanocomposites; however the vGP plot shows a monotonic drop in the phase angle for PPNC-N3 nanocomposite and the polymer matrix (linear PP and compatibilizer in the appropriate ratio). This suggests that the polymer-particle interaction is greatest in case of PPNC-S15 and PPNC-S17 followed by PPNC-S16 and it is outside the test range for PPNC-N3 and the matrix. The melt extensional viscosity data for PPNC-S15, PPNC-S16 and PPNC-S17 shows that these nanocomposites melts show significant strain hardening behavior while PPNC-N3 and the polymer matrix do not show such phenomenon. This confirms that the presence of strain hardening in these nanocomposites is due to greater polymer-particle

interaction. The absence of strain hardening in PPNC-N3 could thus be due to insufficient interactions due to low amount of PP-g-MA. Further a comparison between PPNC-S15, PPNC-S16 and PPNC-S17 shows that the low frequency plateau modulus is greater for PPNC-S15 and PPNC-S17 melts, which explains why PPNC-S16 shows lower extent of strain hardening behavior compared to PPNC-S15 and PPNC-S17.

## 6.4. Conclusions

In composites where the organoclay was used without additional treatment, hydrogen bonding on the surfaces of the organoclay holds the compatibilizer chains. Comparison of composites with compatibilizers having different chain lengths revealed that the length of compatibilizing polymer chain that is anchored at one or more clay surfaces must be sufficient to affect the dynamics of the entanglement network during extensional flow and produce strain hardening in the melt. Further van-Gurp Palmen plots were used to obtain a qualitative estimate of low frequency plateau modulus, which was used to explain the strain hardening phenomenon in linear PP/clay nanocomposite melts. The extent of strain hardening increased with an increase in the low frequency plateau modulus of the polymer nanocomposite melt.

| Specimen | PP 6523 (wt%) | PP-g-MA (wt%) | | | | | Nanoclay (wt%) | |
|---|---|---|---|---|---|---|---|---|
| | | AC 950 | PO 1020 | PO 1015 | Bond. 1001CN | Bond. 1001 | I.44P | Silated I.44P |
| PPNC-N2 | 68.0 | 24.0 | -- | -- | -- | -- | 8.0 | -- |
| PPNC-N3 | 85.0 | -- | -- | -- | 12.0 | -- | -- | 3.0 |
| PPNC-S6 | 85.0 | -- | -- | 12.0 | -- | -- | 3.0 | -- |
| PPNC-S7 | 85.0 | -- | -- | 12.0 | -- | -- | -- | 3.0 |
| PPNC-S13 | 85.0 | -- | 12.0 | -- | -- | -- | 3.0 | -- |
| PPNC-S14 | 85.0 | -- | 12.0 | -- | -- | -- | -- | 3.0 |
| PPNC-S15* | 76.0 | -- | -- | -- | 21.0 | -- | -- | 3.0 |
| PPNC-S16 | 76.0 | -- | -- | -- | 21.0 | -- | -- | 3.0 |
| PPNC-S17 | 76.0 | -- | -- | -- | -- | 21.0 | -- | 3.0 |

**Table 6.1:** Composition of linear PP/clay nanocomposites. (*The silated clay used here is Diamino dimethoxy-silated I.44P, except for PPNC-S15 where it is diamino monomethoxy-silated I.44P).

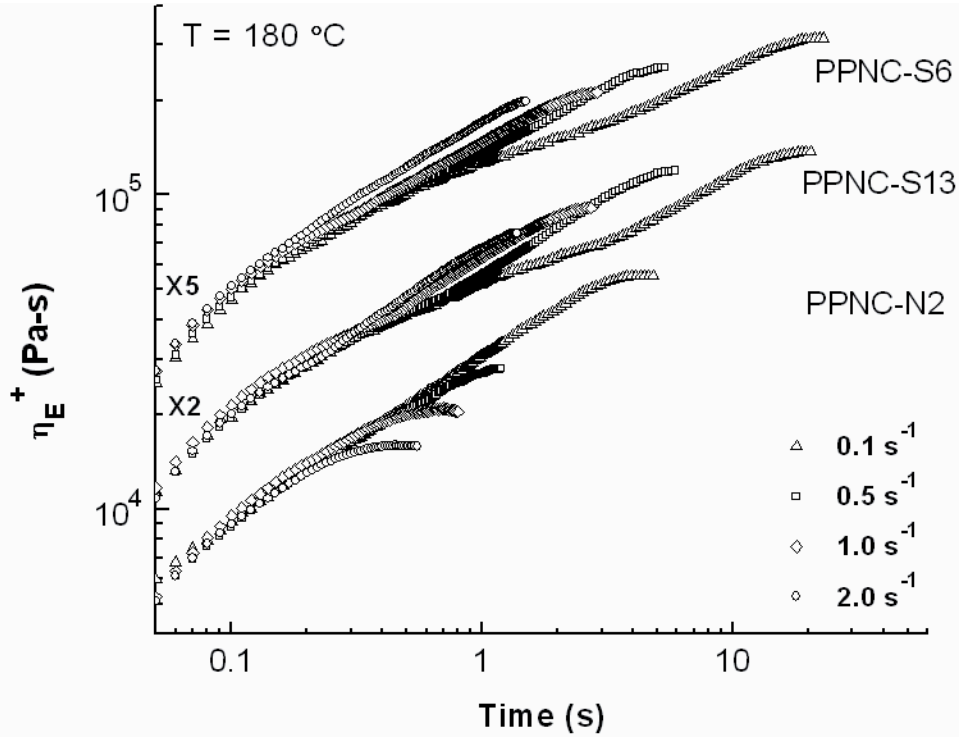


**Figure 6.1:** Melt extensional viscosity comparison for various linear PP/clay nanocomposites, showing the effect of molecular weight of the compatibilizer on the strain hardening characteristics of the derived nanocomposites.

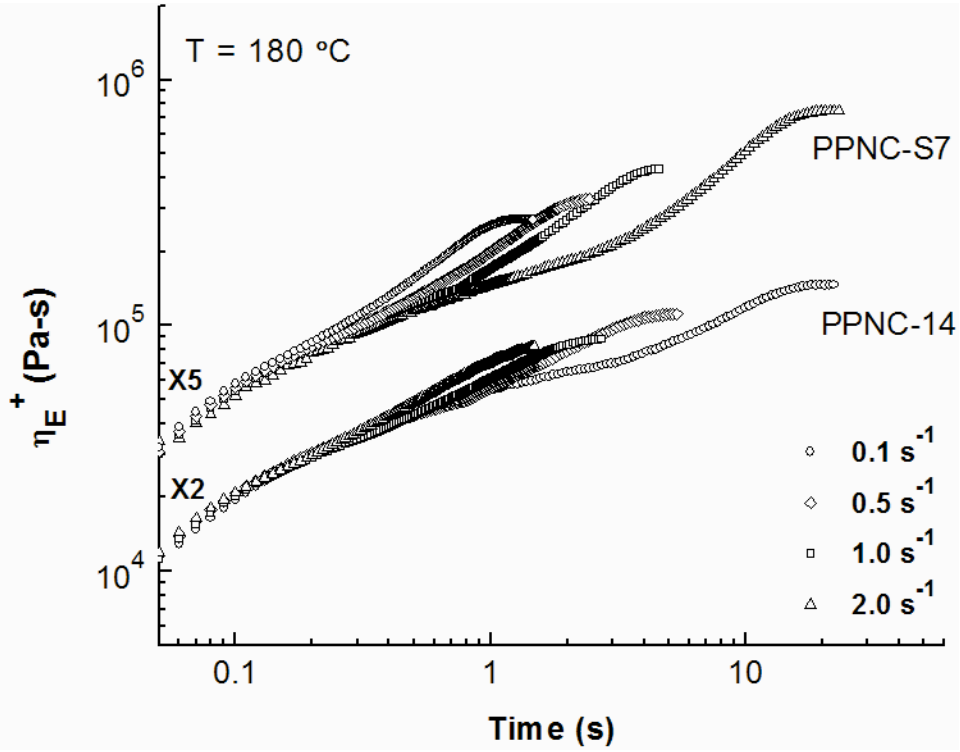


**Figure 6.2:** Melt extensional viscosity comparison for two nanocomposites under uniaxial extensional flow, showing the effect of molecular structure of the compatibilizer on the strain hardening characteristics of the derived nanocomposites (PPNC-S7 is prepared using PO 1015 and PPNC-S14 is prepared using PO 1020).

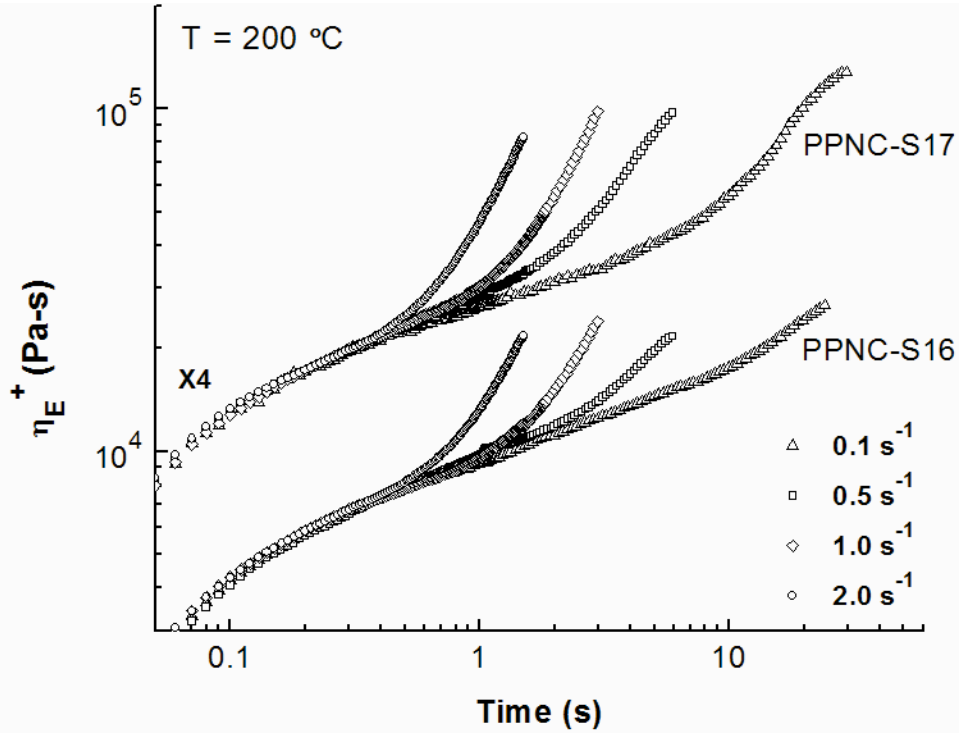


**Figure 6.3:** Melt extensional viscosity comparison for two nanocomposites under uniaxial extensional flow, showing the effect of molecular structure of the compatibilizer on the strain hardening characteristics for nanocomposites having Bondyram 1001 (PPNC-S17) and Bondyram 1001CN (PPNC-S16) as the compatibilizer.

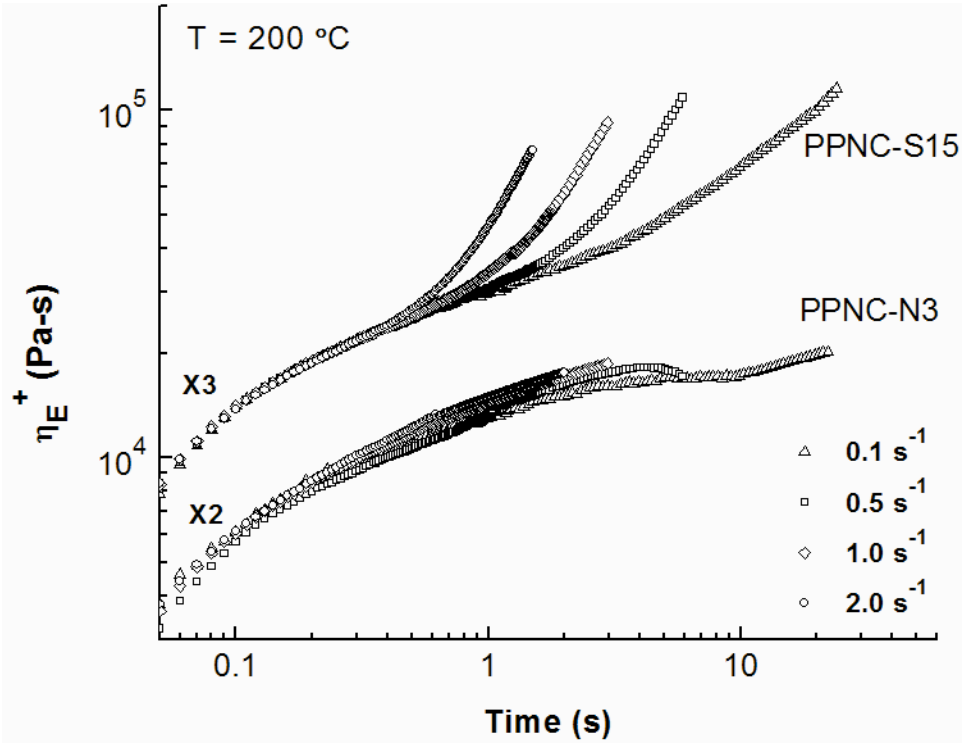


**Figure 6.4:** Melt extensional viscosity data under uniaxial extensional flow, for nanocomposites having Bondyram 1001CN as the compatibilizer. PPNC-N3 is prepared from Diamino dimethoxy silane treated I.44P and has a compatibilizer to clay ratio of 4 and PPNC-S15 is prepared from Diamino monomethoxy silane treated I.44P and has a compatibilizer to clay ratio of 7.

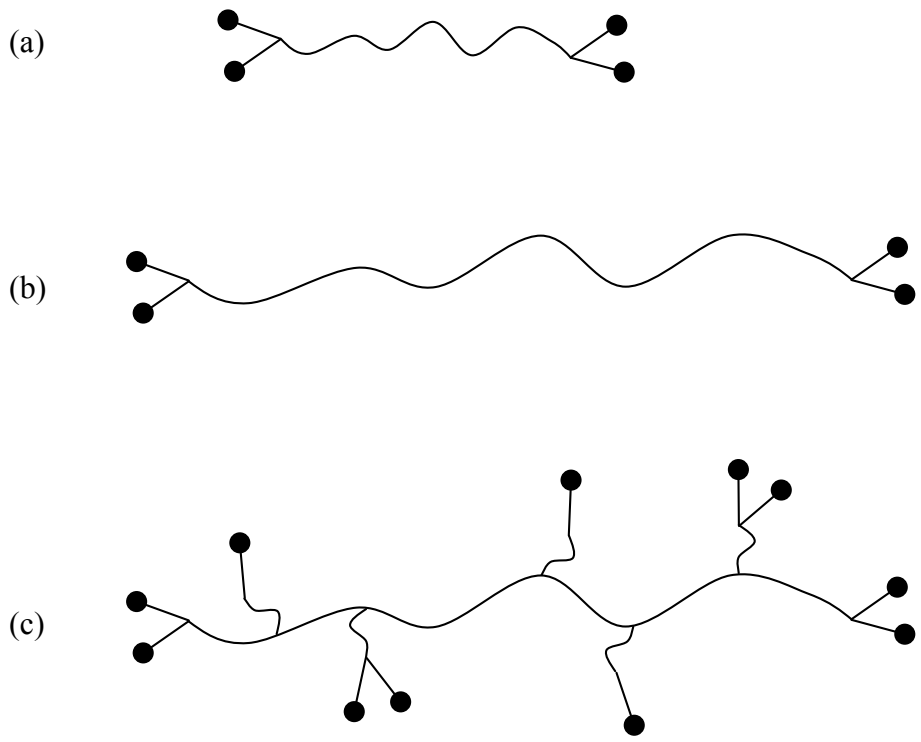


**Figure 6.5:** Molecular structure of PPgMAs. (a) AC-950, (b) PO 1020, and (c) PO 1015

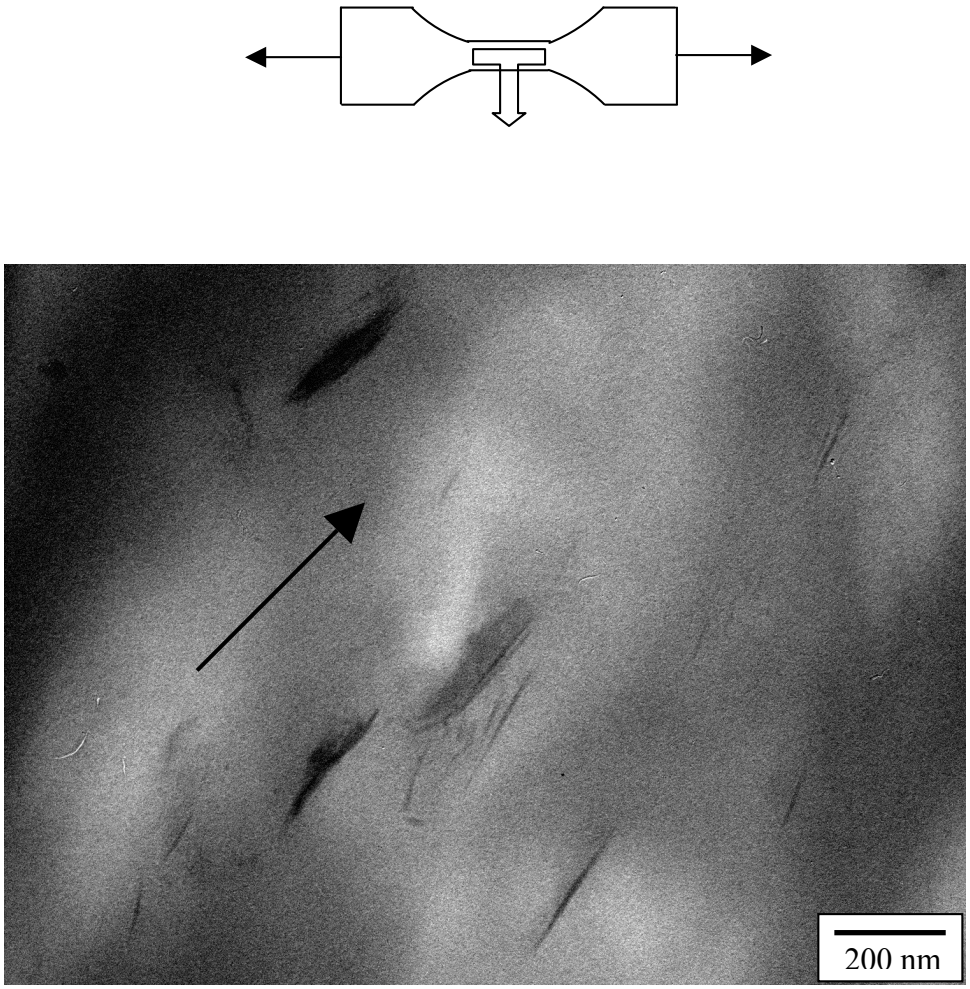


**Figure 6.6:** TEM micrographs of a stretched section of a representative nanocomposite (PPNC-S4) sample. The nanoclay platelets are oriented along the direction of stretch (shown by the arrow). The cartoon shows the section of the stretched samples used for TEM.

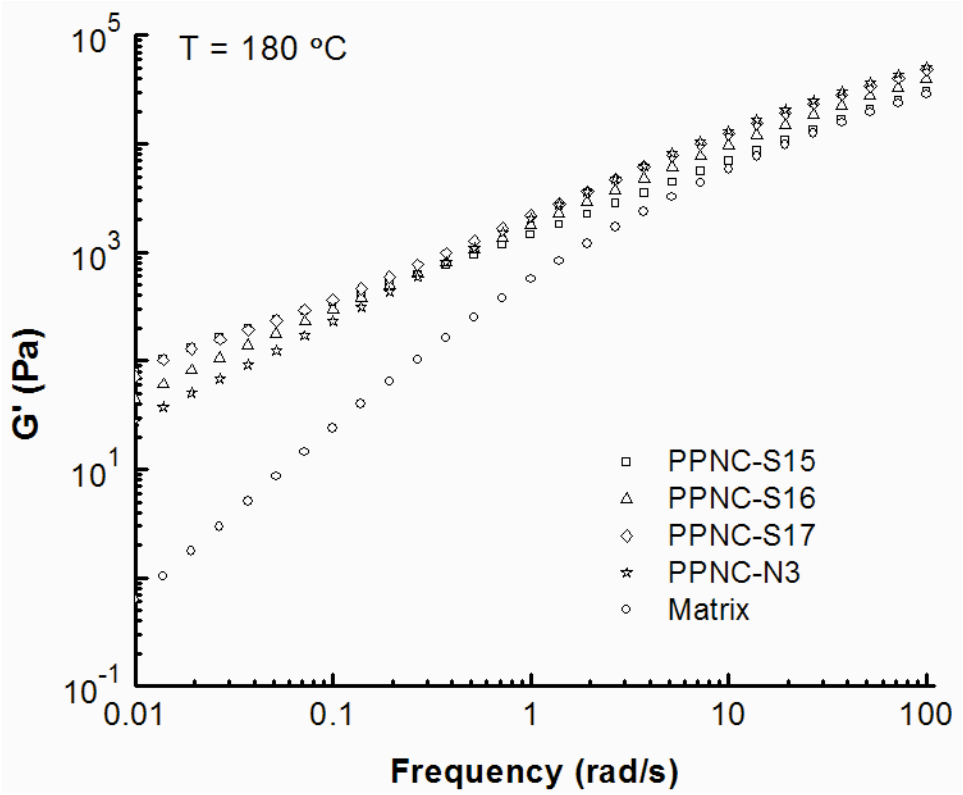


**Figure 6.7:** Variation of storage modulus with frequency for various linear PP-clay nanocomposites and the matrix polymer, prepared using Bondyram 1001CN as the compatibilizer.

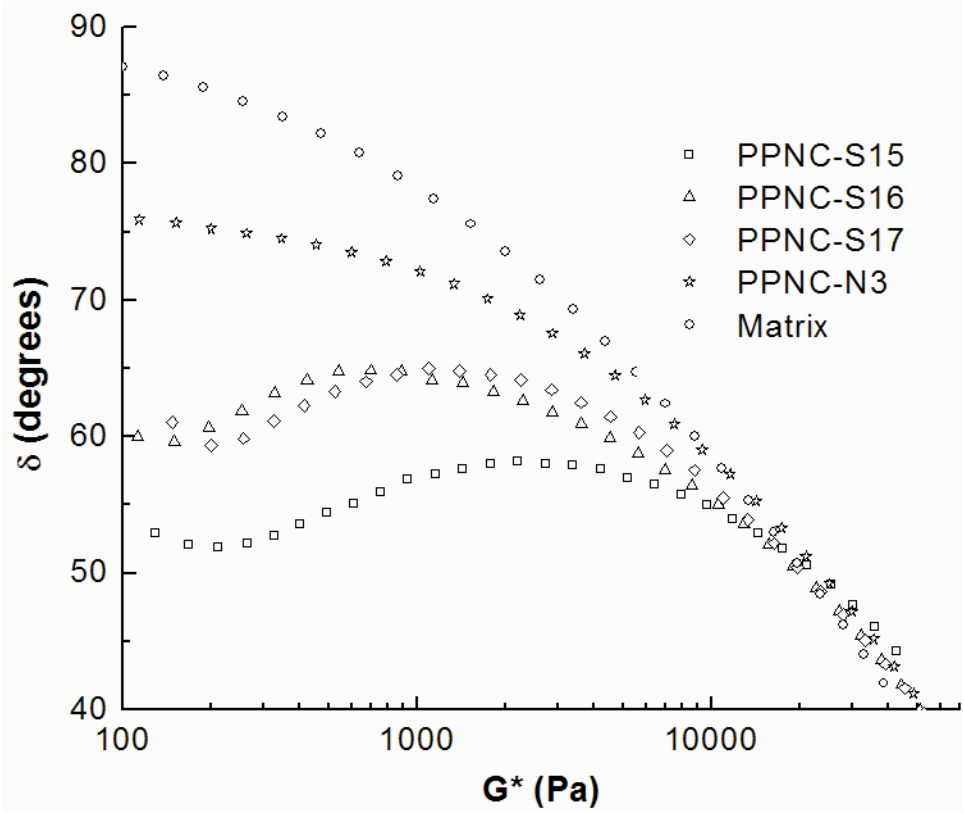


**Figure 6.8:** Van-Gurp Palmen plot for various linear PP-clay nanocomposites prepared using Bondyram 1001CN and Bondyram 1001 as the compatibilizer along with the matrix (linear PP + Bondyram 1001CN).

# 7. EFFECT OF MELT PROCESSING ON STRAIN HARDENING BEHAVIOR OF POLYPROPYLENE CLAY NANOCOMPOSITES - RECYCLABILITY

## 7.1. Introduction

With the growing interest towards sustainability, material recycling is getting serious attention from industries, both from environmental point of view as well as resource management and economics. One of the main objectives of this research is to replace currently used thermosetting foams with completely recyclable thermoplastic foams. Since our objective is to use the polypropylene – clay nanocomposites for foaming applications, it is important to study the effect of reprocessing on nanoclays morphological stability and strain hardening of these nanocomposites. In general, two main factors affecting the polymer properties during any processing operations are temperature and shear. In this study we have studied the effect of temperature and shear on strain hardening separately.

The effect of reprocessing of polypropylene was studied by Incarnato et al [221]. They observed that due to reprocessing, the weight average molecular weight and shear viscosity of the polypropylene decreases due to thermal degradation along with drop in elongation at break with increase in recycling operations. Moreover, in case of polymer clay nanocomposites there is a high likelihood that the dispersed nanoplatelets can agglomerate forming network like structure due to reprocessing [222]. Hence, it is expected that after few recycling operations the virgin polymer might show a drop in mechanical properties and rheological properties [52, 222-227].

In general, melt mixing is used to disperse the nanoclay in the polymer matrix, followed by additional molding or processing steps for the intended applications. Work done by Reichert

et al. [228] and Manias et al. [83] on the effect of additional melt blending on nanolayer morphology resulted in shear induced flocculation of nanolayers, also observed by Okamoto et al. [229]. Reichert et al. [228] also conducted annealing studies of injection molded polypropylene nanocomposites and found a decrease in spacing between the nanolayers due to annealing. Manias et al. [83] reported the effect of thermal annealing on the morphology of PP/clay nanocomposites and Pp-g-MA/clay nanocomposites. They observed severe collapse of clay galleries in case of PP nanocomposite while the PP-g-MA nanocomposite remained stable indicating enhanced stability of the nanoclays morphology due to better coupling between the clay and the matrix.

Another important aspect of nanoclay composites is the anisotropy of the nanoparticles. This allows them to be oriented differently along a particular direction resulting in significant improvement in various material properties [230-232]. Various studies have investigated the effect of shear [233-237] and elongational flow [131] on the orientation of nanoplatelets. Okamoto et al. [131] observed alignment of the nanoplatelets perpendicular to the stretch direction in PP-g-MA/clay nanocomposites under uniaxial extensional flow. as already mentioned in Chapter 6, the reasons for strain hardening in polymer melts is the increase in the chain stretch relaxation time. In organoclay nanocomposites the orientation of nanoparticles could significantly alter this characteristic time. Hence any change in morphology of the nanoclays that can prevent or reduce the orientability of the platelets should result in drop in strain hardening characteristics.

Since recyclability drives the substitution of thermoset polyurethane foams with closed cell PP foams, the effect of re-processing on the melt strain hardening under uniaxial extensional flow was investigated in this chapter. Various nanocomposites were annealed and extruded

though a uniform cross-section die to study the effect of heating and shear flow on the structural morphology and strain hardening of the nanocomposites.

## 7.2. Materials and Experimental Procedures

Various linear PP/clay nanocomposites (PPNC-S3, PPNC-S4, PPNC-S6 and PPNC-S7) prepared using silated and unsilated I.30P and I.44P nanoclays, characterized in Chapters 3 and 4, were used to study the effect of additional melt processing on the morphology of the nanoclays along with their strain hardening behavior. In order to carry out this study, the effect of processing is divided into two steps – thermal annealing to evaluate thermal stability and shear flow in an extruder to evaluate stability of the nanocomposites under shear flow. This was done so as to understand the individual effect of temperature and shear on the stability and strain hardening of the nanocomposites.

### 7.2.1. Thermal Annealing

In order to study the effect of thermal annealing alone on strain hardening behavior, the PP nanocomposites were thermally annealed at a temperature of 180ºC for 5 hrs in an oven under a blanket of nitrogen atmosphere so as to prevent any oxidative degradation of the nanoclays and the compatibilizer. The annealed samples were then re-molded and tested for strain hardening characteristics. The annealed samples were also characterized for their structural morphology using XRD and shear rheology. A frequency sweep was run on the annealed samples in order to see the effect annealing on the complex viscosity and shear modulus (G' and G") of the samples.

### 7.2.2. Extrusion

To study the effect of shear on strain hardening, various PP/organoclay nanocomposites were extruded through a capillary die (d = 1mm, L/D = 30) at a shear rate of $500s^{-1}$ and a temperature of 180ºC in a Dynisco LCR6000 Capillary rheometer. The PPNC granules were carefully fed into the capillary rheometer with intermittent packing of the melt. The extruded samples were then molded and characterized for various structural and rheological properties. XRD and TEM were used to study the effect of extrusion on the structural morphology of the nanocomposites. Both shear and uniaxial extensional rheology were used to study the rheological properties of the extruded materials. The details of the characterization techniques are presented in Chapter 2.

## 7.3. Results and Discussion

### 7.3.1. Effect of Thermal Annealing

The X-ray diffraction patterns of various linear PP/clay nanocomposites before and after annealing are presented Figures 7.1-7.4. A comparison of the d-spacing before and after annealing reveals that the spacing between the platelets have either remained unchanged or have increased and have not resulted in coarsening of the nanoclays structure. This type of phenomenon has also been reported in literature [238-240] for nanocomposites. Tang et al. [238] and Fordiani et al. [239] reported the structural changes of maleated PP/organoclays due to thermal annealing. FTIR studies conducted on these sample suggested that prolonged annealing of the polymer nanocomposite melt, in presence of oxygen, led to a chemical reaction between the hydroxyl group present at the nanoclays edges and the maleic anhydride group. This led to

greater intercalation of the polymer chains by so called "peeling-off" mechanism. The presence of a small fraction of oxygen promotes this kind of mechanism. Even though we carried out the annealing experiment under nitrogen; presence of traces of oxygen cannot be eliminated. The effect of such reactions should also be reflected in the strain hardening behavior of the nanocomposites, as the weaker hydrogen bonds are now replaced with stronger chemical bonds. The effect of thermal annealing on the melt extensional viscosity data is presented in Figures 7.5-7.8. Figure 7.5 shows a significant increase in the strain hardening behavior for PPNC-S6 after annealing. This is due to the replacement of the weaker H-bonds with chemical bonds between the compatibilizer and the clay. However, thermal annealing resulted in no change in the strain hardening behavior for the silated clay nanocomposites (figure 7.6-7.8). This is because there were chemical bonds between the compatibilizer and the clay even before annealing. Hence, it can be safely concluded that thermal annealing does not result in deterioration of the strain hardening behavior of the PP/clay nanocomposites.

### 7.3.2. Effect of Extrusion

The X-ray diffraction patterns for extruded nanocomposite samples are presented in Figure 7.1-7.4. From the XRD, it is evident that extrusion of the nanocomposites, through a uniform die, resulted in a decrease in d-spacing of the nanocomposites along with a more prominent peak. This indicates that extrusion of the nanocomposites through a uniform die resulted in restacking of the nanolayers. The change in the morphology of the nanocomposites is solely due to shear and not due to temperature as thermal annealing did not result in coarsening of the nanocomposite structure.

From the strain hardening data presented in Figure 7.5-7.8, it is quite evident that thermal annealing alone does not result in decrease in strain hardening characteristics. All four PP nanocomposites subjected to thermal annealing at 180ºC for 5hrs were able to maintain their strain hardening behavior. However, the effect of shear during extrusion has a completely different story. In case of PPNC-S6 and PPNC-S7 nanocomposites, extruded samples resulted in drop in the strain hardening behavior, especially at the higher strain rates. This could possibly be due to re-stacking of the nanoplatelets during extrusion. In general, extrusion of nanocomposites leads to agglomeration of nanoclay platelets (Figure 7.12). This could be either edge-to-edge agglomeration or face-to-edge agglomeration (commonly known as House-of-cards formation). The structure of the nanoclays after extrusion has also been studied by transmission electron microscopy. The TEM micrographs for PPNC-S7 before and after extrusion, presented in Figure 7.9, demonstrate that extrusion led to more edge-to-edge re-stacking of the platelets, thereby affecting the strain hardening characteristics of the nanocomposites. This is because, grafting of the reactive silane coupling agents has occurred primarily at the edges of I.44P clay, resulting in predominantly edge-to-edge aggregation of the nanoclays. The formation of such aggregates increases the resistance towards orientation of the nanoplatelets during the extensional flow, thereby reducing the strain hardening characteristics.

On the other hand, extrusion of PPNC-S4 nanocomposites resulted in complete loss in the strain hardening characteristics while PPNC-S3 nanocomposites retains most of its strain hardening characteristics even after extrusion. This could be due to severe agglomeration of the clay platelets in case of PPNC-S4. The TEM micrographs for PPNC-S3 and PPNC-S4 nanocomposites are presented in Figures 7.10 and 7.11. In case of PPNC-S3, extrusion through a uniform die did result in some re-stacking of the nanoclays that has been reflected in a small

drop in the strain hardening characteristics. However, extrusion of PPNC-S4 resulted in severe face-to-edge kind of agglomeration. This results in decrease in anisotropy of the nanoparticles thereby making it difficult to orient these agglomerates along the direction of stretch, resulting in complete loss of strain hardening behavior in extruded PPNC-S4 nanocomposite. The formation of such aggregates for PPNC-S4 could be explained using a simple cartoon shown in Figure 7.13.

The diamino dimethoxy-silane treated clay platelet have face grafted silanes with two hydrolysable groups; one of them is involved in the condensation reaction with the active sites of the nanoclay, while the other one is unreacted. These unreacted hydroxyl groups during the extrusion process could interact with those of neighboring clay platelets forming a house of cards structure. These structures might no longer behave as a nanoplatelet and orientating these agglomerated structures during extensional flow to further assist orientation of polymer chains is highly improbable. While in case of diamino monomethoxy-silane treated I.30P nanocomposites (PPNC-S3) due to the absence of any free hydrolysable groups on the silane molecule attached to the clay surface, this kind of re-agglomeration is not possible, thereby being able to retain its strain hardening characteristics. Hence, diamino monomethoxy-silane treated I.30P-PP nanocomposites is a potential candidate for producing foams that can be reused, as these nanocomposites can maintain their strain hardening behavior under uniaxial extensional flow, an indispensable property for producing high quality polymer foams, even after reprocessing.

To further verify the formation of such agglomerates, shear modulus and viscosity of these samples were measured. A significant drop in the storage modulus and/or complex viscosity at low frequency is an indication of loss of polymer-particle network. It has been well established in literature that exfoliation of nanoclays leads to significant increase in both storage

modulus and complex viscosities at low frequency region as compared to nanocomposites with poor dispersion of clay platelets [69, 71, 74, 92]. Figure 7.14 shows the effect of extrusion on storage modulus and Figure 7.15 shows the effect of extrusion on complex viscosity for PPNC-S3 and PPNC-S4 nanocomposites. It is evident from the figures that there is a significant drop in both storage modulus and complex viscosity for PPNC-S4 compared to PPNC-S3. This is due to the formation of face-to-face aggregates for PPNC-S4 that significantly lowers the reinforcement effect of nanoclays on the polymer matrix, thereby affecting both its shear and extensional rheology.

## 7.4. Conclusions

Recyclability of linear PP/clay nanocomposites drives the substitution of thermoset polyurethane foams with closed cell PP foams. To study the effect of re-processing on the melt strain hardening, various nanocomposites were annealing and extruded though a uniform cross-section die to study the effect of heating and shear flow on the structural morphology and strain hardening of the nanocomposites. The results indicated that annealing had no negative impact on morphology or strain hardening of the nanocomposites. However, extrusion of these nanocomposites indicated that nanocomposites prepared using multiple hydrolysable groups resulted in formation of face-to-face nanolayer aggregates that are difficult to orient during uniaxial extensional flow and thus resulted in loss of the strain hardening behavior. The formation of such agglomerates has been verified by transmission electron microscopy. Shear rheology results showed a drop in storage modulus and complex viscosity for samples confirming the formation of agglomerates during extrusion. However, the formation of agglomerates can be avoided by the use of amino silanes having only one hydrolysable group.

Such nanocomposites showed retention of strain hardening behavior after extrusion and hence can be used as a potential candidate for the replacement of thermoset polymers for applications where strain hardening in polymer melt is essential.

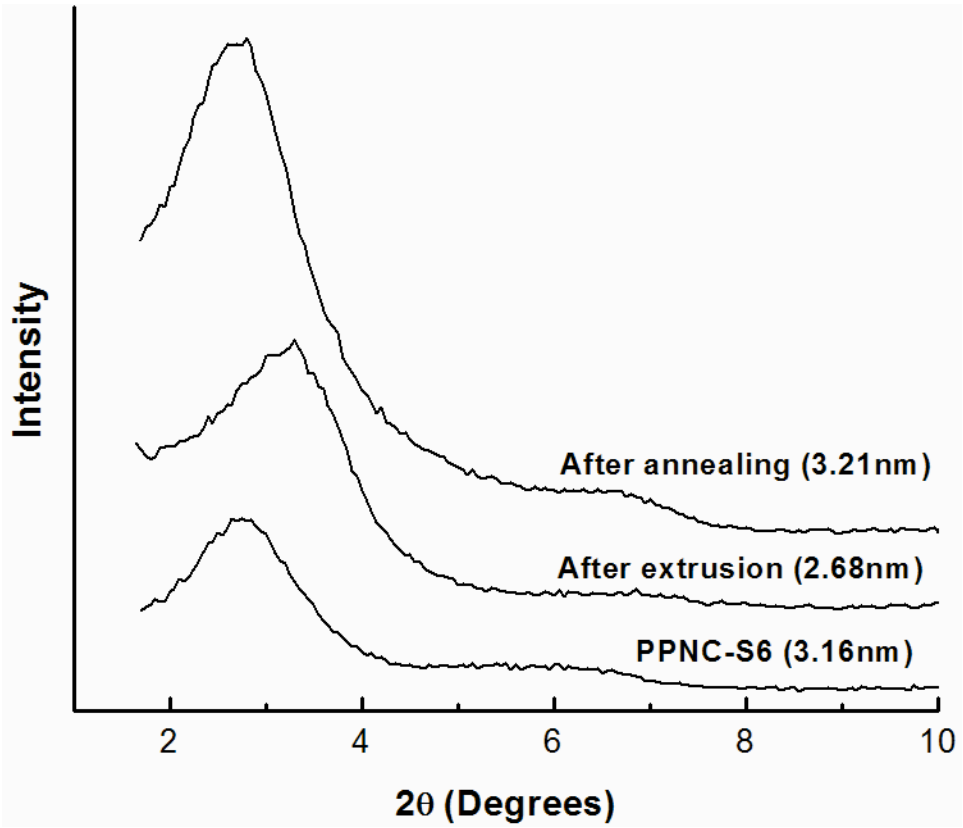


**Figure 7.1:** X-ray diffraction pattern showing the effect of thermal annealing and extrusion for PPNC-S6 nanocomposites.

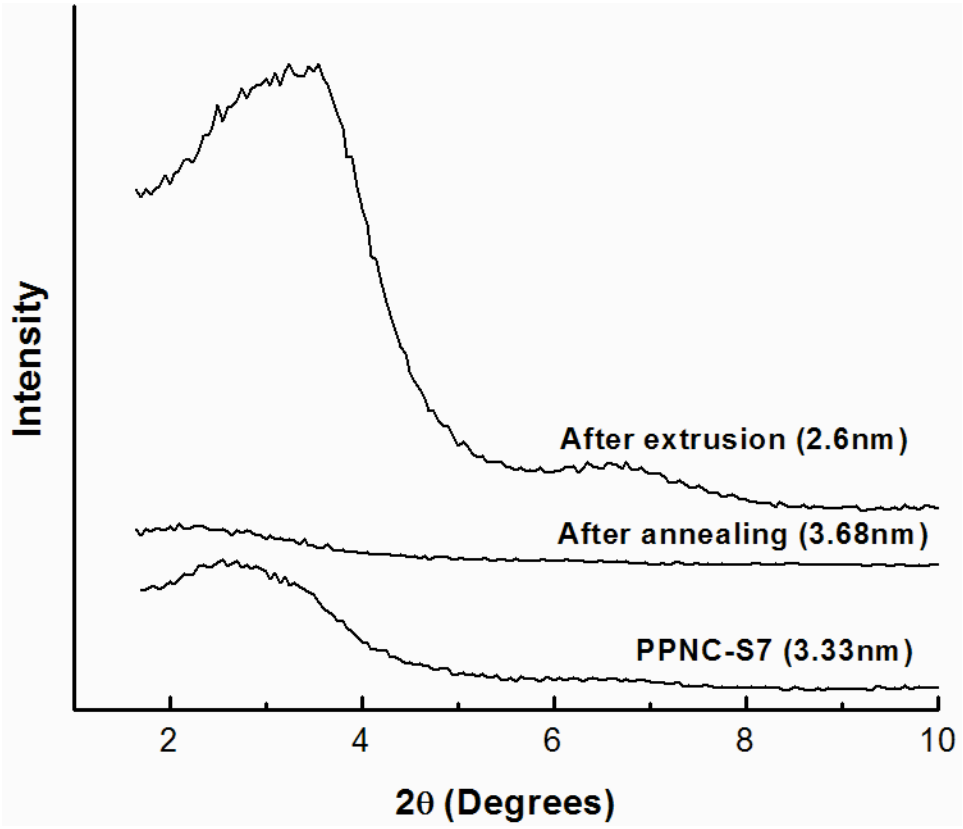


**Figure 7.2:** X-ray diffraction pattern showing the effect of thermal annealing and extrusion for PPNC-S7 nanocomposites.

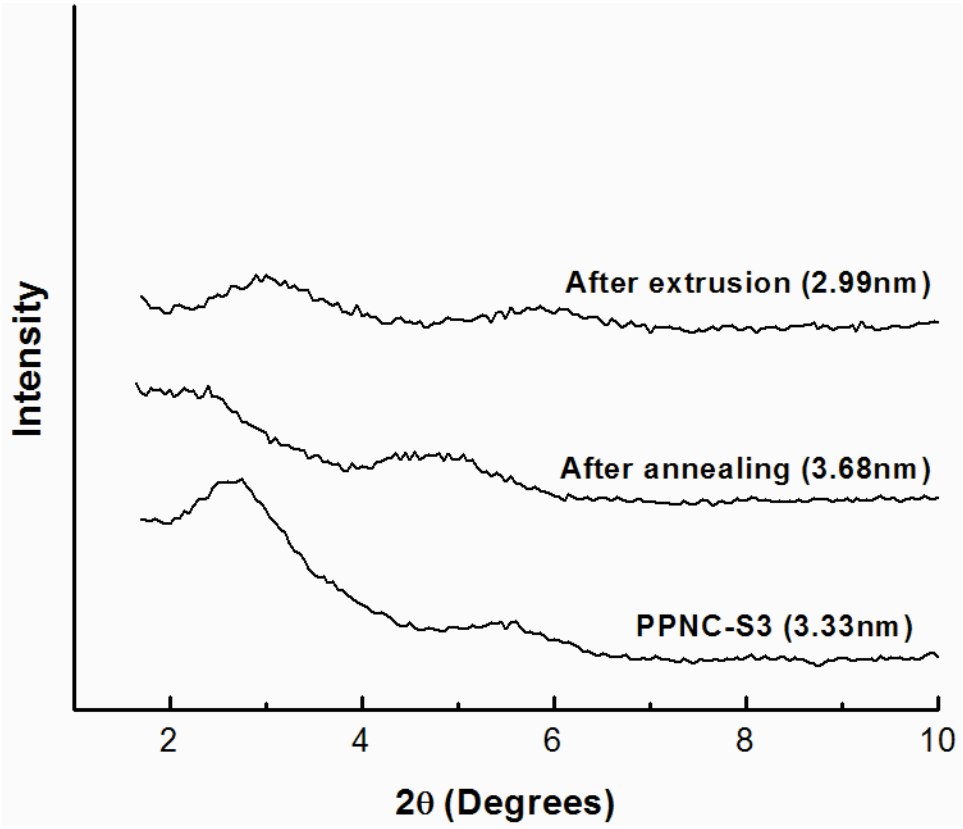


**Figure 7.3:** X-ray diffraction pattern showing the effect of thermal annealing and extrusion for PPNC-S3 nanocomposites.

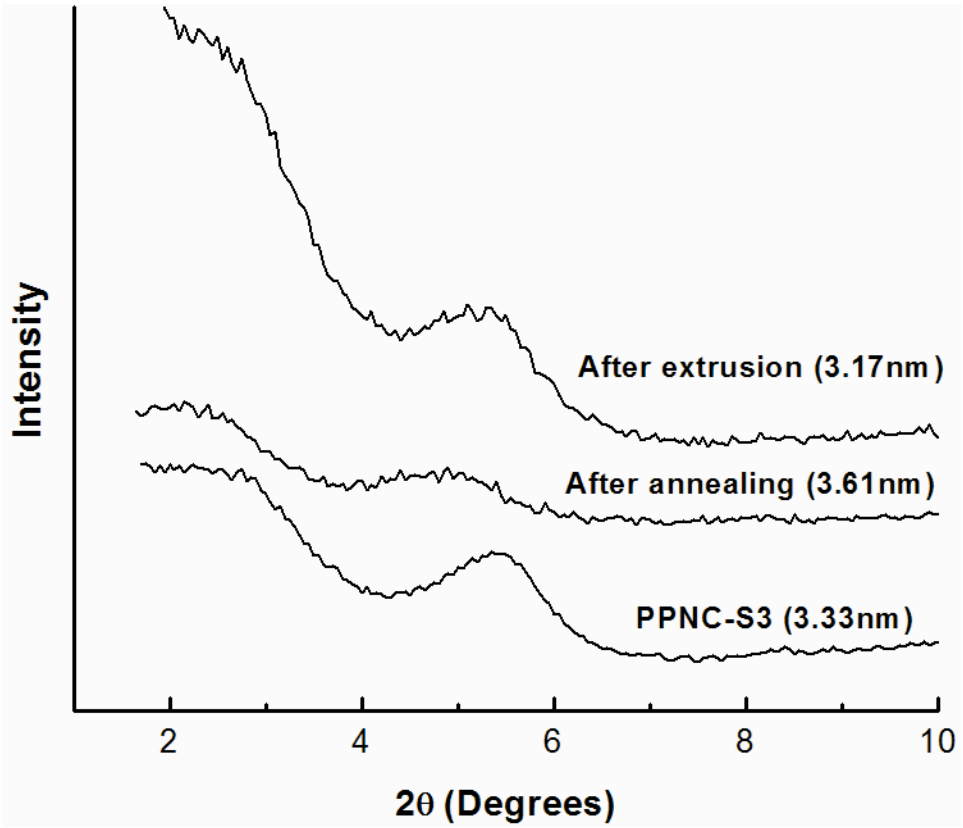


**Figure 7.4:** X-ray diffraction pattern showing the effect of thermal annealing and extrusion for PPNC-S4 nanocomposites.

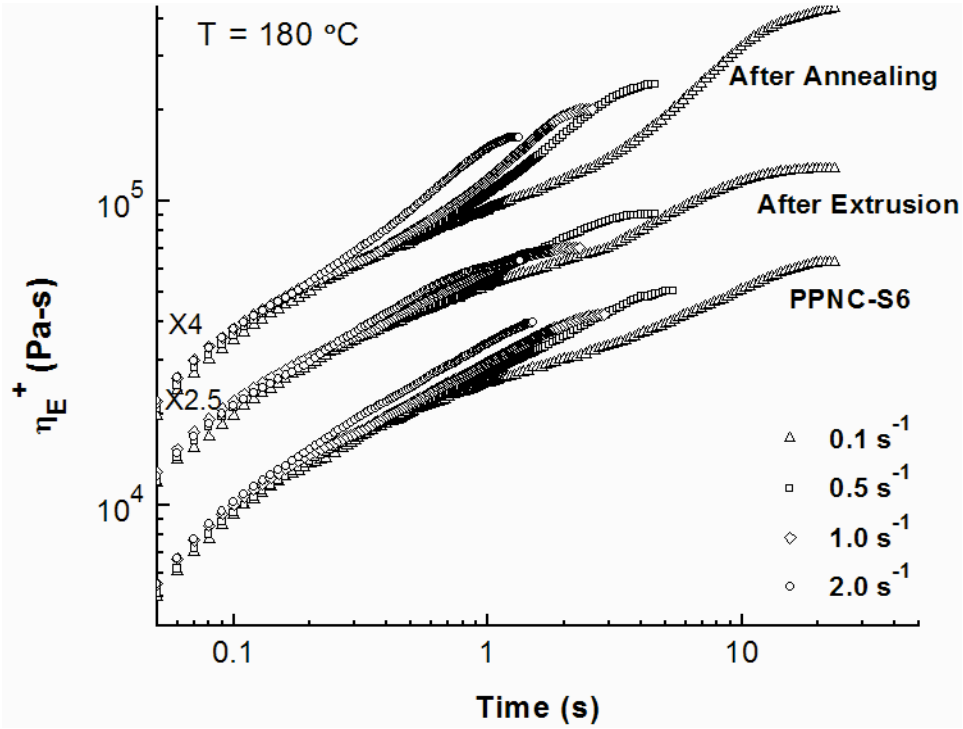


**Figure 7.5:** Melt extensional viscosity of PPNC-S6 nanocomposites, showing the effect of thermal annealing and extrusion on strain hardening under uniaxial extensional flow.

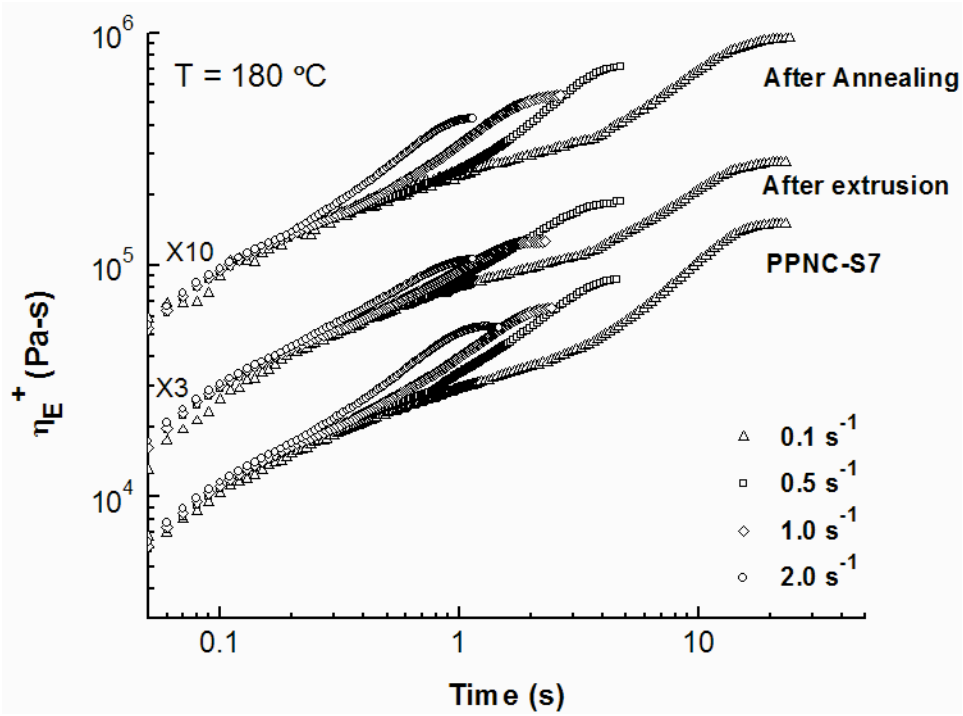


**Figure 7.6:** Melt extensional viscosity of PPNC-S7 nanocomposites, showing the effect of thermal annealing and extrusion on strain hardening under uniaxial extensional flow.

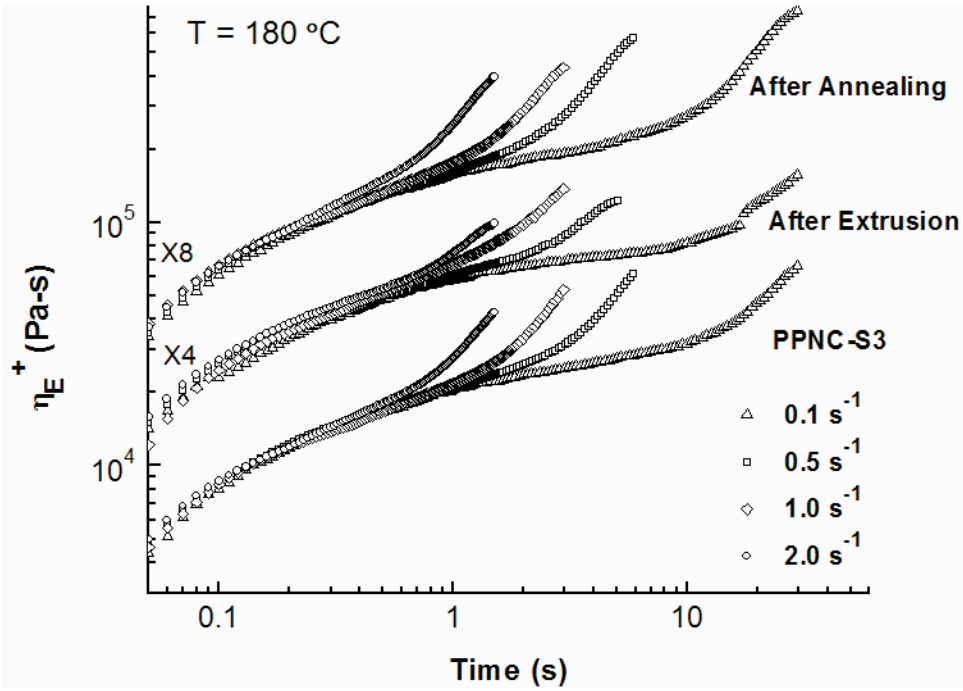


**Figure 7.7:** Melt extensional viscosity of PPNC-S3 nanocomposites, showing the effect of thermal annealing and extrusion on strain hardening under uniaxial extensional flow.

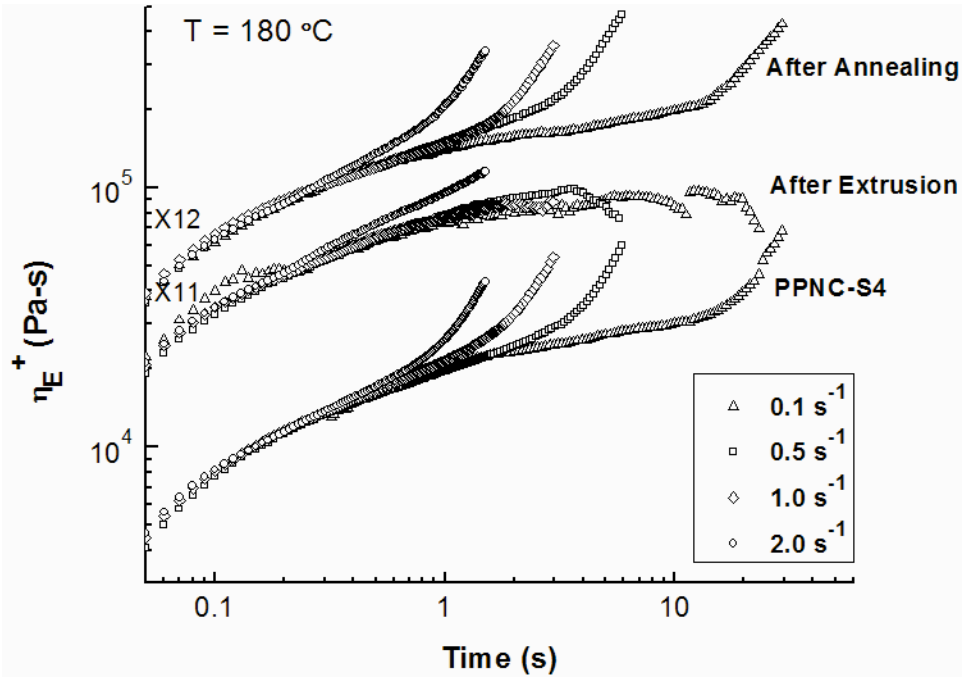


**Figure 7.8:** Melt extensional viscosity of PPNC-S4 nanocomposites, showing the effect of thermal annealing and extrusion on strain hardening under uniaxial extensional flow.

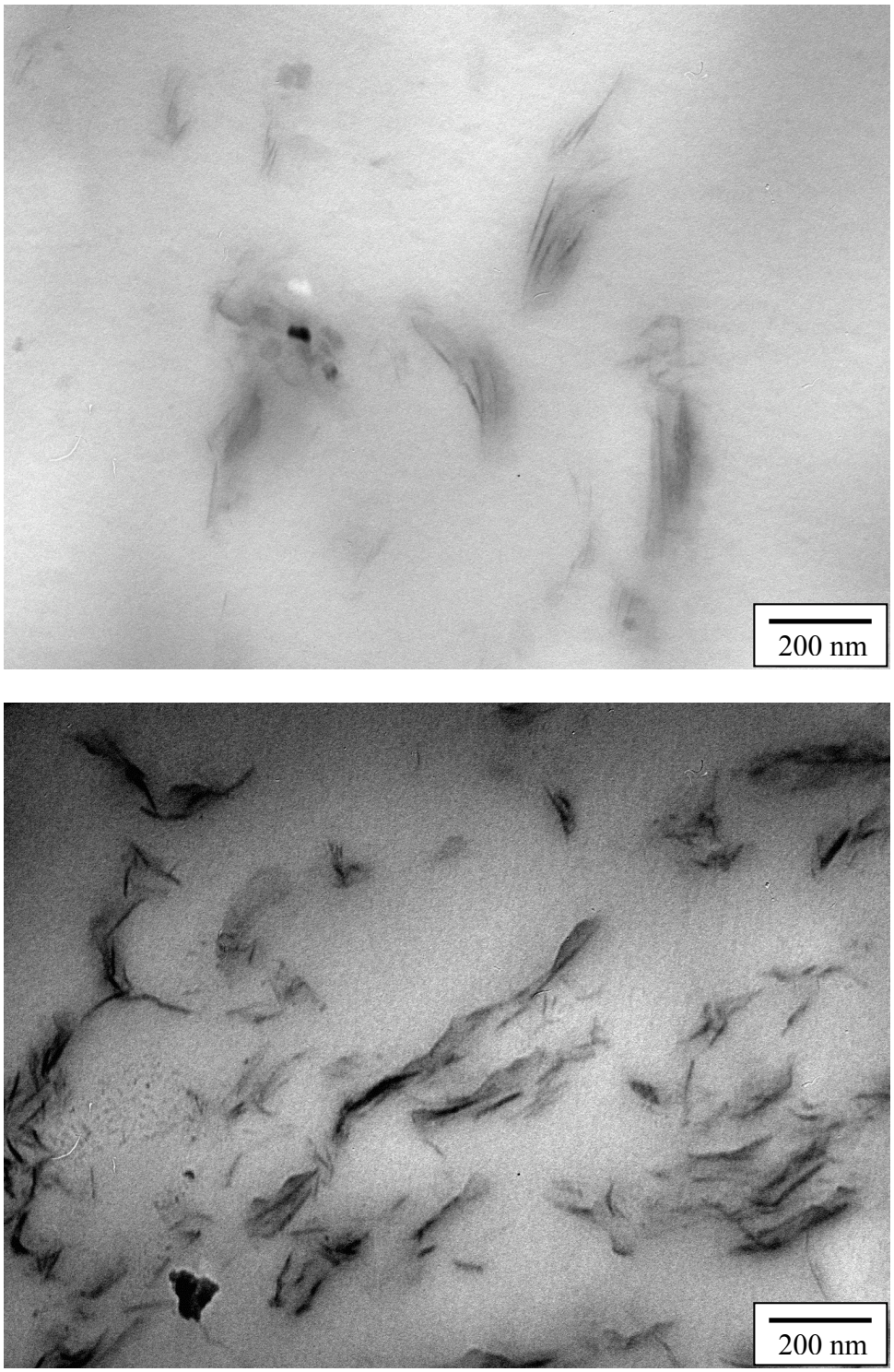


**Figure 7.9:** TEM micrographs of linear PP/diamino dimethoxy silated I.44P (PPNC-S7) nanocomposites showing the effect of extrusion on nanoclay dispersion (top: before extrusion, bottom: after extrusion).

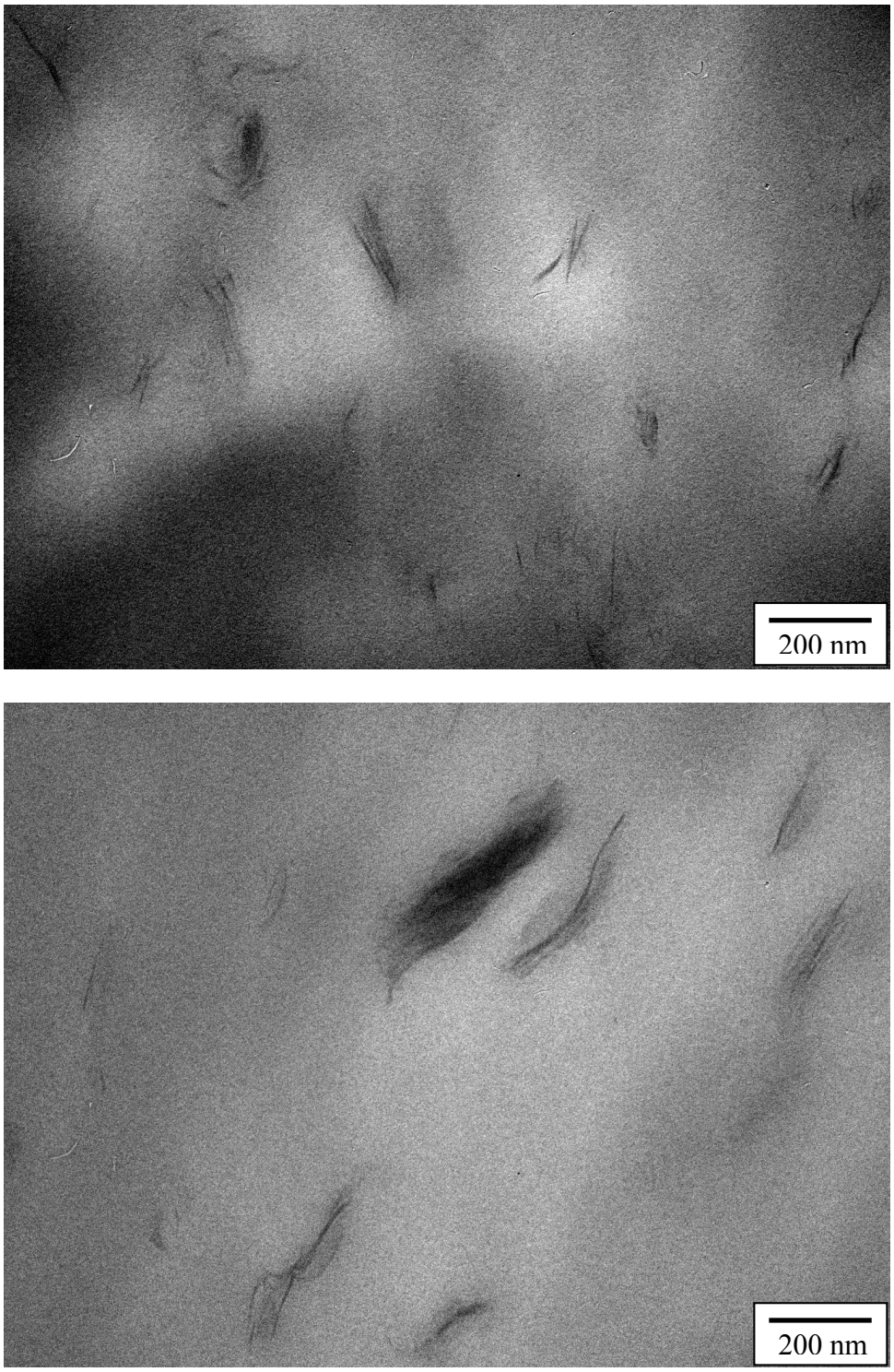


**Figure 7.10:** TEM micrographs of linear PP/diamino monomethoxy silated I.30P (PPNC-S3) nanocomposites showing the effect of extrusion on nanoclays dispersion (top: before extrusion, bottom: after extrusion).

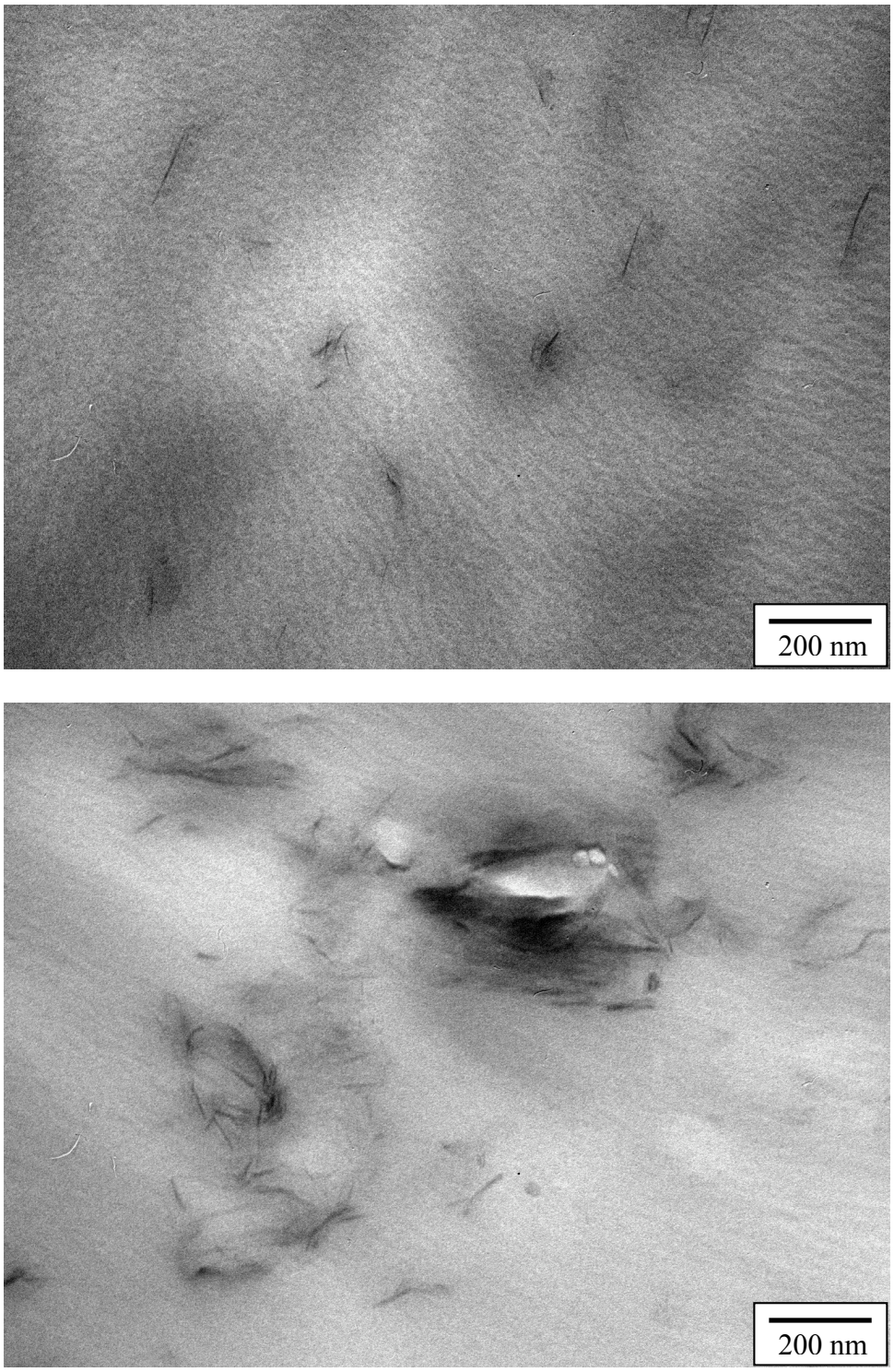


**Figure 7.11:** TEM micrographs of linear PP/diamino dimethoxy silated I.30P (PPNC-S4) nanocomposites showing the effect of extrusion on nanoclays dispersion (top: before extrusion, bottom: after extrusion).

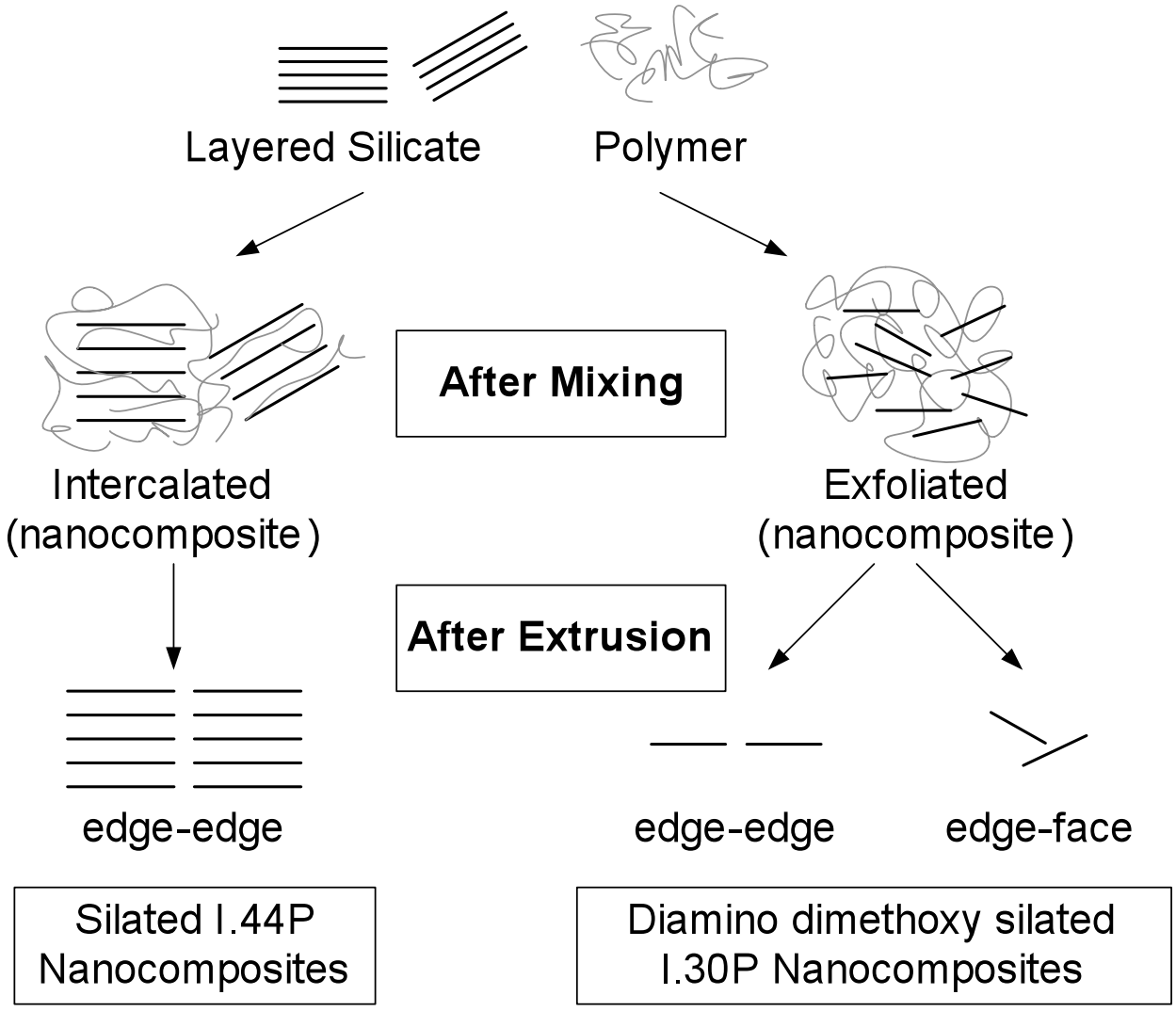


**Figure 7.12:** Schematic representing state of nanolayers dispersion/agglomeration after mixing and after extrusion through a capillary die.

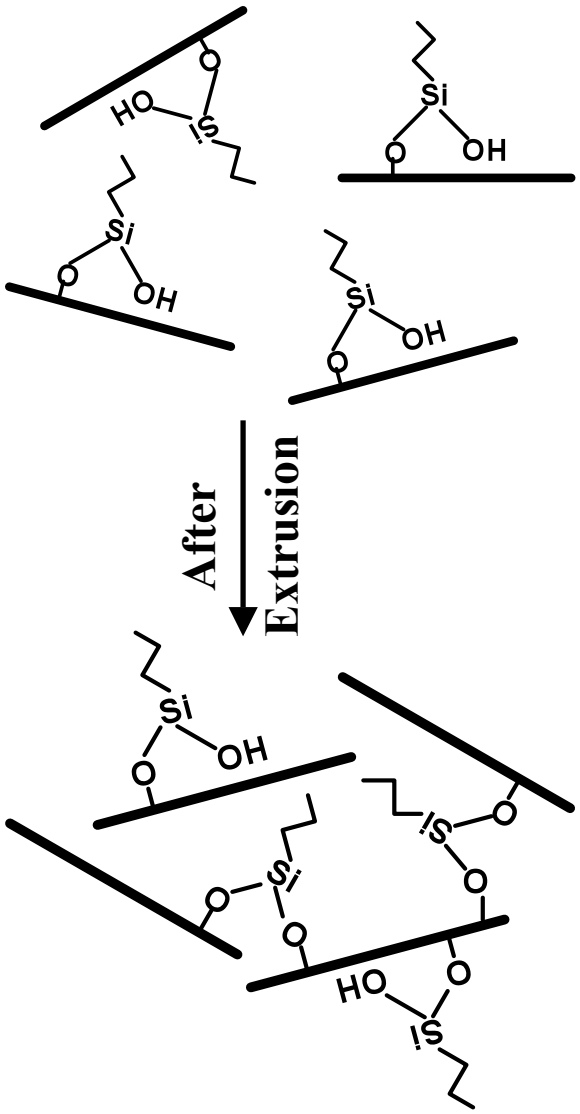


**Figure 7.13:** Schematic representing agglomeration of diamino dimethoxy silated I.30P layers in PPNC-S4 due to extrusion through a capillary die.

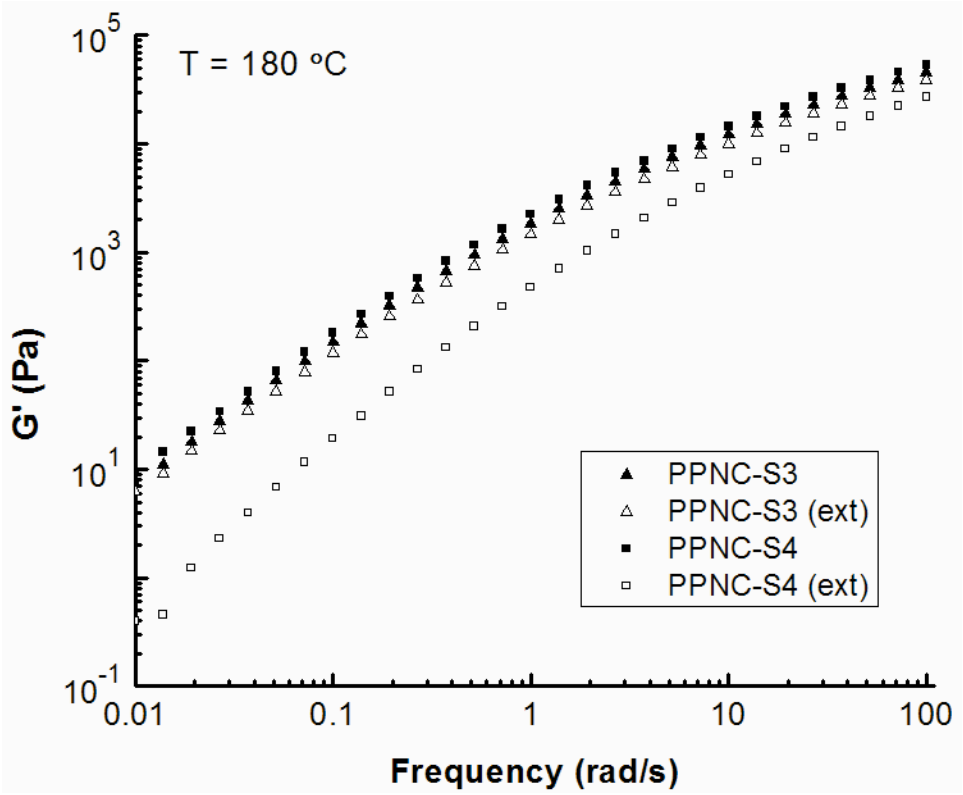


**Figure 7.14:** Effect of extrusion on storage modulus (G') of PPNC-S3 and PPNC-S4 nanocomposites. (open symbols: before extrusion and closed symbol: after extrusion)

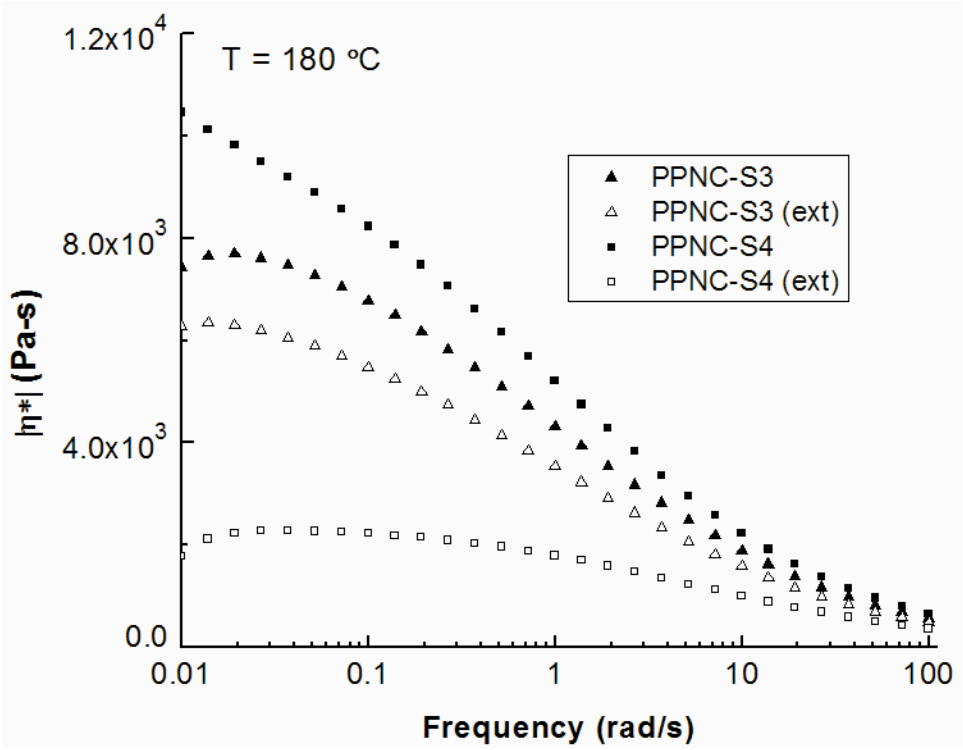


**Figure 7.15:** Effect of extrusion on complex viscosity of PPNC-S3 and PPNC-S4 nanocomposites. (open symbols: before extrusion and closed symbol: after extrusion)

# 8. CONCLUSIONS AND RECOMMENDATIONS

## 8.1. Conclusions

This study was focused towards improving the strain hardening property of linear polypropylene using a suitable compatibilizer and organically modified montmorillonite as nanoclays for foaming applications. This was achieved by improving the interactions between the different components of a polypropylene nanocomposite system — bulk polypropylene, maleated polypropylene and the nanoclay intercalated with long chain alkyl ammonium surfactants. The objectives of this research were (1) to understand the effects of composition on melt extensional strain hardening in nanocomposites of linear polypropylene with nanoclay, compatibilizer and various coupling agents and (2) to evaluate selected nanocomposite formulations in extrusion foaming with chemical blowing agents.

Nanocomposites were prepared with organically modified montmorillonite, maleic anhydride grafted polypropylene as compatibilizer and linear polypropylene as the bulk matrix. Compatibilizers with different molecular weights and molecular structure (polypropylene homopolymer or ethylene-propylene copolymer) were used. The organoclays were also treated with amino silane coupling agents to increase the interaction between nanoclays and the compatibilizer. The nanocomposites were characterized by X-Ray diffraction, TEM, melt extensional rheometry and DSC. Selected nanocomposites were foamed in a single screw extruder using a chemical blowing agent. The extrusion foaming process was optimized for each nanocomposites based on their melting crystallization temperature. The cellular structure of the extruded foam samples was characterized by scanning electron microscopy and its image analysis was used to obtain average cell size and cell density of the foam samples.

When several polypropylene clay nanocomposites all with good dispersion of the dialkyl amine treated organoclay were foamed by extrusion with a chemical blowing agent, systematic variations in foam quality were obtained based on differences among them in tensile melt strength and in crystallization behavior. Even among nanocomposites without any melt strain hardening, decreasing the rate of crystallization led to closed cell foams with smaller cell size and higher cell density. Among nanocomposites where significant strain hardening was observed in extensional flow along with the slower rates of crystallization, the extruded polypropylene nanocomposite foams displayed the smallest cell sizes and the greatest cell density by reducing cell coalescence. These enhancements may be attributed to attachment of high molecular weight PP-g-MA chains to the surfaces of nanolayers due to hydrogen bonding, providing greater constraints on chain stretch relaxation and also slowing down the crystallization. The foam extrudates were compared with those prepared from a blend of linear and branched polypropylene. The cell size and cell density of foam prepared from the blend of linear and branched polypropylene was significantly higher than that prepared from the linear polypropylene/clay nanocomposites. This was due to absence of any nucleating agent present in the blend. Hence nanoclays acts as both rheology modifier as well as nucleating agent and thus improves the quality of foam produced form the linear PP/clay nanocomposites.

The organoclays and the compatibilizer present in the nanocomposites have mainly electrostatic or hydrogen bonding type interactions, which are weaker forces of attraction. In order to replace these weaker forces of attraction, the organoclays were further treated with amino silane coupling agents. The amino silane treated nanoclays resulted in either edge grafting or face and edge grafting depending upon the amount of intercalant already present in the clay galleries. Characterization of the silated clays using BET, TGA, and XRD confirmed that

organoclays with low surfactant content (I.30P) resulted in face and edge grafting of the silanes while the high surfactant containing I.44P organoclays led to edge grafting of the clays. The amino groups of the face and/or edge grafted silanes is believed to react with the maleic anhydride group of the selected compatibilizer to replace the weaker forces of attraction with stronger chemical bonds. This resulted in nanocomposites with significant increase in melt strain hardening compared to the unsilated clay nanocomposites. These nanocomposites were further evaluated for extrusion foaming using a chemical blowing agent. It was found that the nanocomposites showing melt strain hardening behavior that remained unchanged with strain rates resulted in foams with lowest possible cell size and highest cell densities within the scope of this research.

To further understand the effect of compatibilizer molecular structure on the strain hardening behavior of the nanocomposites, compatibilizers having different chain lengths and different chain structure were selected. It is known that grafting of maleic anhydride on polypropylene occur predominantly at the two ends of the polypropylene chan. Hence if a ethylene – propylene copolymer is selected for maleation, then along with the two ends of the polymer backbone, grafting of maleic anhydride groups will also take place at additional sites along the ethylene-propylene copolymer chain. A comparison of composites with compatibilizers having different chain lengths revealed that the length of compatibilizing polymer chain that is anchored at one or more clay surfaces must be sufficient to affect the dynamics of the entanglement network during extensional flow and produce strain hardening in the melt. Further, it was also found that maleated copolymer of propylene and ethylene with high molecular weight provided greater improvements in strain hardening with the use of silated clays. This is because the entangled network formed between polymer-clay systems would

involve greater number of clay layers/galleries and thereby would significantly increase the characteristic chain stretch relaxation time. With the help of van-Gurp Palmen plots, it was shown that nanocomposites having higher low frequency plateau modulus showed stronger strain hardening behavior.

Since recyclability of linear PP/nanocomposites drives the substitution of thermoset polyurethane for various foaming applications, the effect of re-processing on melt strain hardening was also investigated. Various nanocomposites prepared different silane treated clay were annealed and extruded though a uniform cross-section die to study the effect of heating and shear flow on the structural morphology and strain hardening of the nanocomposites. The results showed that annealing had no negative impact on morphology or strain hardening of the nanocomposites. However, extrusion of these nanocomposites indicated that nanocomposites prepared using multiple hydrolysable groups resulted in formation of layered aggregates that are difficult to orient during uniaxial extensional flow and thus resulted in loss of the strain hardening behavior. This was verified both by transmission electron microscopy and by shear rheology. The nanocomposites prepared using diamino dimethoxy silated I.30P showed a significant drop in both storage modulus and complex viscosity after extrusion. This can happen if the polymer-particle network is destroyed due to extrusion. Hence proper selection of clay treatment and compatibilizer can lead to linear polypropylene nanocomposites that can show significant improvement in strain hardening characteristics, an indispensible property for foaming polymers.

## 8.2. Recommendations

Based on the results of this research, the following recommendations can be made for future research:

a) It was found in this study that the use amino silane coupling agents in synthesizing linear PP/clay resulted insignificant increase in strain hardening behavior of the polymer melt under uniaxial extensional flow. Since, the amino groups predominantly react with the maleic anhydride group of the compatibilizer, the use of surfactant can be eliminated. Hence, nanoclays treated with just amino silanes could provide enough interaction between the clay and the compatibilizer to produce strain hardening effect in linear PP/clay nanocomposite melt.

b) The use of amino silanes (amino propyl trimethoxy silanes) has been well reported in literature for improving the interaction between the clay and the compatibilizer. However, there has not been a single report that mentions about the improvement in the strain hardening characteristics of the polymer melt. This could be due to short length of the linker (three carbon) between the amine and the silicon groups. In our research, we have used silanes with five carbon linker length and observed significant improvement in strain hardening characteristics of the resulting nanocomposites. Hence, the use of longer linker length in the silane coupling agents needs to be evaluated in order to study the effects of chain length, between the amine and the silicon group, on the coupling between the clay and the bulk polypropylene and thereby on its melt strain hardening property.

c) The dispersion of clay layers has always been challenging in polypropylenes. In this study we used batch mixing process to achieve intercalation of the polymer chains

within the clay galleries. For successful implementation of this research for industrial purposes, continuous extrusion process needs to be evaluated for dispersion of nanoclays and melt strain hardening of the resulting nanocomposites.

d) This research presented a qualitative understanding of the formation of polymer/clay entangles network using van-Gurp Palmen plots. A more quantitative approach could be taken to understand the formation of such networks and its effect on strain hardening behavior of the nanocomposites.

# REFERENCES

# REFERENCES


1. X. Cao, L. J. Lee, T. Widya and C. Macosko, "Polyurethane/clay nanocomposites foams: processing, structure and properties," *Polymer,* **46**(3), 775-783 (2005).

2. L. Domeier, A. Nissen, S. Goods, L. Whinnery and J. McElhanon, "Thermomechanical Characterization of Thermoset Urethane Shape-Memory Polymer Foams," *Journal of Applied Polymer Science,* **115**(6), 3217-3229 (2010).

3. A. Guo, I. Javni and Z. Petrovic, "Rigid polyurethane foams based on soybean oil," *Journal of Applied Polymer Science,* **77**(2), 467-473 (2000).

4. Y. H. Hu, Y. Gao, D. N. Wang, C. P. Hu, S. Zu, L. Vanoverloop and D. Randall, "Rigid polyurethane foam prepared from a rape seed oil based polyol," *Journal of Applied Polymer Science,* **84**(3), 591-597 (2002).

5. W. J. Seo, H. C. Jung, J. C. Hyun, W. N. Kim, Y. B. Lee, K. H. Choe and S. B. Kim, "Mechanical, morphological, and thermal properties of rigid polyurethane foams blown by distilled water," *Journal of Applied Polymer Science,* **90**(1), 12-21 (2003).

6. T. Widya and C. W. Macosko, "Nanoclay-modified rigid polyurethane foam," *Journal of Macromolecular Science-Physics,* **B44**(6), 897-908 (2005).

7. K. S. Chian and L. H. Gan, "Development of a rigid polyurethane foam from palm oil," *Journal of Applied Polymer Science,* **68**(3), 509-515 (1998).

8. I. Javni, W. Zhang, V. Karajkov, Z. S. Petrovic and V. Divjakovic, "Effect of nano- and micro-silica fillers on polyurethane foam properties," *Journal of Cellular Plastics,* **38**(3), 229-239 (2002).

9. L. J. Lee, C. C. Zeng, X. Cao, X. M. Han, J. Shen and G. J. Xu, "Polymer nanocomposite foams," *Composites Science and Technology,* **65**(15-16), 2344-2363 (2005).

10. A. M. Trater, S. Alavi and S. S. H. Rizvi, "Use of non-invasive X-ray microtomography for characterizing microstructure of extruded biopolymer foams," *Food Research International,* **38**(6), 709-719 (2005).

11. S. Arif, G. Burgess, R. Narayan and B. Harte, "Evaluation of a biodegradable foam for protective packaging applications," *Packaging Technology and Science,* **20**(6), 413-419 (2007).

12. Q. Fang and M. A. Hanna, "Characteristics of biodegradable Mater-Bi (R)-starch based foams as affected by ingredient formulations," *Industrial Crops and Products,* **13**(3), 219-227 (2001).

13. G. M. Glenn and D. W. Irving, "STARCH-BASED MICROCELLULAR FOAMS," *Cereal Chemistry,* **72**(2), 155-161 (1995).

14. Y. Nabar, R. Narayan and M. Schindler, "Twin-screw extrusion production and characterization of starch foam products for use in cushioning and insulation applications," *Polymer Engineering and Science,* **46**(4), 438-451 (2006).

15. Y. U. Nabar, D. Draybuck and R. Narayan, "Physicomechanical and hydrophobic properties of starch foams extruded with different biodegradable polymers," *Journal of Applied Polymer Science,* **102**(1), 58-68 (2006).

16. R. Narayan, "Commercializing biobased, biodegradable starch foam plastics: From R&D to marketplace," *Abstracts of Papers of the American Chemical Society,* **229**, U277-U277 (2005).

17. R. L. Shogren, J. W. Lawton, W. M. Doane and K. F. Tiefenbacher, "Structure and morphology of baked starch foams," *Polymer,* **39**(25), 6649-6655 (1998).

18. J. L. Willett and R. L. Shogren, "Processing and properties of extruded starch/polymer foams," *Polymer,* **43**(22), 5935-5947 (2002).

19. D. Jovanovic, G. E. Engels, J. A. Plantinga, M. Bruinsma, W. van Oeveren, A. J. Schouten, M. J. A. van Luyn and M. C. Harmsen, "Novel polyurethanes with interconnected porous structure induce in vivo tissue remodeling and accompanied vascularization," *Journal of Biomedical Materials Research Part A,* **95A**(1), 198-208 (2010).

20. V. Mourino, P. Newby and A. R. Boccaccini, "Preparation and Characterization of Gallium Releasing 3-D Alginate Coated 45S5 Bioglass (R) Based Scaffolds for Bone Tissue Engineering," *Advanced Engineering Materials,* **12**(7), B283-B291 (2010).

21. L. Y. Lee, S. H. Ranganath, Y. L. Fu, J. L. Zheng, H. S. Lee, C. H. Wang and K. A. Smith, "Paclitaxel release from micro-porous PLGA disks," *Chemical Engineering Science,* **64**(21), 4341-4349 (2009).

22. A. Streubel, J. Siepmann and R. Bodmeier, "Floating matrix tablets based on low density foam powder: effects of formulation and processing parameters on drug release," *European Journal of Pharmaceutical Sciences,* **18**(1), 37-45 (2003).

23. R. Garg and G. Das Gupta, "Preparation and Evaluation of Gastroretentive Floating Tablets of Silymarin," *Chemical & Pharmaceutical Bulletin,* **57**(6), 545-549 (2009).

24. K. A. Arora, A. J. Lesser and T. J. McCarthy, "Preparation and characterization of microcellular polystyrene foams processed in supercritical carbon dioxide," *Macromolecules,* **31**(14), 4614-4620 (1998).

25. H. Janani and M. H. N. Famili, "Investigation of a Strategy for Well Controlled Inducement of Microcellular and Nanocellular Morphologies in Polymers," *Polymer Engineering and Science,* **50**(8), 1558-1570 (2010).

26. B. Zhu, W. B. Zha, J. T. Yang, C. L. Zhang and L. J. Lee, "Layered-silicate based polystyrene nanocomposite microcellular foam using supercritical carbon dioxide as blowing agent," *Polymer,* **51**(10), 2177-2184 (2010).

27. J. Shen, C. C. Zeng and L. J. Lee, "Synthesis of poly styrene-carbon nanofibers nanocomposite foams," *Polymer,* **46**(14), 5218-5224 (2005).

28. X. M. Han, C. C. Zeng, L. J. Lee, K. W. Koelling and D. L. Tomasko, "Extrusion of polystyrene nanocomposite foams with supercritical CO2," *Polymer Engineering and Science,* **43**(6), 1261-1275 (2003).

29. N. H. Abu-Zahra, A. M. Alian, R. Perez and H. Chang, "Extrusion of Rigid PVC Foam with Nanoclay: Synthesis and Characterization," *Journal of Reinforced Plastics and Composites,* **29**(8), 1153-1165 (2010).

30. C. A. Diaz and L. M. Matuana, "Continuous Extrusion Production of Microcellular Rigid PVC," *Journal of Vinyl & Additive Technology,* **15**(4), 211-218 (2009).

31. V. Kumar and J. E. Weller, "A process to produce microcellular PVC," *International Polymer Processing,* **8**(1), 73-80 (1993).

32. G. T. Lim, V. Altstadt and F. Ramsteiner, "Understanding the Compressive Behavior of Linear and Cross-linked Poly(vinyl chloride) Foams," *Journal of Cellular Plastics,* **45**(5), 419-439 (2009).

33. J. Sandler, F. Wollecke, V. Altstadt, E. Wettstein and D. Rakutt, "Principal correlation of PVC melt elongational properties with foam cell morphology," *Cellular Polymers,* **19**(6), 371-388 (2000).

34. A. K. Bledzki, M. Rohleder, H. Kirschling and A. Chate, "Microcellular Polycarbonate with Improved Notched Impact Strength Produced by Injection Moulding with Physical Blowing Agent," *Cellular Polymers,* **27**(6), 327-345 (2008).

35. Y. K. Kwon and H. K. Bae, "Production of microcellular foam plastics by supercritical carbon dioxide," *Korean Journal of Chemical Engineering,* **24**(1), 127-132 (2007).

36. M. Mitsunaga, Y. Ito, S. S. Ray, M. Okamoto and K. Hironaka, "Intercalated polycarbonate/clay nanocomposites: Nanostructure control and foam processing," *Macromolecular Materials and Engineering,* **288**(7), 543-548 (2003).

37. S. G. Kim, J. W. S. Lee, C. B. Park and M. Sain, "Enhancing Cell Nucleation of Thermoplastic Polyolefin Foam Blown with Nitrogen," *Journal of Applied Polymer Science,* **118**(3), 1691-1703.

38. M. A. Rodriguez-Perez, F. Hidalgo, E. Solorzano and J. A. de Saja, "Measuring the time evolution of the gas pressure in closed cell polyolefin foams produced by compression moulding," *Polymer Testing,* **28**(2), 188-195 (2009).

39. M. A. Rodriguez-Perez, J. Lobos, C. A. Perez-Munoz and J. A. De Saja, "Mechanical Response of Polyethylene Foams with High Densities and Cell Sizes in the Microcellular Range," *Journal of Cellular Plastics,* **45**(5), 389-403 (2009).

40. Z. Zakaria, Z. M. Ariff and C. S. Sipaut, "Effects of Parameter Changes on the Structure and Properties of Low-Density Polyethylene Foam," *Journal of Vinyl & Additive Technology,* **15**(2), 120-128 (2009).

41. M. Antunes, J. I. Velasco, V. Realinho and E. Solorzano, "Study of the Cellular Structure Heterogeneity and Anisotropy of Polypropylene and Polypropylene Nanocomposite Foams," *Polymer Engineering and Science,* **49**(12), 2400-2413 (2009).

42. M. Guo, M. Heuzey and P. J. Carreau, "Cell structure and dynamic properties of injection molded polypropylene foams," *Polymer Engineering and Science,* **47**(7), 1070-1081 (2007).

43. P. C. Lee, W. Kaewmesri, J. Wang, C. B. Park, J. Pumchusak, R. Folland and A. Praller, "Effect of die geometry on foaming behaviors of high-melt-strength polypropylene with CO2," *Journal of Applied Polymer Science,* **109**(5), 3122-3132 (2008).

44. C. Liu, D. Wei, A. Zheng, Y. Li and H. Xiao, "Improving foamability of polypropylene by grafting modification," *Journal of Applied Polymer Science,* **101**(6), 4114-4123 (2006).

45. H. E. Naguib and C. B. Park, "Strategies for achieving ultra low-density polypropylene foams," *Polymer Engineering and Science,* **42**(7), 1481-1492 (2002).

46. H. E. Naguib, C. B. Park and N. Reichelt, "Fundamental foaming mechanisms governing the volume expansion of extruded polypropylene foams," *Journal of Applied Polymer Science,* **91**(4), 2661-2668 (2004).

47. C. B. Park and L. K. Cheung, "A study of cell nucleation in the extrusion of polypropylene foams," *Polymer Engineering and Science,* **37**(1), 1-10 (1997).

48. J. Stange and H. Munstedt, "Effect of long-chain branching on the foaming of polypropylene with azodicarbonamide," *Journal of Cellular Plastics,* **42**(6), 445-467 (2006).

49. W. G. Zheng, Y. H. Lee and C. B. Park, "Use of Nanoparticles for Improving the Foaming Behaviors of Linear PP," *Journal of Applied Polymer Science,* **117**(5), 2972-2979 (2010).

50. R. Dhavalikar, M. Yamaguchi and M. Xanthos, "Molecular and structural analysis of a triepoxide-modified poly(ethylene terephthalate) from rheological data," *Journal of Polymer Science, Part A: Polymer Chemistry,* **41**(7), 958-969 (2003).

51. Y. W. Di, S. Iannace, E. Di Maio and L. Nicolais, "Poly(lactic acid)/organoclay nanocomposites: Thermal, rheological properties and foam processing," *Journal of Polymer Science Part B-Polymer Physics,* **43**(6), 689-698 (2005).

52. I. Pillin, N. Montrelay, A. Bourmaud and Y. Grohens, "Effect of thermo-mechanical cycles on the physico-chemical properties of poly(lactic acid)," *Polymer Degradation and Stability,* **93**(2), 321-328 (2008).

53. N. Kakarala, "Trends in Automotive plastics," *Society of Plastics Engineers Tech. Papers* (1999).

54. S. Shah and N. Kakarala, "Requirements for rapid growth of all olefinic automotive interiors," *Society of Plastics Engineers Tech. Papers* (2000).

55. S. Mehta, F. M. Mirabella, K. Rufener and A. Bafna, "Thermoplastic olefin/clay nanocomposites: Morphology and mechanical properties," *Journal of Applied Polymer Science,* **92**(2), 928-936 (2004).

56. J. K. Mishra, K. J. Hwang and C. S. Ha, "Preparation, mechanical and rheological properties of a thermoplastic polyolefin (TPO)/organoclay nanocomposite with reference to the effect of maleic anhydride modified polypropylene as a compatibilizer," *Polymer,* **46**(6), 1995-2002 (2005).

57. S. Wong, H. E. Naguib and C. B. Park, "Effect of processing parameters on the cellular morphology and mechanical properties of thermoplastic polyolefin (TPO) microcellular foams," *Advances in Polymer Technology,* **26**(4), 232-246 (2007).

58. J. Stange and H. Munstedt, "Rheological properties and foaming behavior of polypropylenes with different molecular structures," *Journal of Rheology,* **50**(6), 907-923 (2006).

59. P. Spitael and C. W. Macosko, "Strain hardening in polypropylenes and its role in extrusion foaming," *Polymer Engineering and Science,* **44**(11), 2090-2100 (2004).

60. S. Doroudiani, C. B. Park and M. T. Kortschot, "Effect of the crystallinity and morphology on the microcellular foam structure of semicrystalline polymers," *Polymer Engineering and Science,* **36**(21), 2645-2662 (1996).

61. J. Reignier, R. Gendron and M. F. Champagne, "Autoclave Foaming of Poly(e-Caprolactone) Using Carbon Dioxide: Impact of Crystallization on Cell Structure," *Journal of Cellular Plastics,* **43**, 459-489 (2007).

62. D. Klempner, V. Sendijarevic and R. M. Aseeva, *Handbook of polymeric foams and foam technology* (Hanser Publishers, Munich, Cincinnati, 2004).

63. J. E. Martini, N. P. Suh and F. A. Waldman, "Microcellular closed cell foams and their method of manufacture," U.S. Pat. 4,473,665 (1984).

64. J. L. Throne, *Thermoplastic foam extrusion : an introduction* (Hanser Publishers, Munich, Germany and Cincinnati, Ohio, 2004).

65. J. S. Colton and N. P. Suh, "The Nucleation of Microcellular Thermoplastic Foam with Additives .1. Theoretical Considerations," *Polymer Engineering and Science,* **27**(7), 485-492 (1987).

66. N. H. Fletcher, "Size Effect in Heterogeneous Nucleation," *Journal of Chemical Physics,* **29**(3), 572-576 (1958).

67. D. F. Baldwin, C. B. Park and N. P. Suh, "An extrusion system for the processing of microcellular polymer sheets: Shaping and cell growth control," *Polymer Engineering and Science,* **36**(10), 1425-1435 (1996).

68. C. B. Park, L. K. Cheung and S. W. Song, "The effect of talc on cell nucleation in extrusion foam processing of polypropylene with CO2 and isopentane," *Cellular Polymers,* **17**(4), 221-251 (1998).

69. M. Alexandre and P. Dubois, "Polymer-layered silicate nanocomposites: preparation, properties and uses of a new class of materials," *Materials Science & Engineering R-Reports,* **28**(1-2), 1-63 (2000).

70. H. Fischer, "Polymer nanocomposites: from fundamental research to specific applications," *Materials Science & Engineering C-Biomimetic and Supramolecular Systems,* **23**(6-8), 763-772 (2003).

71. E. P. Giannelis, "Polymer layered silicate nanocomposites," *Advanced Materials,* **8**(1), 29-35 (1996).

72. G. Lagaly, "Introduction: from clay mineral-polymer interactions to clay mineral-polymer nanocomposites," *Applied Clay Science,* **15**(1-2), 1-9 (1999).

73. S. Pavlidou and C. D. Papaspyrides, "A review on polymer-layered silicate nanocomposites," *Progress in Polymer Science,* **33**(12), 1119-1198 (2008).

74. S. S. Ray and M. Okamoto, "Polymer/layered silicate nanocomposites: a review from preparation to processing," *Progress in Polymer Science,* **28**(11), 1539-1641 (2003).

75. A. Usuki, M. Kawasumi, Y. Kojima, A. Okada, T. Kurauchi and O. Kamigaito, "Swelling Behavior of Montmorillonite Cation Exchanged for Omega-Amino Acids by Epsilon-Caprolactam," *Journal of Materials Research,* **8**(5), 1174-1178 (1993).

76. A. Usuki, Y. Kojima, M. Kawasumi, A. Okada, Y. Fukushima, T. Kurauchi and O. Kamigaito, "Synthesis of Nylon 6-Clay Hybrid," *Journal of Materials Research,* **8**(5), 1179-1184 (1993).

77. H. Heinz, R. A. Vaia, R. Krishnamoorti and B. L. Farmer, "Self-assembly of alkylammonium chains on montmorillonite: Effect of chain length, head group structure, and cation exchange capacity," *Chemistry of Materials,* **19**(1), 59-68 (2007).

78. M. Kawasumi, N. Hasegawa, M. Kato, A. Usuki and A. Okada, "Preparation and mechanical properties of polypropylene-clay hybrids," *Macromolecules,* **30**(20), 6333-6338 (1997).

79. T. Lan, P. D. Kaviratna and T. J. Pinnavaia, "On the Nature of Polyimide Clay Hybrid Composites," *Chemistry of Materials,* **6**(5), 573-575 (1994).

80. H. Z. Shi, T. Lan and T. J. Pinnavaia, "Interfacial effects on the reinforcement properties of polymer-organoclay nanocomposites," *Chemistry of Materials,* **8**(8), 1584-& (1996).

81. J. I. Velasco, M. Ardanuy, V. Realinho, M. Antunes, A. I. Fernandez, J. I. Gonzalez-Pena, M. A. Rodriguez-Perez and J. A. de Saja, "Polypropylene/clay nanocomposites: Combined effects of clay treatment and compatibilizer polymers on the structure and proverties," *Journal of Applied Polymer Science,* **102**(2), 1213-1223 (2006).

82. P. Reichert, H. Nitz, S. Klinke, R. Brandsch, R. Thomann and R. Mulhaupt, "Poly(propylene)/organoclay nanocomposite formation: Influence of compatibilizer functionality and organoclay modification," *Macromolecular Materials and Engineering,* **275**(2), 8-17 (2000).

83. E. Manias, A. Touny, L. Wu, K. Strawhecker, B. Lu and T. C. Chung, "Polypropylene/Montmorillonite nanocomposites. Review of the synthetic routes and materials properties," *Chemistry of Materials,* **13**(10), 3516-3523 (2001).

84. M. T. Ton-That, F. Perrin-Sarazin, K. C. Cole, M. N. Bureau and J. Denault, "Polyolefin nanocomposites: Formulation and development," *Polymer Engineering and Science,* **44**(7), 1212-1219 (2004).

85. T. D. Fornes, D. L. Hunter and D. R. Paul, "Nylon-6 nanocomposites from alkylammonium-modified clay: The role of alkyl tails on exfoliation," *Macromolecules,* **37**(5), 1793-1798 (2004).

86. N. Hasegawa, M. Kawasumi, M. Kato, A. Usuki and A. Okada, "Preparation and mechanical properties of polypropylene-clay hybrids using a maleic anhydride-modified polypropylene oligomer," *Journal of Applied Polymer Science,* **67**(1), 87-92 (1998).

87. M. Kato, A. Usuki and A. Okada, "Synthesis of polypropylene oligomer-clay intercalation compounds," *Journal of Applied Polymer Science,* **66**(9), 1781-1785 (1997).

88. A. Usuki, M. Kato, A. Okada and T. Kurauchi, "Synthesis of polypropylene-clay hybrid," *Journal of Applied Polymer Science,* **63**(1), 137-139 (1997).

89. N. Hasegawa, H. Okamoto, M. Kato and A. Usuki, "Preparation and mechanical properties of polypropylene-clay hybrids based on modified polypropylene and organophilic clay," *Journal of Applied Polymer Science,* **78**(11), 1918-1922 (2000).

90. N. Hasegawa, H. Okamoto, M. Kawasumi, M. Kato, A. Tsukigase and A. Usuki, "Polyolefin-clay hybrids based on modified polyolefins and organophilic clay," *Macromolecular Materials and Engineering,* **280**(7-8), 76-79 (2000).

91. N. Hasegawa and A. Usuki, "Silicate laver exfoliation in polvolefin/clay nanocomposites based on maleic anhydride modified polyolefins and organophilic clay," *Journal of Applied Polymer Science,* **93**(1), 464-470 (2004).

92. T. G. Gopakumar, J. A. Lee, M. Kontopoulou and J. S. Parent, "Influence of clay exfoliation on the physical properties of montmorillonite/polyethylene composites," *Polymer,* **43**(20), 5483-5491 (2002).

93. H. Ishida, S. Campbell and J. Blackwell, "General approach to nanocomposite preparation," *Chemistry of Materials,* **12**(5), 1260-1267 (2000).

94. B. K. Deka and T. K. Maji, "Effect of coupling agent and nanoclay on properties of HDPE, LDPE, PP, PVC blend and Phargamites karka nanocomposite," *Composites Science and Technology,* **70**(12), 1755-1761 (2010).

95. C. C. Zeng, X. M. Han, L. J. Lee, K. W. Koelling and D. L. Tomasko, "Polymer-clay nanocomposite foams prepared using carbon dioxide," *Advanced Materials,* **15**(20), 1743-1747 (2003).

96. Z. H. Guo, L. J. Lee and D. L. Tomasko, "CO2 Permeability of Polystyrene Nanocomposites and Nanocomposite Foams," *Industrial & Engineering Chemistry Research,* **47**(23), 9636-9643 (2008).

97. J. Shen, X. Cao and L. J. Lee, "Synthesis and foaming of water expandable polystyrene-clay nanocomposites," *Polymer,* **47**(18), 6303-6310 (2006).

98. X. M. Han, K. W. Koelling, D. L. Tomasko and L. J. Lee, "Effect of die temperature on the morphology of microcellular foams," *Polymer Engineering and Science,* **43**(6), 1206-1220 (2003).

99. J. Shen, X. M. Han and L. J. Lee, "Nucleation and reinforcement of carbon nanofibers on polystyrene nanocomposite foam," *Society of Plastics Engineers Tech. Papers,* **63**, 2597-2601 (2005).

100. M. Okamoto, P. H. Nam, P. Maiti, T. Kotaka, T. Nakayama, M. Takada, M. Ohshima, A. Usuki, N. Hasegawa and H. Okamoto, "Biaxial flow-induced alignment of silicate layers in polypropylene/clay nanocomposite foam," *Nano Letters,* **1**(9), 503-505 (2001).

101. X. L. Jiang, T. Liu, Z. M. Xu, L. Zhao, G. H. Hu and W. K. Yuan, "Effects of crystal structure on the foaming of isotactic polypropylene using supercritical carbon dioxide as a foaming agent," *Journal of Supercritical Fluids,* **48**(2), 167-175 (2009).

102. W. Zheng, Y. H. Lee and C. B. Park, "Effect of nano particles on foaming behaviors of PP," *Society of Plastics Engineers Tech. Papers,* **64**, 2715-2720 (2006).

103. W. Kaewmesri, P. C. Lee, C. B. Park and J. Pumchusak, "Effects of CO2 and talc contents on foaming behavior of recyclable high-melt-strength PP," *Journal of Cellular Plastics,* **42**(5), 405-428 (2006).

104. J. W. S. Lee, K. Y. Wang and C. B. Park, "Challenge to extrusion of low-density microcellular polycarbonate foams using supercritical carbon dioxide," *Industrial & Engineering Chemistry Research,* **44**(1), 92-99 (2005).

105. D. Dixon, P. J. Martin and H. E. Jones, " Predicting the Performance of Chemical Blowing Agents Using Thermal Analysis Techniques," *Journal of Cellular Plastics,* **36**(4), 310-326 (2000).

106. C. H. Lee, K. J. Lee, H. G. Jeong and S. W. Kim, "Growth of gas bubbles in the foam extrusion process," *Advances in Polymer Technology* **19**(2), 97-112 (2000).

107. A. Ghijsels and J. Declippeleir, "Melt Strength Behavior of Polypropylenes," *International Polymer Processing,* **9**(3), 252-257 (1994).

108. J. G. Burt, "The elements of expansion of thermoplastics: Part II," *Journal of Cellular Plastics,* **14**(6), 341-345 (1978).

109. H. Munstedt, S. Kurzbeck and J. Stange, "Importance of elongational properties of polymer melts for film blowing and thermoforming," *Polymer Engineering and Science,* **46**(9), 1190-1195 (2006).

110. F. J. Stadler, A. Nishioka, J. Stange, K. Koyama and H. Munstedt, "Comparison of the elongational behavior of various polyolefins in uniaxial and equibiaxial flows," *Rheologica Acta,* **46**(7), 1003-1012 (2007).

111. M. Danaei, N. Sheikh and F. A. Taromi, "Radiation Cross-linked Polyethylene Foam: Preparation and Properties," *Journal of Cellular Plastics,* **41**(6), 551-562 (2005).

112. D. H. Han, J. H. Jang, H. Y. Kim, B. N. Kim and B. Y. Shin, "Manufacturing and foaming of high melt viscosity of polypropylene by using electron beam radiation technology," *Polymer Engineering and Science,* **46**(4), 431-437 (2006).

113. C. Gabriel and H. Munstedt, "Strain hardening of various polyolefins in uniaxial elongational flow," *Journal of Rheology,* **47**(3), 619-630 (2003).

114. F. Yoshii, T. Sasaki, K. Makuuchi and N. Tamura, "Durability of Radiation-Sterilized Polymers. 3. Oxidation Layer Determined by Chemiluminescence," *Journal of Applied Polymer Science,* **31**(5), 1343-1350 (1986).

115. A. Yousefi and A. A. Katbab, "Post Irradiation Degradation of Polypropylene Radiation Durability of Polypropylene Stabilized With Phenolic Stabilizer (II) " *Radiation Physics and Chemistry,* **44**(6), 645-649 (1994).

116. J. Stange, C. Uhl and H. Munstedt, "Rheological behavior of blends from a linear and a long-chain branched polypropylene," *Journal of Rheology,* **49**(5), 1059-1079 (2005).

117. S. Kurzbeck, F. Oster and H. Munstedt, "Rheological properties of two polypropylenes with different molecular structure," *Journal of Rheology,* **43**(2), 359-374 (1999).

118. T. J. McCallum, M. Kontopoulou, C. B. Park, E. B. Muliawan and S. G. Hatzikiriakos, "The rheological and physical properties of linear and branched polypropylene blends," *Polymer Engineering and Science,* **47**(7), 1133-1140 (2007).

119. S. H. Tabatabaei, P. J. Carreau and A. Ajji, "Rheological and thermal properties of blends of a long-chain branched polypropylene and different linear polypropylenes," *Chemical Engineering Science,* **64**(22), 4719-4731 (2009).

120. S. H. Tabatabaei, P. J. Carreau and A. Ajji, "Rheological Long-Chain Properties of Blends of Linear and Branched Polypropylenes," *Polymer Engineering and Science,* **50**(1), 191-199 (2010).

121. M. F. Champagne and R. Gendron, "Structural PP Nanocomposites foams prepared by direct CO2 injection," *Society of Plastics Engineers Tech. Papers,* **63**, 1477-1481 (2005).

122. H. E. Naguib, C. B. Park and P. C. Lee, "Effect of talc content on the volume expansion ratio of extruded PP foams," *Journal of Cellular Plastics,* **39**(6), 499-511 (2003).

123. Z. J. Xu, P. Xue, F. H. Zhu and H. M. He, "Effects of formulations and processing parameters on foam morphologies in the direct extrusion foaming of polypropylene using a single-screw extruder " *Journal of Cellular Plastics,* **41**(2), 169-185 (2005).

124. X. L. Jiang, J. B. Bao, T. Liu, L. Zhao, Z. M. Xu and W. K. Yuan, "Microcellular Foaming of Polypropylene/Clay Nanocomposites with Supercritical Carbon Dioxide," *Journal of Cellular Plastics,* **45**(6), 515-538 (2009).

125. M. Antunes, V. Realinho and J. I. Velasco, "Foaming Behaviour, Structure, and Properties of Polypropylene Nanocomposites Foams," *Journal of Nanomaterials,* **2010**, 1-11 (2010).

126. A. Minegishi, A. Nishioka, T. Takahashi, Y. Masubuchi, J. Takimoto and K. Koyama, "Uniaxial elongational viscosity of PS/a small amount of UHMW-PS blends," *Rheologica Acta,* **40**(4), 329-338 (2001).

127. H. Munstedt, "Dependence of the elongational behavior of polystyrene melts on molecular-weight and molecular-weight distribution," *Journal of Rheology,* **24**(6), 847-867 (1980).

128. T. Takahashi, J. I. Takimoto and K. Koyama, "Uniaxial elongational viscosity of various molten polymer composites," *Polymer Composites,* **20**(3), 357-366 (1999).

129. R. K. Gupta, V. Pasanovic-Zujo and S. N. Bhattacharya, "Shear and extensional rheology of EVA/layered silicate-nanocomposites," *Journal of Non-Newtonian Fluid Mechanics,* **128**(2-3), 116-125 (2005).

130. D. G. Seong, T. J. Kang and J. R. Youn, "Rheological characterization of polymer-based nanocomposites with different nanoscale dispersions," *E-Polymers*, - (2005).

131. M. Okamoto, P. H. Nam, P. Maiti, T. Kotaka, N. Hasegawa and A. Usuki, "A house of cards structure in polypropylene/clay nanocomposites under elongational flow," *Nano Letters,* **1**(6), 295-298 (2001).

132. T. Pathak and K. Jayaraman, "Polymer clay nanocomposites with improved melt strength," *Society of Plastics Engineers Tech. Papers,* **65**, 133-137 (2007).

133. Y. Minoura, M. Ueda, S. Mizunuma and M. Oba, "Reaction of Polypropylene with Maleic Anhydride," *Journal of Applied Polymer Science,* **13**(8), 1625-1640 (1969).

134. W. Gianelli, G. Camino, N. T. Dintcheva, S. Lo Verso and F. P. La Mantia, "EVA-montmorillonite nanocomposites: Effect of processing conditions," *Macromolecular Materials and Engineering,* **289**(3), 238-244 (2004).

135. S. Kumar, *Effects of grafting from edges of nanolayers on flow induced structure in polypropylene/clay nanocomposites*, Ph.D., Michigan State University (2005).

136. D. Marchant and K. Jayaraman, "Strategies for optimizing polypropylene-clay nanocomposite structure," *Industrial & Engineering Chemistry Research,* **41**(25), 6402-6408 (2002).

137. H. Shariatpanahi, F. Sarabi, M. Mirali, M. Hemmati and F. Mahdavi, "Polypropylene-Organoclay Nanocomposite: Preparation, Microstructure, and Mechanical Properties," *Journal of Applied Polymer Science,* **113**(2), 922-926 (2009).

138. M. K. Dolgovskij, P. D. Fasulo, F. Lortie, C. W. Macosko, R. A. Ottaviani and W. R. Rodgers, "Effect of Mixer type on exfoliation of Polypropylene Nanocomposites," *Society of Plastics Engineers Tech. Papers* (2003).

139. T. G. Gopakumar and D. J. Y. S. Page, "Compounding of nanocomposites by thermokinetic mixing," *Journal of Applied Polymer Science,* **96**(5), 1557-1563 (2005).

140. D. Marchant, *Characterization and control of exfoliation in melt-processed nanocomposites of PP and clay*, Ph.D., Michigan State University (2003).

141. S. Brunauer, P. H. Emmett and E. Teller, "Adsorption of gases in multimolecular layers," *Journal of the American Chemical Society,* **60**, 309-319 (1938).

142. I. Langmuir, "The constitution and fundamental properties of solids and liquids Part I Solids," *Journal of the American Chemical Society,* **38**, 2221-2295 (1916).

143. B. D. Cullity, *Elements of x-ray diffraction* (Addison-Wesley Pub. Co., Reading, Mass., 1978).

144. C. W. Macosko and R. G. Larson, *Rheology : principles, measurements, and applications* (VCH, New York, NY, 1994).

145. J. M. Dealy and R. G. Larson, *Structure and rheology of molten polymers : from structure to flow behavior and back again* (Hanser Publishers, Munich, Cincinnati, 2006).

146. J. Meissner, T. Raible and S. E. Stephenson, "Rotary Clamp in Uniaxial and Biaxial Extensional Rheometry of Polymer Melts," *Journal of Rheology,* **25**(1), 1-28 (1981).

147. Y. Ema, M. Ikeya and M. Okamoto, "Foam processing and cellular structure of polylactide-based nanocomposites," *Polymer,* **47**(15), 5350-5359 (2006).

148. L. M. Chen, R. Ozisik and L. S. Schadler, "The influence of carbon nanotube aspect ratio on the foam morphology of MWNT/PMMA nanocomposite foams," *Polymer,* **51**(11), 2368-2375 (2010).

149. S. S. Ray and M. Okamoto, "New polylactide/layered silicate nanocomposites, 6 - Melt rheology and foam processing," *Macromolecular Materials and Engineering,* **288**(12), 936-944 (2003).

150. R. Verdejo, P. Werner, J. Sandler, V. Altstadt and M. S. P. Shaffer, "Morphology and properties of injection-moulded carbon-nanofibre poly(etheretherketone) foams," *Journal of Materials Science,* **44**(6), 1427-1434 (2009).

151. N. Katsikis, T. Koniger and H. Munstedt, "Elongational viscosities of polymethylmethacrylate/nano-clay composites," *Applied Rheology,* **17**(5), - (2007).

152. M. Yamaguchi, "Rheological properties of linear and crosslinked polymer blends: Relation between crosslink density and enhancement of elongational viscosity," *Journal of Polymer Science Part B-Polymer Physics,* **39**(2), 228-235 (2001).

153. M. Yamaguchi and K. Suzuki, "Rheological properties and foam processability for blends of linear and crosslinked polyethylenes," *Journal of Polymer Science Part B-Polymer Physics,* **39**(18), 2159-2167 (2001).

154. D. Sikdar, K. S. Katti and D. R. Katti, "Molecular interactions alter clay and polymer structure in polymer clay nanocomposites," *Journal of Nanoscience and Nanotechnology,* **8**(4), 1638-1657 (2008).

155. E. P. Giannelis, "Polymer layered silicate nanocomposites," *Advanced Materials,* **8**(1), 29-& (1996).

156. T. S. Ellis and J. S. D'Angelo, "Thermal and mechanical properties of a polypropylene nanocomposite," *Journal of Applied Polymer Science,* **90**(6), 1639-1647 (2003).

157. R. A. Vaia and E. P. Giannelis, "Lattice model of polymer melt intercalation in organically-modified layered silicates," *Macromolecules,* **30**(25), 7990-7999 (1997).

158. P. B. Messersmith and E. P. Giannelis, "Synthesis and Characterization of Layered Silicate-Epoxy Nanocomposites," *Chemistry of Materials,* **6**(10), 1719-1725 (1994).

159. M. Kawasumi, "The discovery of polymer-clay hybrids," *Journal of Polymer Science Part a-Polymer Chemistry,* **42**(4), 819-824 (2004).

160. K. Jayaraman and S. Kumar, *Polypropylene layered silicate nanocomposites* (eds. Mai, Y. W. & Yu, Z. Z.) (Woodhead Publishing, 2006).

161. Y. Wang, F. B. Chen and K. C. Wu, "Twin-screw extrusion compounding of polypropylene/organoclay nanocomposites modified by maleated polypropylenes," *Journal of Applied Polymer Science,* **93**(1), 100-112 (2004).

162. Y. Wang, F. B. Chen, K. C. Wu and J. C. Wang, "Clay dispersion and physical properties of melt-blended PP/organoclay nanocomposites: effect of interfacial interaction," *Composite Interfaces,* **13**(8-9), 831-852 (2006).

163. N. N. Herrera, J. M. Letoffe, J. P. Reymond and E. Bourgeat-Lami, "Silylation of laponite clay particles with monofunctional and trifunctional vinyl alkoxysilanes," *Journal of Materials Chemistry,* **15**(8), 863-871 (2005).

164. G. X. Chen, H. S. Kim, J. H. Shim and J. S. Yoon, "Role of epoxy groups on clay surface in the improvement of morphology of poly(L-lactide)/clay composites," *Macromolecules,* **38**(9), 3738-3744 (2005).

165. A. M. Shanmugharaj, K. Y. Rhee and S. H. Ryu, "Influence of dispersing medium on grafting of aminopropyltriethoxysilane in swelling clay materials," *Journal of Colloid and Interface Science,* **298**(2), 854-859 (2006).

166. D. W. Kim, K. W. Park, S. R. Chowdhury and G. H. Kim, "Effect of compatibilizer and silane coupling agent on physical properties of ethylene vinyl acetate copolymer/ethylene-1-butene copolymer/clay nanocomposite foams," *Journal of Applied Polymer Science,* **102**(4), 3259-3265 (2006).

167. N. N. Herrera, J. M. Letoffe, J. L. Putaux, L. David and E. Bourgeat-Lami, "Aqueous dispersions of silane-functionalized laponite clay platelets. A first step toward the elaboration of water-based polymer/clay nanocomposites," *Langmuir,* **20**(5), 1564-1571 (2004).

168. H. P. He, J. Duchet, J. Galy and J. F. Gerard, "Grafting of swelling clay materials with 3-aminopropyltriethoxysilane," *Journal of Colloid and Interface Science,* **288**(1), 171-176 (2005).

169. K. A. Carrado, L. Q. Xu, R. Csencsits and J. V. Muntean, "Use of organo- and alkoxysilanes in the synthesis of grafted and pristine clays," *Chemistry of Materials,* **13**(10), 3766-3773 (2001).

170. H. D. Lu, Y. Hu, M. Li, Z. Y. Chen and W. C. Fan, "Structure characteristics and thermal properties of silane-grafted-polyethylene/clay nanocomposite prepared by reactive extrusion," *Composites Science and Technology,* **66**(15), 3035-3039 (2006).

171. S. Kumar and K. Jayaraman, "Polypropylene Clay Nanocomposites with Improved Stability of Morphology to Processing," *Society of Plastics Engineers Tech. Papers,* **52**, 403-407 (2006).

172. M. Buggy, G. Bradley and A. Sullivan, "Polymer-filler interactions in kaolin/nylon 6,6 composites containing a silane coupling agent," *Composites Part a-Applied Science and Manufacturing,* **36**(4), 437-442 (2005).

173. Y. Y. Choi, S. H. Lee and S. H. Ryu, "Effect of silane functionalization of montmorillonite on epoxy/montmorillonite nanocomposite," *Polymer Bulletin,* **63**(1), 47-55 (2009).

174. J. W. Lee, M. H. Kim, W. M. Choi and O. O. Park, "Effects of organoclay modification on microstructure and properties of polypropylene-organoclay nanocomposites," *Journal of Applied Polymer Science,* **99**(4), 1752-1759 (2006).

175. H. Yazdani, J. Morshedian and H. A. Khonakdar, "Effects of silane coupling agent and maleic anhydride grafted polypropylene on the morphology and viscoelastic properties of polypropylene-mica composites," *Polymer Composites,* **27**(5), 491-496 (2006).

176. K. Milczewska, A. Voelkel and J. Jeczalik, "The use of Flory-Huggins parameters to characterization of polymer/filler interactions," *Macromolecular Symposia,* **194**, 305-311 (2003).

177. K. Song and G. Sandi, "Characterization of montmorillonite surfaces after modification by organosilane," *Clays and Clay Minerals,* **49**(2), 119-125 (2001).

178. L. Le Pluart, J. Duchet, H. Sautereau and J. F. Gerard, "Surface modifications of montmorillonite for tailored interfaces in nanocomposites," *Journal of Adhesion,* **78**(7), 645-662 (2002).

179. T. Hameed, D. K. Potter and E. Takacs, "Reactions of Low Molecular Weight Highly Functionalized Maleic Anhydride Grafted Polyethylene with Polyetherdiamines," *Journal of Applied Polymer Science,* **116**(4), 2285-2297 (2010).

180. K. H. Ku and S. C. Kim, "Polypropylene Nanocomposite Using Maleated PP and Diamine," *Journal of Applied Polymer Science,* **113**(3), 1539-1549 (2009).

181. Q. W. Lu, C. W. Macosko and J. Horrion, "Melt amination of polypropylenes," *Journal of Polymer Science Part a-Polymer Chemistry,* **43**(18), 4217-4232 (2005).

182. C. A. Orr, J. J. Cernohous, P. Guegan, A. Hirao, H. K. Jeon and C. W. Macosko, "Homogeneous reactive coupling of terminally functional polymers," *Polymer,* **42**(19), 8171-8178 (2001).

183. Z. Q. Song and W. E. Baker, "Chemical reactions and reactivity of primary, secondary, and tertiary diamines with acid functionalized polymers," *Journal of Polymer Science Part a-Polymer Chemistry,* **30**(8), 1589-1600 (1992).

184. A. Zheng, H. G. Wang, X. S. Zhu and S. Masuda, "Studies on the interface of glass fiber-reinforced polypropylene composite," *Composite Interfaces,* **9**(4), 319-333 (2002).

185. P. Nygard, K. Redford and C. G. Gustafson, "Interfacial strength in glass fibre-polypropylene composites: influence of chemical bonding and physical entanglement," *Composite Interfaces,* **9**(4), 365-388 (2002).

186. W. Najjar, S. Azabou, S. Sayadi and A. Ghorbel, "Catalytic wet peroxide photo-oxidation of phenolic olive oil mill wastewater contaminants - Part 1. Reactivity of tyrosol over (Al-Fe)PILC," *Applied Catalysis B-Environmental,* **74**(1-2), 11-18 (2007).

187. R. Wibulswas, "Batch and fixed bed sorption of methylene blue on precursor and QACs modified montmorillonite," *Separation and Purification Technology,* **39**(1-2), 3-12 (2004).

188. T. Yang, X. D. Wen, J. F. Li and L. M. Yang, "Theoretical and experimental investigations on the structures of purified clay and acid-activated clay," *Applied Surface Science,* **252**(18), 6154-6161 (2006).

189. H. P. He, Q. Zhou, W. N. Martens, T. J. Kloprogge, P. Yuan, X. F. Yunfei, J. X. Zhui and R. L. Frost, "Microstructure of HDTMA(+)-modified montmorillonite and its influence on sorption characteristics," *Clays and Clay Minerals,* **54**(6), 689-696 (2006).

190. K. Ogura and M. Takahashi, "Uniaxial extension behavior of cross-linked poly(methyl methacrylate)s with various degrees of cross-linking," *Journal of the Society of Rheology Japan,* **31**(2), 85-89 (2003).

191. H. Bastian, P. Rubio and M. H. Wagner, "The strain hardening of linear and long-chain branched polymer melts," *Chemie Ingenieur Technik,* **73**(11), 1447-1451 (2001).

192. H. Munstedt, S. Kurzbeck and L. Egersdorfer, "Influence of molecular structure on rheological properties of polyethylenes Part II. Elongational behavior," *Rheologica Acta,* **37**(1), 21-29 (1998).

193. A. Malmberg, C. Gabriel, T. Steffl, H. Munstedt and B. Lofgren, "Long-chain branching in metallocene-catalyzed polyethylenes investigated by low oscillatory shear and uniaxial extensional rheometry," *Macromolecules,* **35**(3), 1038-1048 (2002).

194. D. Auhl, J. Stange, H. Munstedt, B. Krause, D. Voigt, A. Lederer, U. Lappan and K. Lunkwitz, "Long-chain branched polypropylenes by electron beam irradiation and their rheological properties," *Macromolecules,* **37**(25), 9465-9472 (2004).

195. H. E. Naguib, J. X. Xu and C. B. Park, "Effects of belnding of branched and linear polypropylene mateirals on the foamability," *Society of Plastics Engineers Tech. Papers,* **59**, 1623-1630 (2001).

196. S. N. Leung, C. B. Park, D. L. Xu, H. B. Li and R. G. Fenton, "Computer simulation of bubble-growth phenomena in foaming," *Industrial & Engineering Chemistry Research,* **45**(23), 7823-7831 (2006).

197. I. Coccorullo, L. Di Maio, S. Montesano and L. Incarnato, "Theoretical and experimental study of foaming process with chain extended recycled PET," *Express Polymer Letters,* **3**(2), 84-96 (2009).

198. N. S. Ramesh, D. H. Rasmussen and G. A. Campbell, "Numerical and Experimental Studies of Bubble-Growth during the Microcellular Foaming Process," *Polymer Engineering and Science,* **31**(23), 1657-1664 (1991).

199. K. Taki, T. Nakayama, T. Yatsuzuka and M. Ohshima, "Visual observations of batch and continuous foaming processes," *Journal of Cellular Plastics,* **39**(2), 155-169 (2003).

200. P. Etelaaho, K. Nevalainen, R. Suihkonen, J. Vuorinen and P. Jarvela, "Effects of Two Different Maleic Anhydride-Modified Adhesion Promoters (PP-g-MA) on the Structure and Mechanical Properties of Nanofilled Polyolefins," *Journal of Applied Polymer Science,* **114**(2), 978-992 (2009).

201. H. S. Kim, B. H. Lee, S. W. Choi, S. Kim and H. J. Kim, "The effect of types of maleic anhydride-grafted polypropylene (MAPP) on the interfacial adhesion properties of bio-flour-filled polypropylene composites," *Composites Part a-Applied Science and Manufacturing,* **38**(6), 1473-1482 (2007).

202. M. L. Lopez-Quintanilla, S. Sanchez-Valdes, L. F. R. de Valle and R. G. Miranda, "Preparation and mechanical properties of PP/PP-g-MA/Org-MMT nanocomposites with different MA content," *Polymer Bulletin,* **57**(3), 385-393 (2006).

203. W. H. Yuan, M. Guo, Z. A. Miao and Y. Q. Liu, "Influence of maleic anhydride grafted polypropylene on the dispersion of clay in polypropylene/clay nanocomposites," *Polymer Journal,* **42**(9), 745-751 (2010).

204. Y. Wang, F. Chen, Y. Li and K. Wu, "Melt processing of polypropylene/clay nanocomposites modified with maleated polypropylene compatibilizers," *Composites Part B-Engineering,* **35**(2), 111-124 (2004).

205. Y. Minoura, M. Ueda, S. Mizunuma and M. Oba, "The Reaction of Polypropylene with Maleic Anhydride," *Journal of Applied Polymer Science,* **13**, 1625 (1969).

206. Y. H. R. Jois and J. B. Harrison, "Modification of polyolefins: An overview," *Journal of Macromolecular Science-Reviews in Macromolecular Chemistry and Physics,* **C36**(3), 433-455 (1996).

207. G. Moad, "The synthesis of polyolefin graft copolymers by reactive extrusion," *Progress in Polymer Science,* **24**(1), 81-142 (1999).

208. W. Heinen, C. H. Rosenmoller, C. B. Wenzel, H. J. M. deGroot, J. Lugtenburg and M. vanDuin, "C-13 NMR study of the grafting of maleic anhydride onto polyethene, polypropene, and ethene-propene copolymers," *Macromolecules,* **29**(4), 1151-1157 (1996).

209. U. Mierau, D. Voigt, F. Bohme and E. Brauer, "Investigation of grafted impact-resistant polypropylene by temperature rising elution fractionation," *Journal of Applied Polymer Science,* **63**(3), 283-288 (1997).

210. S. H. P. Bettini and J. A. M. Agnelli, "Crafting of maleic anhydride onto polypropylene by reactive processing. I. Effect of maleic anhydride and peroxide concentrations on the reaction," *Journal of Applied Polymer Science,* **74**(2), 247-255 (1999).

211. B. Deroover, M. Sclavons, V. Carlier, J. Devaux, R. Legras and A. Momtaz, "Molecular Characterization of Maleic Anhydride-Functionalized Polypropylene," *Journal of Polymer Science Part a-Polymer Chemistry,* **33**(5), 829-842 (1995).

212. M. Sclavons, M. Laurent, J. Devaux and V. Carlier, "Maleic anhydride-grafted polypropylene: FTIR study of a model polymer grafted by ene-reaction," *Polymer,* **46**(19), 8062-8067 (2005).

213. T. C. B. McLeish and R. G. Larson, "Molecular constitutive equations for a class of branched polymers: The pom-pom polymer," *Journal of Rheology,* **42**(1), 81-110 (1998).

214. P. Olley and M. H. Wagner, "A modification of the convective constraint release mechanism in the molecular stress function model giving enhanced vortex growth," *Journal of Non-Newtonian Fluid Mechanics,* **135**(1), 68-81 (2006).

215. V. H. Rolon-Garrido, R. Pivokonsky, P. Filip, M. Zatloukal and M. H. Wagner, "Modelling elongational and shear rheology of two LDPE melts," *Rheologica Acta,* **48**(6), 691-697 (2009).

216. V. H. Rolon-Garrido and M. H. Wagner, "The MSF model: relation of nonlinear parameters to molecular structure of long-chain branched polymer melts," *Rheologica Acta,* **46**(5), 583-593 (2007).

217. M. H. Wagner, "The rheology of linear and long-chain branched polymer melts," *Macromolecular Symposia,* **236**, 219-227 (2006).

218. M. H. Wagner, S. Kheirandish, J. Stange and H. Munstedt, "Modeling elongational viscosity of blends of linear and long-chain branched polypropylenes," *Rheologica Acta,* **46**(2), 211-221 (2006).

219. S. Trinkle and C. Friedrich, "Van Gurp-Palmen-plot: a way to characterize polydispersity of linear polymers," *Rheologica Acta,* **40**(4), 322-328 (2001).

220. S. Trinkle, P. Walter and C. Friedrich, "Van Gurp-Palmen Plot II - Classification of long chain branched polymers by their topology," *Rheologica Acta,* **41**(1-2), 103-113 (2002).

221. L. Incarnato, P. Scarfato and D. Acierno, "Rheological and mechanical properties of recycled polypropylene," *Polymer Engineering and Science,* **39**(4), 749-755 (1999).

222. G. M. Russo, V. Nicolais, L. Di Maio, S. Montesano and L. Incarnato, "Rheological and mechanical properties of nylon 6 nanocomposites submitted to reprocessing with single and twin screw extruders," *Polymer Degradation and Stability,* **92**(10), 1925-1933 (2007).

223. A. Bonardi, R. Cilloni, V. Paganuzzi and N. Grizzuti, "Effects of degree of recycling on the rheology and processability of thermoplastic polymers," *Journal of Polymer Engineering,* **23**(2), 79-94 (2003).

224. E. T. Kabamba and D. Rodrigue, "The effect of recycling on LDPE foamability: Elongational rheology," *Polymer Engineering and Science,* **48**(1), 11-18 (2008).

225. M. R. Thompson and K. K. Yeung, "Recyclability of a layered silicate-thermoplastic olefin elastomer nanocomposite," *Polymer Degradation and Stability,* **91**(10), 2396-2407 (2006).

226. N. T. Phuong, V. Gilbert and B. Chuong, "Preparation of Recycled Polypropylene/Organophilic Modified Layered Silicates Nanocomposites Part I: The Recycling Process of Polypropylene and the Mechanical Properties of Recycled Polypropylene/Organoclay Nanocomposites," *Journal of Reinforced Plastics and Composites,* **27**(18), 1983-2000 (2008).

227. I. Rex, B. A. Graham and M. R. Thompson, "Studying single-pass degradation of a high-density polyethylene in an injection molding process," *Polymer Degradation and Stability,* **90**(1), 136-146 (2005).

228. P. Reichert, B. Hoffmann, T. Bock, R. Thomann, R. Mulhaupt and C. Friedrich, "Morphological stability of poly(propylene) nanocomposites," *Macromolecular Rapid Communications,* **22**(7), 519-523 (2001).

229. M. Okamoto, H. Sato, H. Taguchi and T. Kotaka, "Shear-induced aggregation behavior in lipophilized smectite clay/styrene suspension," *Nihon Reoroji Gakkaishi,* **28**(4), 199-200 (2000).

230. M. Bartholmai and B. Schartel, "Layered silicate polymer nanocomposites: new approach or illusion for fire retardancy? Investigations of the potentials and the tasks using a model system," *Polymers for Advanced Technologies,* **15**(7), 355-364 (2004).

231. J. Gilman, "Flammability and thermal stability studies of polymer layered-silicate (clay) nanocomposites," *Applied Clay Science,* **15**(1-2), 31-49 (1999).

232. Q. Zhang, Y. Wang and Q. Fu, "Shear-induced change of exfoliation and orientation in polypropylene/montmorillonite nanocomposites," *Journal of Polymer Science Part B-Polymer Physics,* **41**(1), 1-10 (2003).

233. A. Bafna, G. Beaucage, F. Mirabella and S. Mehta, "3D Hierarchical orientation in polymer-clay nanocomposite films," *Polymer,* **44**(4), 1103-1115 (2003).

234. Y. Kojima, A. Usuki, M. Kawasumi, A. Okada, T. Kurauchi, O. Kamigaito and K. Kaji, "Novel Preferred Orientation in Injection-Molded Nylon 6-Clay Hybrid," *Journal of Polymer Science Part B-Polymer Physics,* **33**(7), 1039-1045 (1995).

235. G. Schmidt, A. I. Nakatani, P. D. Butler, A. Karim and C. C. Han, "Shear orientation of viscoelastic polymer-clay solutions probed by flow birefringence and SANS," *Macromolecules,* **33**(20), 7219-7222 (2000).

236. K. Varlot, E. Reynaud, M. H. Kloppfer, G. Vigier and J. Varlet, "Clay-reinforced polyamide: Preferential orientation of the montmorillonite sheets and the polyamide crystalline lamellae," *Journal of Polymer Science Part B-Polymer Physics,* **39**(12), 1360-1370 (2001).

237. Y. Kojima, A. Usuki, M. Kawasumi, A. Okada, Y. Fukushima, T. Kurauchi and O. Kamigaito, "Mechanical-Properties of Nylon 6-Clay Hybrid," *Journal of Materials Research,* **8**(5), 1185-1189 (1993).

238. Y. Tang and M. Lewin, "Maleated polypropylene OMMT nanocomposite: Annealing, structural changes, exfoliated and migration," *Polymer Degradation and Stability,* **92**(1), 53-60 (2007).

239. F. Fordiani, T. Aubry and Y. Grohens, "Structural Changes Evidenced by Rheology in PPgMA Nanocomposites During Oxidative Ageing," *Journal of Applied Polymer Science,* **114**(6), 4011-4019 (2009).

240. H. O. Pastore, A. Frache, E. Boccaleri, L. Marchese and G. Camino, "Heat induced structure modifications in polymer-layered silicate nanocomposites," *Macromolecular Materials and Engineering,* **289**(9), 783-786 (2004).